UNIVERSITÀ
DEGLI STUDI
DI PADOVA

Sede amministrativa: Università degli studi di Padova

Dipartimento di Ingegneria dell'Informazione

SCUOLA DI DOTTORATO DI RICERCA IN: Ingegneria dell'Informazione

INDIRIZZO: Bioingegneria

CICLO XXIV

DIFFUSION TENSOR IMAGING AND FIBER TRACTOGRAPHY: NEW APPROACHES TO STUDY ALTERED MICROSTRUCTURE AND EVALUATION IN DIFFERENT PATHOLOGIES

Direttore della scuola: Ch.mo Prof. Matteo Bertocco

Supervisore: Prof. Alessandra Bertoldo

Dottorando: Letizia Squarcina

Contents

Sommario

L'imaging da tensore di diffusione (diffusion tensor imaging, DTI) è una tecnica di risonanza magnetica (magnetic resonance imaging, MRI) non invasiva, che permette di ottenere informazioni riguardanti la direzionalità della struttura microscopica del cervello. Il segnale di risonanza di diffusione, ottenuto dall'applicazione di gradienti magnetici in diverse direzioni, è infatti sensibile al movimento delle molecole di acqua all'interno di una struttura. Dal momento che il movimento di diffusione dell'acqua è di natura anisotropa all'interno della materia bianca cerebrale, una misura della sua variazione permette di stimare la direzionalità delle strutture, nello specifico fibre formate da insiemi di assoni, presenti al suo interno. Si rende possibile quindi localizzare le fibre di materia bianca che collegano diverse zone del cervello, tramite tecniche definite di trattografia, e derivare indici di quantificazione della diffusione, quali la sua intensità il grado di anisotropia nei tessuti cerebrali. In caso sia presente uno stato patologico, questo può essere evidenziato sia da una variazione dei diversi indici di diffusione, introdotti al capitolo 1, che da una anomala ricostruzione dei tratti cerebrali. Scopo di questa tesi è la valutazione di nuovi approcci per quantificare il danno ai tessuti cerebrali in diverse patologie.

In questa tesi, ai capitoli 1 e 2 , sarà data un'introduzione alle basi della tecnica di imaging DTI e al modello utilizzato per l'interpretazione dei dati. Inoltre, sarà data una panoramica dello stato dell'arte relativo a tale tecnica. Il metodo

più utilizzato per l'analisi di immagini DTI prevede l'assunzione di un modello monoesponenziale, da cui viene stimato un tensore di diffusione simmetrico tramite il fit dei dati misurati. Successivamente, da una scomposizione di tale tensore in autovettori e autovalori, vengono derivate quantità scalari dette indici di diffusione. Due degli indici più utilizzati sono la fractional anisotropy (FA) e la mean diffusivity (MD), che quantificano rispettivamente il grado di anisotropia e l'intensità della diffusione all'interno di un voxel. È stato dimostrato che tali indici sono sensibili ai cambiamenti patologici nella microstruttura dei tessuti.

Nel capitolo 3, vengono presentate le due maggiori categorie in cui possono venire suddivisi gli algoritmi di trattografia: trattografia deterministica e probabilistica. Gli algoritmi deterministici prevedono di ricostruire la direzione di un fascio di fibre connettendo voxel adiacenti, seguendo la direzione predominante della diffusione all'interno dei voxel stessi. Tale direzione viene definita dall'autovettore corrispondente all'autovalore maggiore, tra quelli in cui è stato scomposto il tensore. Gli algoritmi che seguono un approccio probabilistico, invece, considerano oltre ai dati misurati anche il rumore, che è caratteristica intrinseca dei dati DTI. Questi algoritmi forniscono come output una mappa dove ad ogni voxel corrisponde un grado di connettività del voxel stesso. Spesso tale valore rappresenta la probabilità di un dato voxel di essere connesso sia alla regione di interesse (ROI) da cui il procedimento di tracking è stato fatto partire, sia alla ROI dove il tratto termina. Nel capitolo 4 viene presentato lo stato dell'arte relativo alla trattografia.

Nel capitolo 5 vengono riportati i risultati ottenuti dall'applicazione di un nuovo algoritmo di trattografia deterministica a pazienti affetti da sclerosi multipla (multiple sclerosis, MS), al fine di studiare quantitativamente l'effetto della patologia nei tratti di materia bianca. Un approccio innovativo per la valutazione della connettività cerebrale viene definito nel capitolo 6, dove vi sono anche i

risultati della sua applicazione a immagini ottenute da pazienti affetti da traumi cerebrali (traumatic brain injuries, TBI). Tale approccio consiste nella creazione di un template di connessioni che dal talamo raggiungono diverse aree corticali, ottenendole dall'applicazione di un algoritmo di trattografia probabilistica a dati ottenuti da volontari sani. L'utilizzo di tale template in pazienti TBI ha permesso di valutare il danno alla materia bianca senza effettuare la stima dei tratti nei cervelli patologici, dove può essere critica a causa del danno cerebrale potenzialmente esteso. Inoltre, tale metodologia è completamente automatica e poco computazionalmente pesante, e non richiede alcuna conoscenza pregressa sul danno cerebrale subito dai pazienti.

Due metodologie per la valutazione della diffusione cerebrale di pazienti affetti da sclerosi multipla, schizofrenia e disturbo bipolare vengono descritte nel capitolo 7. Vengono considerate sia una metodologia che considera le caratteristiche di diffusione all'interno di determinate ROI patologiche, in rapporto a tessuto sano, sia una metodologia che considera l'intero volume cerebrale. Per i pazienti affetti da sclerosi multipla, è stata utilizzata una metodologia che prevede di comparare direttamente i valori di diffusione relativi a specifiche ROI, posizionate in aree patologiche di materia grigia, con i valori di diffusione della materia grigia sana. Si è visto che i valori di FA sono alterati nelle ROI patologiche, e che l'alterazione persiste nel tempo. Nei pazienti schizofrenici o affetti da disturbo bipolare è stato usato un metodo, la tract-based spatial statistics, che permette di considerare l'intero volume acquisito, al fine di identificare differenze nella diffusione rispetto ad individui sani.

Summary

Diffusion tensor imaging (DTI) is a non-invasive magnetic resonance imaging (MRI) technique that allows one to infer information about the directionality of brain microstructure. The DT signal, obtained from the application of magnetic gradients in different directions, is sensitive to the displacement of water molecules inside a structure. Since water diffuses in an anisotropic way inside the white matter of the brain, a measure of the water displacement gives an estimation of the directionality of the structures, as fibers of axons, present in said white matter. It is then possible to delineate the bundles of white matter that connect different parts of the brain, with tractography techniques, and to investigate the diffusion properties of brain tissues, as the grade of anisotropy or the magnitude of the diffusion itself. Pathology is reflected both in an abnormal fiber reconstruction and in variations in diffusion indexes, introduced in chapter 1. Aim of this work is to evaluate new approaches to quantify brain tissue damage in different pathologies.

In this thesis, in chapter 1 and 2, an overview on the basis of diffusion imaging and on the underlying model will be given, as well as a report of the state of the art literature on the topic. In order to characterize the anisotropy of diffusivity inside the white matter, the most widely used DTI analysis method requires to quantify a symmetric diffusion tensor matrix by linear regression and, successively, to derive, from the eigenvalues of the estimated tensor matrix, scalar quantities called

diffusion indexes. Fractional anisotropy (FA) and mean diffusivity (MD) are two of the main DTI indices which respectively quantify the degree of anisotropy and the intensity of diffusion inside a voxel. These indices have been shown to be sensitive to changes in the tissue microstructure.

In chapter 3, the two main typologies of tracking algorithms are presented. Two main approaches are used for brain fiber tracking: deterministic and probabilistic tractography. Deterministic tractography algorithms allow the reconstruction of fiber bundles directions, connecting adjacent voxels following the predominant diffusion direction, determined by the direction of the eigenvector of the tensor with the highest eigenvalue. Probabilistic tractography approaches take into account the noise that inherently affects DTI data, and give as an output a brain map where a value of connectivity is given for each voxel. This value often represents the probability of a given voxel to be connected to both the starting tract region of interest (ROI), called seed, and the ROI where the tract terminates. In chapter 4, a review of the literature regarding tractography is given.

In chapter 5, a novel deterministic tractography algorithm has been applied to multiple sclerosis (MS) patients, to study quantitatively the affected white matter bundles. A novel approach for the evaluation of brain connectivity based on a template of white matter fibers is described in chapter 6, and the results of its application on traumatic brain injury (TBI) patients are reported. This approach consists in creating a template of connections from the thalamus to the cortex, generating it from probabilistic tractography of healthy volunteers. Then, the template has been applied to TBI patients in order to assess the damage to the white matter, avoiding the direct application of tracking algorithm in damaged tissue, that can be critical. It also has the advantages to be less time-consuming than tractography and to be completely data-driven, so no prior knowledge of the TBI damage is required to evaluate the pathology.

Then in chapter 7, two methods for the study of the diffusion characteristics of the brain of multiple sclerosis, schizophrenia and bipolar disorder patients are delineated. The evaluation of disease is done both by considering known altered tissue regions of interest (ROIs) and utilizing completely data-driven methods. A ROI approach is utilized for the analysis of gray matter lesions in multiple sclerosis. It is shown that FA is altered in the presence of lesions, and that the alterations persist also if longitudinal studies are conducted. A whole-brain statistical method, known as tract-based spatial statistics, has been utilized to investigate changes in white matter tracts in psychiatric patients, specifically schizophrenia and bipolar disorder patients, in respect to healthy individuals.

Chapter 1

Diffusion Tensor Imaging: Theory and Applications

1.1 Introduction

The sensitivity of magnetic resonance techniques to water diffusion has been considered for the first time in 1950, with a research conducted by E. Hahn [1]. It was found that there is an attenuation of the measured signal, related to the diffusion of water inside the considered tissue. Later [2, 3], this propriety was exploited creating ad-hoc sequences that allow the quantification of water diffusion. This technique has been called diffusion tensor imaging. Given that the central nervous system (CNS) is characterized by organized structures, within which water diffuses following precise directions, diffusion tensor imaging has become a popular tool for the investigation of brain tissues characteristics. In 1990 Moseley [4] demonstrated that water diffusion is anisotropic in white matter and Le Bihan [5] showed that, assuming that the estimated direction of predominant diffusion coincides with the direction of white matter fibers, the directionality of diffusion inside the brain can be shown. After Pierpaoli and colleagues [6] evaluated quantitative indices that can depict the integrity of brain tissues, applications of DTI became widespread as a method to study brain structure and modifications due

to disease. Early applications of DTI included stroke [7], multiple sclerosis [8] and schizophrenia [9]. In the last years DTI applications increased, and diffusion analysis has become an important tool in research and in clinical practice, with applications that cover several neuropathology fields of research , from healthy brain structure, as in brain development and aging studies, to neuropsychological diseases as dementia to genetic disorders as Huntington disease [10]. This development has been made possible also by technical advancements, as the growth of intensity of MRI magnetic fields (from <1T, to 1.5T, to 3T and beyond) and the possibility of increasing the number of magnetic gradient available for DTI experiments (from 6, to 32, to 64 and, now, to hundreds).

1.2 Diffusion in water and in tissue

Diffusion is a physical process that consists in the random motion of molecules in a medium, driven by kinetic energy. It has been described initially according to Fick's first law, which states that, when there is a difference in concentration, molecules move creating a net flux from regions with high concentration towards regions with low concentration:

$$J = -D\nabla c, \tag{1.1}$$

where J is the net flux, c is the gradient of concentration and D the diffusion coefficient. D is dependent only on the dimension of the particle diffusing, the microstructure characteristics and the temperature of the medium, and it is described by the Stokes - Einstein equation:

$$D = \frac{RT}{N_A}\frac{1}{6\pi r\eta}, \tag{1.2}$$

where R is the ideal gas constant, N_A the Avogadro number, r the particle radius and η and T the viscosity and the temperature of the medium measured in Kelvin

respectively.

When there isn't any gradient in concentration, the net flux disappears, but molecules continue to move, maintaining a thermodynamic equilibrium. This phenomenon has been referred to as Brownian motion, and it's been described in a stochastic fashion. The movement of particles can be represented by a Gaussian displacement distribution, dependent from D; the probability for a molecule to have traveled a distance x in the time t is defined as:

$$p(x,t) = \frac{e^{-x^2/4Dt}}{\sqrt{4\pi Dt}}. \tag{1.3}$$

According to this, the mean square displacement during the time Δt is:

$$< x^2 >= 2\mathrm{D}\Delta\mathrm{t} \tag{1.4}$$

where Δt is the time during which the particle moves.

When there aren't boundaries for the motion of molecules, diffusion is free and it follows the model of random Brownian motion. In this case, the diffusion is called isotropic. When, on the other hand, the movement of particles is hindered by obstacles, diffusion will happen preferentially in the direction where there is no impediment, and the diffusion will be called anisotropic.

This is particularly important when the focus is posed, as in this thesis, in the diffusion of water within biological tissue. As a matter of fact, living tissues are composed of organized structures that guide the movement of water, which hence doesn't happen freely. Often these structures are not visible with conventional magnetic resonance techniques, because their dimensions are even magnitude of orders smaller than the resolution of a magnetic resonance image.

This is particularly important when the interest is in brain images. In fact, brain tissues are highly characterized by their diffusion properties, and white matter, gray matter and cerebro-spinal fluid (CSF), that are the three components of the

brain, can be differentiated based on the way water diffuses.

Neural tissue is formed of neurons, neural cells that have a body, from which dendrites depart, and an axon. Dendrites are branches that extend for a limited space from the body, along which the neural signal travels, towards said body. The axon is an elongated structure that can reach up to 1m in length (in the case of spinal cord neurons), with the purpose of connecting different neurons or regions. White matter is constituted of axons organized in fibers, where they are parallel one to another. Water diffuses more easily along the axons than perpendicularly to their axes. This is because in traveling perpendicularly to the axon, molecules encounter membranes, which are an obstacle to diffusion. Moreover, axons are covered with myelin, which is a substance that enhances the conductivity of electricity and modules the anisotropy of diffusion inside the white matter. Although the primary source of anisotropy of diffusion inside the brain is the high level of organization of structures and fibers, myelin has a non-negligible effect on water diffusion [11]. In the gray matter there are the bodies of the neurons, along with the dendrites, and glial cells. Here water diffuses without a preferential direction, and more freely and with more intensity than in white matter. CSF occupies, in a healthy brain, around 10% of the cerebral volume [12]. It's a fluid with characteristics that can be assimilated to water, hence there are no barriers to diffusion, that happens in a isotropic fashion and with high magnitude, compared to the rest of the brain.

Diffusion in tissues can be analyzed in vivo thanks to diffusion tensor imaging (DTI), whose basics will be explained in section 1.3. With this technique, it is possible to derive measures of diffusion in the tissues, as presented in section 1.4 and 1.5, that can then be used to investigate the health of the tissues and, as is of interest in this thesis, of the brain.

1.3 Measuring diffusion with diffusion tensor imaging

Magnetic resonance imaging (MRI) is based on the property of nuclei to have a spin, associated with a magnetic momentum, which causes them to align to an external static magnetic field. When such a field is applied, protons precess with a frequency given by the Larmor equation:

$$\upsilon = \gamma B, \tag{1.5}$$

where B is the magnitude of the external field and γ is a constant, called gyromagnetic ratio, which is intrinsic to the specific nucleus. If a second magnetic pulse, with the same frequency υ is applied, the magnetic momentum of protons rotate by an angle, called flip angle, specific for a definite MR sequence. When the magnetic pulse is turned off, protons tend to return to their equilibrium state within a period of time that is characteristic of the specific examined tissue. In this way, the spins induce a current in the receiver coil, which is the signal used to generate MR images. If the applied field suffers from inhomogeneities, as it is the case with real non-ideal MRI scanners, there are variations in the frequencies to wich the nuclei precess, which lead, over time, to loss of signal.

To avoid this problem, the spin-echo sequence is used, where protons are exited with a 90 degrees pulse, followed, after a time $T_E/2$ by a 180 degrees refocusing pulse, as first proposed by [1]. After the 180° pulse, the polarity of the protons is reversed, so that after a time equal to the time past before the refocusing pulse, the protons are in phase again, and no signal is lost due to spurious dephasing. After the time T_E an echo is detected by the receiver coils. A modification of this sequence is the basis for diffusion tensor imaging.

This behavior of protons to acquire a phase proportional to the applied external magnetic field can be used to detect diffusion in tissues, with DTI, that is acquired with the pulse sequence presented in [3]. It consists in applying linearly

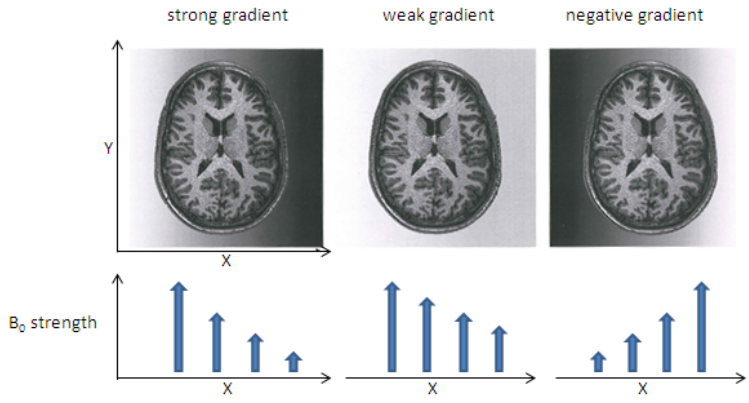

Figure 1.1: Graphical representation of a linearly modulated magnetic gradient applied along a direction. The shade represents the intensity of the gradient in a specific location.

modulated magnetic gradients, so that a particular location in space corresponds to a defined value of the applied field. A graphical representation of magnetic gradients is shown in figure 1.1

The magnetic field inside the MRI scanner is then

$$B = B_0 + G_x(x) + G_y(y) + G_z(z). \tag{1.6}$$

where the gradients are applied for the duration of the time $\delta < T_E/2$. After a time $\Delta t < T_E/2$, during which the refocusing 180° pulse has been applied, the same gradient is turned on again. A representation of this sequence is in figure 1.2.

If spins have not moved from their initial locations, the gradients have no effect and after the rephasing pulse the nuclei are in phase. If there is movement along the direction of the gradient, during the two diffusion-weighting gradients the nuclei are subject to fields of different intensities, and they will no longer be in phase after refocusing. In this case, the phase shift of each particle is proportional to the distance it covered. This causes an attenuation of the received signal S in respect to the signal measured with no weighting-diffusion gradients S_0, that follows, under the assumption that diffusion can be described by a Gaussian

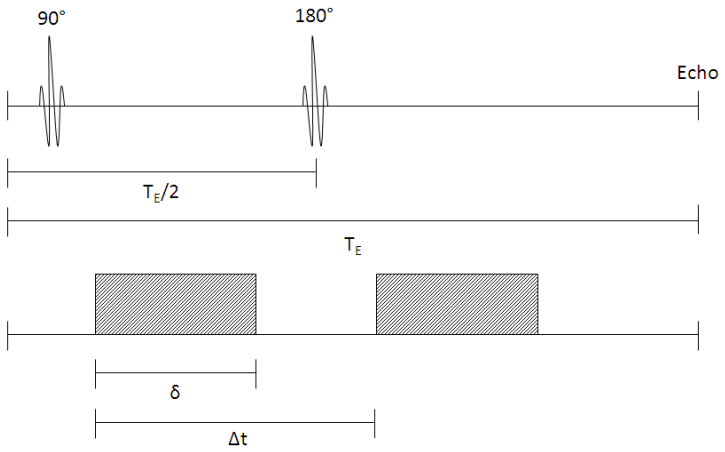

Figure 1.2: Diffusion tensor MR sequence. The two diffusion-weighting gradients have the same magnitude and the same duration δ. In this figure, only a direction has been considered for simplicity. Figure modified from [13].

function, the Stejskal - Tanner equation:

$$S = S_0 e^{-bD}, \tag{1.7}$$

where D is the diffusion coefficient and b depends on the sequence settings [14]. In the case of rectangular gradients, b is

$$b = (\gamma G \delta)^2 (\Delta t - \delta/3), \tag{1.8}$$

where Δt is the separation time between the two gradients and δ the time of application of gradients. The value of D measured in eq. 1.7 is relative only to the diffusion that take place along the direction of the application of the gradient. When diffusion is isotropic, the scalar D completely describes the process, but if the diffusion has different behavior depending on the observed direction, the information that can be extracted from just one measure is not enough to characterize the phenomenon. In tissues, because the diffusion is hindered by barriers, the estimated coefficient D is called apparent diffusion coefficient (ADC), since it appears to be lower than the coefficient in free water D [15]. Hence, to completely

describe diffusion that is not isotropic, measures along more than one direction are needed.

1.4 The diffusion tensor model

Anisotropic diffusion is modeled using the diffusion tensor. The tensor is a 3x3 matrix that takes into account the different diffusion in different directions, thus modeling diffusion in all three dimensions. The 1.7 then becomes

$$S = S_0 e^{-b\mathbf{g}^{\mathbf{T}}\mathbf{D}\mathbf{g}} \tag{1.9}$$

where $\mathbf{g}$ is the unit vector that represents the direction along which the gradient has been applied, and the diffusion coefficient D is replaced by the tensor $\mathbf{D}$:

$$\begin{pmatrix} D_{xx} & D_{xy} & D_{xz} \\ D_{yx} & D_{yy} & D_{yz} \\ D_{zx} & D_{zy} & D_{zz}. \end{pmatrix} \tag{1.10}$$

The elements D_{xx}, D_{yy} and D_{zz} are the apparent diffusion coefficients along the three axes, and the off-diagonal elements represent the correlation between these measures. Thus, the tensor $\mathbf{D}$ is a symmetric covariance matrix, defined by six independent parameters.

Equation 1.7 then becomes

$$\ln \frac{S}{S_0} = - \begin{pmatrix} \sqrt{b_x} & \sqrt{b_y} & \sqrt{b_z} \end{pmatrix} \begin{pmatrix} D_{xx} & D_{xy} & D_{xz} \\ D_{yx} & D_{yy} & D_{yz} \\ D_{zx} & D_{zy} & D_{zz} \end{pmatrix} \begin{pmatrix} \sqrt{b_x} \\ \sqrt{b_y} \\ \sqrt{b_z}, \end{pmatrix} \tag{1.11}$$

where b_x, b_y and b_z now contain information about the applied gradient direction. For the estimation of the six independent elements of $\mathbf{D}$, six acquisitions, each along one direction, are needed, and a single acquisition with no gradient applied S_0. For example, when a gradient is applied along the direction x, the 1.11,

combined with eq. 1.8 becomes

$$\ln \frac{S}{S_0} = -(\gamma\delta)^2 \begin{pmatrix} G_x & 0 & 0 \end{pmatrix} \begin{pmatrix} D_{xx} & D_{xy} & D_{xz} \\ D_{yx} & D_{yy} & D_{yz} \\ D_{zx} & D_{zy} & D_{zz} \end{pmatrix} \begin{pmatrix} G_x \\ 0 \\ 0 \end{pmatrix}, \tag{1.12}$$

then

$$S = S_0 e^{-(\gamma G_x \delta)^2 (\Delta t - \delta/3) D_{xx}}. \tag{1.13}$$

As can be seen, from the measurement along x it is possible to estimate the parameter D_{xx}. In the same way, the other parameters of $\mathbf{D}$ can be inferred from other six acquisition along independent directions.

Typically, in a DTI acquisition scheme, the number of directions along which diffusion is measured is much higher than six, that is the minimum, to mitigate noise effects. In this way, the system to be solved to estimate all the parameters becomes ovedetermined, and a process of fitting is then needed. If a magnetic gradient is applied along a generic direction, the eq. 1.11 becomes

$$\begin{aligned} \ln \frac{S_0}{S} = {} & D_{xx} b_x + D_{yy} b_y + D_{zz} b_z + 2D_{xy}\sqrt{b_x}\sqrt{b_y} + \\ & + 2D_{xz}\sqrt{b_x}\sqrt{b_z} + 2D_{yz}\sqrt{b_y}\sqrt{b_z}. \end{aligned} \tag{1.14}$$

that, if two vectors $\mathbf{b}$ and $\mathbf{D}$ are defined as follows:

$$\begin{aligned} \mathbf{b} &= \begin{pmatrix} b_x & b_y & b_z & \sqrt{b_x b_y} & \sqrt{b_x b_z} & \sqrt{b_y b_z} \end{pmatrix} \\ \mathbf{D} &= \begin{pmatrix} D_{xx} & D_{yy} & D_{zz} & 2D_{xy} & 2D_{xz} & 2D_{yz} \end{pmatrix}^T \end{aligned} \tag{1.15}$$

reduces to

$$\ln(\frac{S_0}{S}) = \mathbf{bD} \tag{1.16}$$

This is a linear equation that can be solved, in respect to D, with a linear least

square fitting process,where

$$\hat{\mathbf{D}} = \underset{\mathrm{D}}{\operatorname{argmin}} \left\| \ln\left(\frac{\mathrm{S}_0}{\mathrm{S}}\right) - \mathbf{bD} \right\|^2 \tag{1.17}$$

and

$$\hat{\mathbf{D}} = (\mathbf{B^T B})^{-1}\mathbf{B^T} \ln\left(\frac{S_0}{S}\right). \tag{1.18}$$

In this case, the data are fitted to the model without considering the noise. If it is taken into account, the data can be fitted with a weighted least squares method, where voxels weights are inversely proportional to the level of the noise that affects the data:

$$\hat{\mathbf{D}}_W = \left(\mathbf{B^T W B}\right)^{-1}\mathbf{B^T} \ln\left(\frac{S_0}{S}\right), \tag{1.19}$$

where $\mathbf{W}$ is a diagonal weighting matrix, whose values are proportional to the estimated noise.

1.5 DTI-derived indices

Once the tensor $\mathbf{D}$ is completely characterized, as shown in the previous section, it is possible to derive quantities that describe concisely the process of diffusion for every considered voxel. The tensor $\mathbf{D}$ can be diagonalized into its three eigenvectors $\mathbf{v_1}$, $\mathbf{v_2}$ and $\mathbf{v_3}$ and eigenvalues λ_1, λ_2 and λ_3, where λ_1 is the biggest eigenvalue and λ_3 the smallest one. $\mathbf{D}$ can be represented by an ellipsoid with axes of length λ_1, λ_2 and λ_3. It can be assimilated to a sphere, if the three eigenvalues have the same value, or it can assume a more elongated shape, when one of the eigenvalues is predominant. Moreover, it can assume intermediate shapes, depending on the relationships between the eigenvalues. A graphical example is provided in figure 1.3.

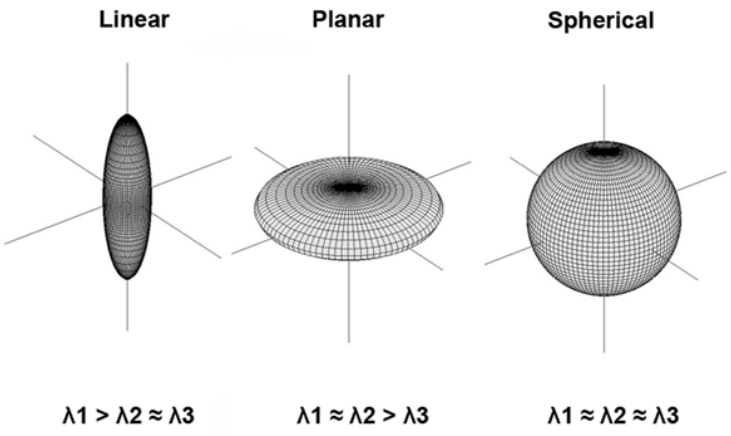

Figure 1.3: The diffusion ellipsoid can assume different shapes, according to the relationship between its axes. Figure modified from [16].

One of the most widely clinically used diffusion parameters is mean diffusivity, or average ADC. It is defined as proportional to the trace of the tensor, and can be defined as a directionally averaged diffusivity:

$$\text{MD} = \frac{\text{tr}(\mathbf{D})}{3} = \frac{D_{xx} + D_{yy} + D_{zz}}{3} = \frac{\lambda_1 + \lambda_2 + \lambda_3}{3} = \text{averageADC}. \tag{1.20}$$

MD gives a quantification of the magnitude of diffusion. The values of the tensor eigenvalues can be combined also to give anisotropy-related indices, like fractional anisotropy (FA) and relative anisotropy (RA): in fact, the information of the possible predominance of an eigenvalue - and associated eigenvector - on the others, gives the idea of how much the diffusion is, in a particular voxel, following a preferential direction. FA is defined [17] as the variance of the three eigenvalues, normalized for the general amplitude of diffusivity, and is described as follows:

$$\text{FA} = \sqrt{\frac{1}{2}} \frac{\sqrt{(\lambda_1 - \lambda_2)^2 + (\lambda_2 - \lambda_3)^2 + (\lambda_3 - \lambda_1)^2}}{\sqrt{\lambda_1^2 + \lambda_2^2 - \lambda_3^2}}. \tag{1.21}$$

FA describes the portion of the tensor which results from anisotropy, and gives a

measure of the directionality of diffusion. RA, that is defined as:

$$\text{RA} = \sqrt{\frac{1}{2}} \frac{\sqrt{(\lambda_1^2 - \lambda_2^2)^2 + (\lambda_2^2 - \lambda_3^2)^2 + (\lambda_3^2 - \lambda_2^2)^2}}{\lambda_1 + \lambda_2 + \lambda_3} \tag{1.22}$$

describes the ratio between anisotropic and anisotropic portion of the diffusion tensor. Another anisotropy index is volume ratio (VR), which is the ratio of the volume of the diffusion ellipsoid to the volume of a sphere with a radius equal to the mean of the eigenvalues:

$$\text{VR} = \frac{\lambda_1 \lambda_2 \lambda_3}{\left(\frac{(\lambda_1 + \lambda_2 + \lambda_3)}{3}\right)^3}. \tag{1.23}$$

These three indices range from 0 to 1, where in the case of FA and RA o indicates perfect isotropy and 1 perfect anisotropy (i.e. diffusion occurring along just one direction), and in the case of VR the interpretation of the values is the opposite.

Another two used measures are radial and axial diffusivity. Axial diffusivity is the amount of diffusion along the principal direction, λ_1, and radial diffusivity (RD) describes the amount of mean diffusion that occurs along the two minor axes of the diffusion ellipsoid:

$$\text{RD} = \frac{\lambda_2 + \lambda_3}{2}. \tag{1.24}$$

If the just introduced indices are calculated across the brain, in all voxels, maps of the brain isotropy can be derived. White and grey matter present a higher contrast in FA and RA images than in conventional MRI images, whereas MD presents less variability across the whole brain parenchyma. An example of said maps, for a subject, is shown in figure 1.4.

Maps can also be obtained of the three eigenvectors $\mathbf{v_1}$, $\mathbf{v_2}$ and $\mathbf{v_3}$: they will

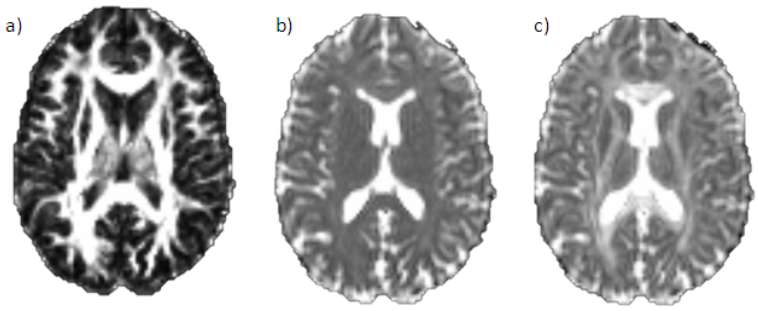

Figure 1.4: Diffusion indices maps for a subject, in the same slice: FA (a), MD (b) and AD (c). As can be seen, FA distinguishes between white and grey matter with a high contrast, which is lower in the MD image. Similar maps can be obtained for all other diffusion measures. Data taken with a 3T MRI scanner.

be composed of sets of three maps, representing $\mathbf{v}_{i,x}$, $\mathbf{v}_{i,y}$ and $\mathbf{v}_{i,z}$. If every direction is associated to a color, these maps can be viewed as a RGB image. It is a convention that red stands for left-right diffusion direction, green for the superior-inferior and blue for the anterior-posterior. The map of the first eigenvector is related to the underlying direction of diffusion in the tissue, as can be seen in figure 1.5.

The diffusion indices described in this section are reported concisely in table 1.1.

Index	Acronym	Formula	Range	Unit
Mean diffusivity	MD	$\frac{\lambda_1+\lambda_2+\lambda_3}{3}$	Not defined	m^2/s
Fractional anisotropy	FA	$\sqrt{\frac{1}{2}}\frac{\sqrt{(\lambda_1-\lambda_2)^2+(\lambda_2-\lambda_3)^2+(\lambda_3-\lambda_1)^2}}{\sqrt{\lambda_1^2+\lambda_2^2-\lambda_3^2}}$	$0 \div 1$	Dimensionless
Relative anisotropy	RA	$\sqrt{\frac{1}{2}}\frac{\sqrt{(\lambda_1^2-\lambda_2^2)^2+(\lambda_2^2-\lambda_3^2)^2+(\lambda_3^2-\lambda_2^2)^2}}{\lambda_1+\lambda_2+\lambda_3}$	$0 \div 1$	Dimensionless
Volume ratio	VR	$\frac{\lambda_1\lambda_2\lambda_3}{\left(\frac{(\lambda_1+\lambda_2+\lambda_3)}{3}\right)^3}$	$0 \div 1$	Dimensionless
Axial diffusivity	AD	λ_1	Not defined	m^2/s
Radial diffusivity	RA	$\frac{\lambda_2+\lambda_3}{2}$	Not defined	m^2/s

Table 1.1: The most used diffusion indices that can be estimated from the decomposition in eigenvectors and eigenvalues of the tensor $\mathbf{D}$.

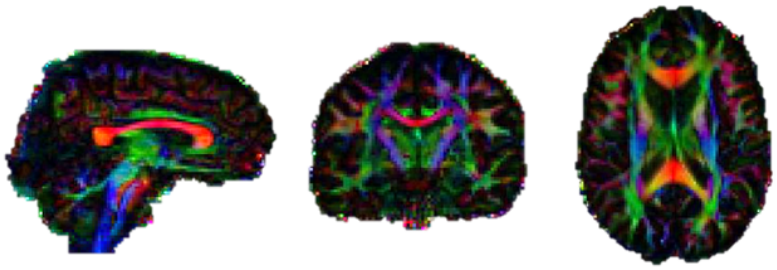

Figure 1.5: Color-coded map of the principal direction of diffusion. $\mathbf{v_1}$ map has been multiplied by FA, so that the voxels with a high level of anisotropy appear brighter. This gives more clarity to the color map. From the left: coronal, sagittal and horizontal view.

Clinical applications of diffusion metrics are reviewed in the next chapter.

1.6 Artifacts in DTI images

Noise is inherent to DTI data, and moreover DTI is obviously very sensitive to motion, since water motion is in fact the quantity that it is measured and estimated. The displacements that DTI measures are of the orders of micrometers: even a slight movement of the subject being scanned, also arising from respiration, blood flow, eye motion, or cardiac pulsation, would corrupt the data heavily [18, 19]. This is the main reason single-shot EPI sequences are used. These kind of sequences though are susceptible of other artifacts, as eddy currents. Eddy currents are distortion of the images caused by the changing magnetic field, that affect the different DTI volumes causing a misalignment of structures by means of shears, stretches, and translations. To reduce their effect, parallel imaging is adopted, and during postprocessing the images belonging to the different volumes are registered to reduce misalignments, as is done in FSL software (`www.fmrib.ox.ac.uk/fsl`). Another artifact that could affect DTI data is ghosting [20], caused by nsufficient or incorrect fat-suppression, that can be eliminated with the optimization of the acquisition scheme.

1.7 Beyond the tensor model

The tensor model has the advantage of being simple, but has the disadvantage of not allowing the identification of different fiber populations that can be present together in the same voxel. To overcome this drawback, several techniques have been proposed. One example is Diffusion Spectrum Imaging (DSI) [21]. With this technique, data are acquired in q-space (that is the space in which MRI data are measured, prior to being transformed into images by Fourier transform), which is sampled intensively (in the case of [21] 515 values of q-encoding were considered) and then the probability density function (PDF) of displacement $p(r)$ is obtained with the 3D Fourier transform of the signal modulus:

$$p\left(r\right) = \sum_{k=0}^{N-1} |S\left(q\right)| e^{-i2\pi \frac{r}{N} n}. \tag{1.25}$$

Then, the orientation density function (ODF), that represents the possible directions of diffusion, is estimated from the spectrum described above with an angular projection:

$$ODF(\mathbf{u}) = \int p\left(\rho \mathbf{u}\right) \rho^2 d\rho$$

where u is the 3D unit vector and $\rho^2 d\rho$ is the 3D volume element for which the integral is computed. The local maxima of the ODF are then used to define the direction of diffusion, and with a tracking algorithm fiber bundles can be reconstructed, as can be seen in figure 1.6.

Tuch and colleagues [22] proposed a method in which the sampling is done on a spherical shell in q-space in hundred of directions, that allows a reduction of acquisition time in respect to DSI. A mixture model that represents fibers populations is then applied to the data. This approach has been called high angular resolution diffusion imaging (HARDI). Later [23] a completely model-free method, q-ball imaging, that employs the Radon transform of the diffusion PDF, has been

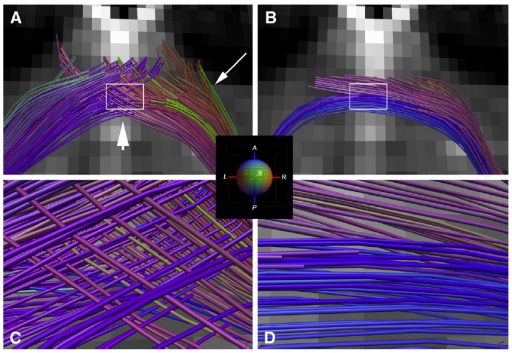

Figure 1.6: Figure from [21]. Reconstructed fiber using DSI (left) and applying DTI on the same data (right) in the optic chiasm of monkey. As can be seen, DSI succeeds in reconstructing crossing fibers better than DTI. A and B are magnified in C and D respectively. The small inset figure shows the color coding that is used for the depiction of the fibers, to which the colors corresponding to theirs endpoints have been assigned.

presented. The Radon transform of the PDF provides a good approximation of the ODF.

Other models for the estimation of diffusion data obtained from intensely sampled q-space employ multi-fiber models, in which the measured intensities are fitted to models that are the combination of different fibers populations, as in [24, 25], or the combination of different fibers populations and a compartment that accounts for extra-axonal diffusion [26].

These techniques are though not used in the clinical practice, because of the large amount of time that the acquisition takes and because their application are still mostly restricted to research. In clinical settings, the amount of available time is limited, and this is also the reason why the conventional tensor model is used in this thesis, since the focus is posed on the development of techniques that can be useful from a clinical point of view.

Chapter 2

Diffusion indices in healthy and pathological brain tissue

2.1 Evaluation of diffusion indices in healthy

As introduced in section 1.5, DTI-derived indices can be used to investigate the structure of the cerebral tissues. The most widely used diffusion indices are FA and MD, because they have been found to relate well with tissue diffusion changes and give a concise representation of diffusion characteristics. The values of FA and MD of a voxel or a region of interest (ROI), in fact, relate strictly to the functionality and the microstructure of the underlying brain tissues. An increase in water diffusion in white matter could reveal a deterioration of the axons, as well as changes in the fractional anisotropy. In example, a change in FA due to an increase of radial diffusivity could be a sign of degeneration of white matter fibers, when the diffusion occurs not only along the fibers but also perpendicularly to them. In gray matter, areas of increased FA or MD could also highlight structural damage. The detection of such changes can be of great importance in the evaluation of the brain health.

Before evaluating the alteration of diffusion indices in pathologic brains, it is es-

sential to understand what is their behaviour in healthy tissues, and which are the critical factors that need a careful evaluation.

In [17] it is found that, in healthy, diffusion parameters, especially MD, have a low variability across subjects. Therefore, a change in their values in patients, in respect to healthy volunteers, could be crucial in the evaluation of brain damage. Moreover, it the same work of Pierpaoli et al., it is shown that anisotropy indices vary inside the white matter, revealing that DTI measures reflect differences in the local architecture and microstructure. In particular, anisotropy measures are lower in the white matter of subcortical regions, and higher in the white matter of corpus callosum or in the pyramidal tract, that are directionally organized structures. Also in [27] it is demonstrated that different anisotropy values in white matter correspond to areas with different axonal organization. They showed that DTI anisotropy images allow the detection of highly myelinated structures, as the internal capsula or the optic radiation, not visible in conventional T1 or T2-weighted MRI images. Using anisotropy measures, also substructures of the thalamus and of the occipital white matter, which appear homogeneous with conventional imaging techniques, are clearly visible. It is also demonstrated that anisotropy values are consistent across different subjects, providing a basis for their use in the evaluation of diseased brains.

Inter-subject similarity of FA and MD values have also been demonstrated by Pfefferbaum et al. [28] to be high. In their work, FA and MD measurement with the same scanner, in different times, showed a mean percentage variability of respectively 1.9% and 2.6% between the different measures, across 10 healthy subjects. Although they found a bias when they compared diffusion indices obtained with different scanners, they demonstrated that FA and MD can be compared longitudinally and across subjects, using the same scanner, in a reliable fashion. They also provided typical diffusion values for healthy. Mean FA and

MD in the supratentorial brain (white matter, gray matter and CSF) was, in this study, respectively, around 0.2 (dimensionless) and $4.3 \times 10^{-4}\text{mm}^2/\text{s}$. When supratentorial white matter only was considered, the reported values were around 0.4 (dimensionless) and $4.3 \times 10^{-4}\text{mm}^2/\text{s}$ for FA and MD, whereas when they restricted the study to only a region of corpus callosum, characterized from a highly directional structure, the values they found were around 0.6 (dimensionless) and $4 \times 10^{-4}\text{mm}^2/\text{s}$.

Although it is certain that there is a variability across scanners, these values can be considered representative for healthy brains. When DTI data are used for tractography, a FA value that is generally accepted to indicate the transition from white to gray matter is 0.2 [29].

In [30], the effect of the field intensity (1.5 T and 3T) on the evaluation of diffusion parameters is evaluated. It is found that it affects the computation, confirming the previous finding that diffusion measurement taken with very different scanners are not comparable. In [31] it's shown that also the b-value can be an important factor that adds a bias in the computation of FA. These findings suggest that, in addition to external factors such as motion, noise and image registration, there are internal factors, i.e. field strength and b-values, that are to be kept in consideration when the reliability of a study is being evaluated. Nevertheless, in [32] typical FA and ADC values are reported for a healthy population, both at 1.5T and 3T. Those values are here reported in table 2.1.

As can be seen, in accordance with the initial findings of [17] and [27], FA values show a regional variability, with the highest values in the corpus callosum, whereas ADC shows less regional variations. The low inter-subject variability in diffusion indices found in all studies confirms that the values found in healthy can be used as a term of comparison when investigating the structure of damaged brain.

Typical applications of DTI in disease are, among others, in cerebral ischemia,

		1.5T (n=10)		3T (n=10)		
Region	FA or ADC	Mean	SD	Mean	SD	P value*
Basal pons	FA right	0.637	0.081	0.670	0.081	
	FA left	0.663	0.076	0.667	0.042	
	ADC right	0.746	0.039	0.730	0.065	
	ADC left	0.747	0.033	0.726	0.054	
Mesencephalon	FA right	0.791	0.041	0.825	0.038	0.019
	FA left	0.805	0.027	0.828	0.036	
	ADC right	0.760	0.054	0.737	0.061	
	ADC left	0.742	0.036	0.721	0.041	
Capsula interna	FA right	0.778	0.037	0.747	0.046	
	FA left	0.746	0.042	0.748	0.040	
	ADC right	0.681	0.017	0.699	0.026	0.044
	ADC left	0.672	0.020	0.682	0.034	
Corona radiata	FA right	0.520	0.040	0.483	0.043	0.02
	FA left	0.550	0.041	0.521	0.051	
	ADC right	0.643	0.028	0.659	0.028	
	ADC left	0.671	0.017	0.647	0.043	0.015
Centrum semiovale	FA right	0.539	0.062	0.502	0.064	
	FA left	0.567	0.067	0.493	0.065	0.004
	ADC right	0.668	0.035	0.703	0.036	0.01
	ADC left	0.676	0.028	0.709	0.040	0.022
CC genu	FA	0.853	0.040	0.838	0.030	
	ADC	0.756	0.070	0.758	0.044	
CC corpus	FA	0.665	0.080	0.669	0.057	
	ADC	0.858	0.079	0.850	0.116	
CC splenium	FA	0.868	0.050	0.862	0.050	
	ADC	0.684	0.054	0.711	0.033	

Table 2.1: Healthy regional mean FA and ADC values, measured at 1.5 and 3T. CC = corpus callosum. *Statistical difference between mean values for 1.5 T vs 3 T; values reported when $p<0.05$. Table from [32].

brain maturation, traumatic brain injury, multiple sclerosis, Alzheimer's disease and tumors [33]. DTI allows the assessment of the acute stage of ischemia even when conventional MRI doesn't show any changes [34]: in ischemic areas, ADC and FA show relevant changes in time in respect to healthy tissue, and also allow differentiating acute and chronic ischemic regions. Brain maturation can also be followed with DTI, because FA and ADC vary with age [35, 36]. ADC and FA, that at birth are respectively higher and lower than in adult brains, undergo substantial changes in the first 6 months after birth, related to decline in water content and progressive myelination, to reach adult values in a non-linear fashion. Aging has also been investigated with DTI, and it is been found i.e. in [37] that

ADC increases and FA decreases with age, especially in subjects older than 40 years and in densely packed areas as the corpus callosum. Decrease in FA have been found in Alzheimer's disease [38], related to progression of disease, and in [39] axonal degeneration in cognitive tracts has been documented. ADC maps can help in the differentiation of tumoral tissue in respect to healthy brain matter [40, 41], and changes in MD and FA have been demonstrated in the tissue around the tumors, especially gliomas.
Applications of DTI in multiple sclerosis, traumatic brain injuries, schizophrenia and bipolar disorder will be briefly covered in the next sections and more diffusely in the next chapters, as they are the pathologies that have been considered of interest in this thesis.

2.2 Evaluation of diffusion indices in pathological brains

2.2.1 Diffusion indices evaluation in multiple sclerosis

Multiple sclerosis (MS) is a chronic demyelinating disease that manifests itself with the presence of demyelinated plaques, or lesions, in the central nervous system (CNS). An example of how these lesions are visualized on MRI images is presented in figure 2.1. It is a major cause of disability in young individuals, and it presents in different phenotypes:

- relapsing-remitting multiple sclerosis (RRMS), which is characterized by episodes (relapses) when new symptoms appear, followed by periods of remission, that can be complete;

- secondary-progressive multiple sclerosis (SPMS), where the disease progresses steadily, with or without relapses, often occurring after RRMS;

- primary progressive multiple sclerosis (PPMS), defined by a progressive worsening of the disease, without relapses or remissions;

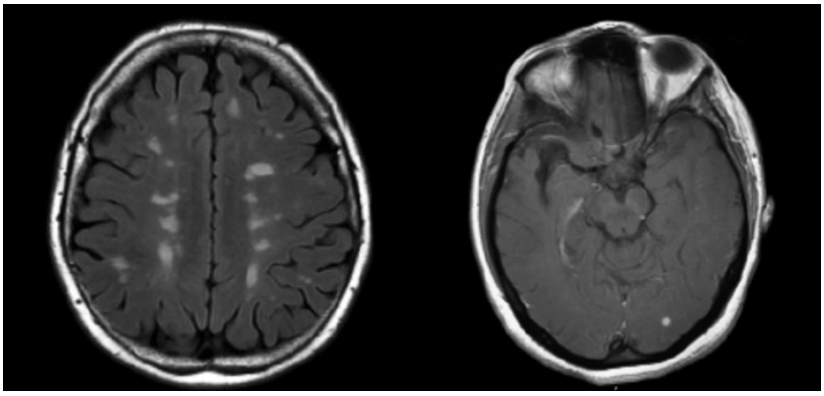

Figure 2.1: Figure from [42]: White matter MS lesions in a patient, identified on a coupled T1-FLAIR-DTI image acquired at 3T. Lesions are visible as hyperintense spots and well identifiable.

- progressive relapsing multiple sclerosis (PRMS), where a steady progression of the disease is coupled with superimposed relapses, without complete remissions;

Lesions are characterized by a phase during which they are active and inflammatory processes occur, followed by a chronic phase, in which they become formed by scar tissue (sclerosis). Symptoms vary greatly, from mild numbness to paralysis. Gravity of disease is graded according to the expanded disability status scale (EDSS) [43], that quantifies the disability using 10 different classes. The progression of the disease and the specific symptoms are unpredictable, but can be managed through medication. Causes of MS are, to date, unknown, even if the major theories comprehend autoimmune, environmental, infectious and genetic etiology.

DTI is a well-established method for the evaluation of multiple sclerosis brain matter. MS studies have been focused mostly on the differentiation of white matter MS lesions from healthy tissue and on the characterization of the diffusion properties of white matter of patients in respect to healthy. In example, in [44] it is shown that diffusivity is increased in multiple sclerosis white matter lesions, thus demonstrating a microstructural damage in the integrity of the tis-

sue. Also fractional anisotropy is abnormal in demyelinating lesions, and some damage is detectable also in normal-appearing white matter (NAWM), as shown e.g. in [45, 46, 47, 48, 49]. In particular, FA is lower in lesions than in NAWM, and lower here than in white matter of healthy individuals. For MD, the opposite is true: it is higher in plaques than in NAWM, and higher in NAWM than in healthy white matter. FA and MD allow also the differentiation between types of lesion, since their values are more far from healthy mean values when the white matter considered regions are more disrupted. Recently, the same findings for lesions and NAWM have been confirmed using 3T DTI-MRI [42] and also in pediatric patients [50, 51]. Even if DTI in MS lesions allows the determination of architectural damage in MS white matter, it does not differentiate if the damage is permanent, i.e. due to axonal loss, or transient, i.e. due to edema or demyelination followed by remyelination [52]. DTI indices can though determine if lesions are active or inactive, and differentiate between different types of lesions, based on the extent of deterioration of white matter. Also whole-brain analysis has been used to investigate white matter differences between patients and healthy individuals, and for example in [53, 54, 55], widespread damage has been found in terms of altered diffusion indices.

Also gray matter has been investigated using DTI, although less extensively. Some studies, e.g. [56, 57, 58] found an increased MD in normal appearing gray matter (NAGM) of patients when compared to healthy controls, and that there is some differentiation using diffusion indices on the basis of the MS phenotype. DTI has also been shown to be sensitive to variations over short periods of time [59, 60] in NAGM. In [61] a change in cortical gray matter of patients has been detected, in term of higher MD and reduced FA, in specific areas, that suggest that microstructural destruction due to inflammation and demyelination is present also in gray matter. Gray matter lesions are less investigated with DTI, but for example in [62] FA is found to be increased, probably due to microglial activation. The work of this thesis regarding MS brain diffusivity focuses on gray

matter lesions, and is described in chapter 7

Even if there is some modest correlation between DTI measures values and clinical findings, the interpretation of this kind of results is not straightforward, especially when dealing with MS-related disability or with the possibility of a prediction of the progression of the disease.

2.2.2 Diffusion indices evaluation in traumatic brain injury

Traumatic brain injury (TBI) is the commonest cause of death and disability in the under 40s [63]. It can be defined as damage to the brain provoked by a sudden trauma, as a collision with an object or a penetration of a sharp object into the brain tissues. It mostly occurs in traffic-related accidents, falls and assaults. Injuries are classified on the basis of their severity [64] into three categories: possible, mild and severe TBI. This system of classification integrates the duration of loss of consciousness, length of post-traumatic amnesia, lowest recorded Glasgow Coma Scale in the first 24 hours, and initial neuroimaging results.

TBI has a strong impact on patients and society, as patients who survive are often left with long-lasting disability, often the result of cognitive and neuropsychiatric problems [65], which include memory, language, social and sensory difficulties. Head injury can result in diffuse traumatic axonal injury (DAI) (often called also traumatic axonal injury (TAI), which is scattered damage to the axons in the brain tissue [66] and usually associated to TBI shearing injuries, induced by acceleration or deceleration [67]. These forces provoke the tissue to slide and the axons to stretch, that causes the axons cytoskeleton to break and subsequential possible neuron death. Detection of this type of damage is difficult and can only be diagnosed definitively postmortem, but DTI shows promising results in the evaluation of the microscopic integrity of the TAI-affected white matter. TAI is found to be a key pathological factor in the development of TBI-related problems [68, 69, 70, 71, 72].

DTI has been demonstrated to be useful for the characterization of TBI-related brain deterioration: in example, in [73] two patients with severe head injury, and no abnormalities on conventional MRI, were studied. Altered MD and, to a lesser extent, FA were found in both cases in specific regions, probably due to TAI and axonal loss or fiber disorganization. A reduction in FA and a reduction in the intensity of the dominant eigenvector of the tensor was found in several ROIs in [74], where 5 patients were investigated shortly after the injury. Also in this case, no damage was visible in tomography images, nor in conventional MR images. The same result has been confirmed in e.g. [69] for 46 mild TBI patients. In all studies, altered ROIs were found especially in the corpus callosum and in the internal capsula. At group level, Nakayama et al. [75, 76] found that taking into account the whole white matter and doing a voxel-based analysis, i.e. a statistic comparison for every voxel considered, it is possible to detect FA reduction and a MD growth in areas of the corpus callosum, internal capsula and some subcortical areas, confirming the previous ROI-based results. An example from [76] is reported in figure 2.2.
In [77] mean FA of the whole white matter is found to correlate with TBI severity, and recently in [78] FA values in the corpus callosum and in frontal white matter have been related with cognitive measures.

2.2.3 Diffusion indices evaluation in schizophrenia and bipolar disorder

Bipolar disorder and schizophrenia are two major psychiatric diseases. Bipolar disorder manifests itself with violent shifts in mood, i.e. episodes of mania (characterized by extreme euphoria and hyperactivity, often with delusional symptoms) and of depression, with variable duration. Between episodes, patients can experience periods without any symptoms. Schizophrenia symptoms include hallucinations, delusions, movement disorders and cognitive abnormalities, especially

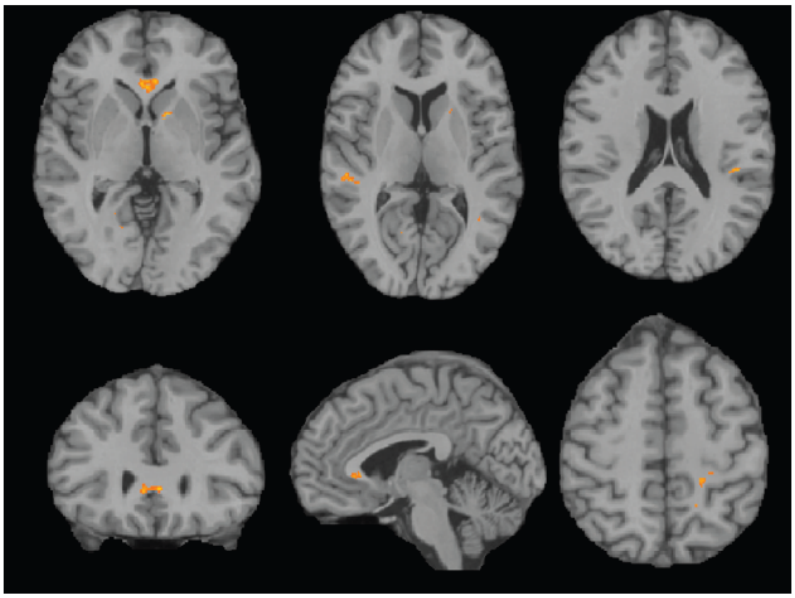

Figure 2.2: Image from [76]. Reduced FA is found in mild TBI patients in multiple white matter clusters bilaterally.

involving executive function and working memory. Both diseases are debilitating for the affected individuals, and have a certain degree of overlap in symptoms.

In the last years, DTI has been used in bipolar disorder, revealing white matter abnormalities especially in prefrontal, parietal, temporal and occipital lobes, internal capsule, uncinate fasciculus, superior longitudinal fasciculus and corpus callosum [79]. With a ROI-based study, in [80] reduced FA was found in the proximity of corpus callosum, and the same result was confirmed by Wang et al [81], both with a ROI-based analysis and with a voxel-based approach, as can be seen in figure 2.3. In [82] reduced FA and high MD were found in temporal and occipital white matter areas, using a voxel-based approach. Abnormalities in FA were found also widespread across white matter tracts i.e. in [83], that have been confirmed when considering tracts belonging to the emotional network [84]. In some cases, elevated FA was found in particular white matter areas, as a part of corpus callosum or left uncinate fasciculus or optic radiation [85, 86]. All

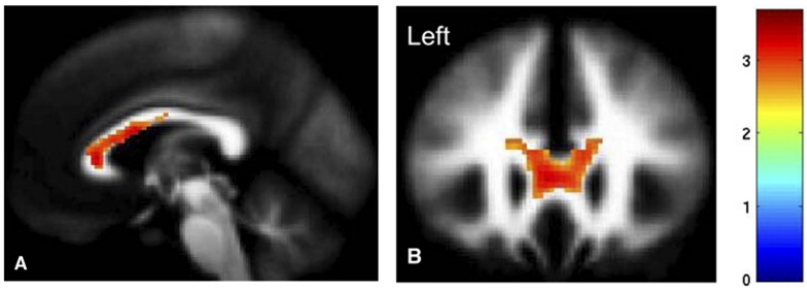

(a) Cluster of voxels with reduced FA found in corpus callosum with a voxel-based analysis.

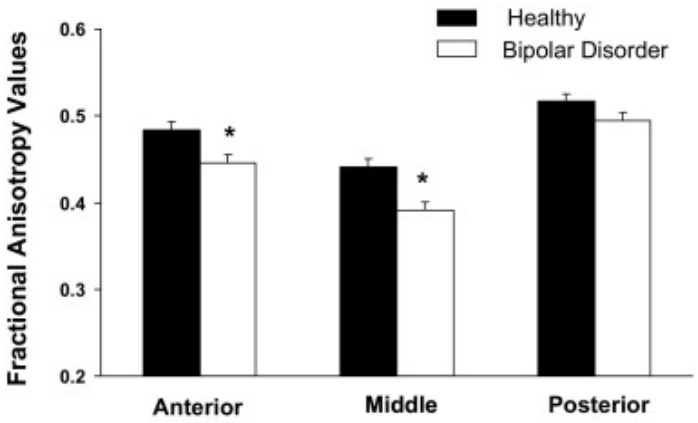

(b) FA values histograms of three ROIs placed in the corpus callosum: anterior, middle and posterior corpus callosum. In all three ROIs, patients show reduced FA, which is statistically relevant for anterior and middle corpus callosum

Figure 2.3: Figures modified from [81]: reduced FA is found in corpus callosum for bipolar disorder patients both using a voxel-based approach (a) and a ROI-based approach (b).

these findings point towards microstructural changes that redefine directionality of fiber, either reducing diagonal fibers and increasing FA [86] or disrupting white matter structure, in the case of reduced FA.

In the case of schizophrenia, DTI studies focus on finding differences in the brain connections in respect to healthy, in particular in cortico-cortical connectivity [87]. Studies have been conducted both using ROI approaches and considering the whole brain using voxel-based analysis. With the first approach, difference between patients and healthy were found, particularly regarding reduced anisotropy and higher diffusivity in the corpus callosum e.g. in [88]. Reduced anisotropy

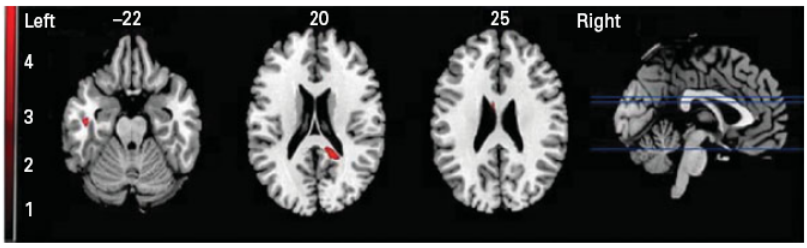

Figure 2.4: Figure from [94]. Using a voxel-based method, reduced FA was found for patients suffering from schizophrenia in corpus callosum, and in the temporal white matter.

was also found in the cingulate fasciculus (a white matter bundle connecting the cingulate gyrus to the middle temporal cortex), that could be related to lack of executive function ([89, 90]). A decrease in FA is also found in the middle pedunculus (that connect the pons, a structure belonging to the brain stem, to the cerebellum) in e.g. [91] and in internal capsula [92]. Differences in FA were found both in anterior and posterior white matter regions [93]. Conducting a whole-brain analysis, a disruption in white matter integrity was found for patients suffering from schizophrenia. In example in [94], reduced FA was found in small clusters in corpus callosum and in the left temporal lobe white matter, as reported in figure 2.4, and in right anterior cingulum in [95].

Chapter 3

Diffusion Tensor Tractography: Structural Connectivity

3.1 Structural connectivity measured with DTI

Different areas of the brain are connected by neural axons that bundle together in fibers, also called tracts. These bundles also carry the information, in form of electric impulses, and are surrounded by myelin, that acts as insulator. The vast majority of white matter fibers connect areas that are near, thus are particularly short [96]. Long fibers can connect the two hemispheres of the brain, passing through the corpus callosum, that is a thick bundles of nerve fibers, and connecting symmetric areas of the brain. DTI tractography is the first non-invasive method to detect white matter tracts in vivo, whereas before the advent of this technology only invasive studies using tracers (in animals) or post-mortem dissection studies were possible.

Methods to investigate structural connectivity can be divided into two main techniques: deterministic tractography, that will be presented in section 3.2, and probabilistic tractography, that will be discussed in section 3.3.

3.2 Deterministic Tractography

Deterministic tractography algorithms have the aim of forming lines (called streamlines) that follow the path of a specific white matter tract from a starting brain area to other areas connected by neural fibers. The underlying principle is the strong assumption that the principal direction of the estimated diffusion tensor coincides with the direction of the underlying fiber. One of the first approaches has been described by Mori et al [29]: this method, called fiber-assignment by continuous tracking (FACT), gives as an output a three-dimensional trajectory that follows white matter tracts. The trajectory starts in the middle of a seed voxel, follows the principal direction of that voxel and, at the boundary with an adjacent one, it changes direction to the principal eigenvector of the diffusion tensor estimated for the new voxel. The tensor is computed for every voxel and there considered constant. The tracking is then done in a continuous two-dimensional space: this allows the voxels to be intersected at any given point in the boundary. This avoid gross deviations from the fiber's real trajectory, as happens if tracking space is considered discrete (i.e. if the tract trajectory comprehends a whole voxel). This concept is illustrated graphically in figure 3.1. The termination of the tract is done when the change in direction exceeds a threshold, which is evaluated by the following coefficient:

$$R = \sum_{i=0}^{s} \sum_{j=0}^{s} \frac{\left| \mathbf{v}_{1i} \cdot \mathbf{v}_{1j} \right|}{s(s-1)}, \tag{3.1}$$

where $\mathbf{v_{1i}}$ represents the principal eigenvector of the diffusion tensor $\mathbf{D}$ at the i-th voxel, and s the number of nearby data point considered. Being this coefficient the sum of the inner products of the considered vectors, if these are aligned, R has high values. If the diffusion direction becomes unsure, the directions of the principal eigenvectors are different for adjacent voxels, and the value of R drops. In [29] fiber reconstruction is stopped when $R < 0.8$.

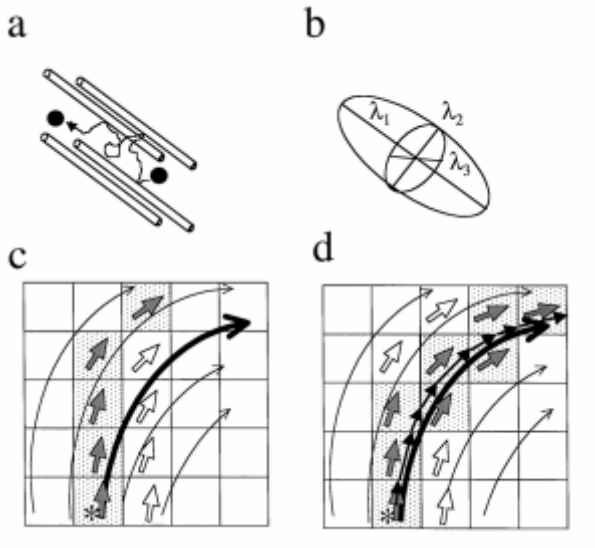

Figure 3.1: Figure from [29]. a) schematic representation of the structure underlying a voxel, where water diffuses in an anisotropic fashion; b) diffusion tensor reconstructed from the diffusion in a); c) tracking of the white matter fiber represented in a) using the principal eigenvector estimated in b) considering a discrete 2D space; d) tractography of the same fiber using a continuous 2D space. It can be seen how the trajectory deviates from the true trajectory when a discrete field is considered, and how this is minimized when using a continuous vector field.The true fiber trajectory is depicted with the bolded line, and the reconstructed trajectory is formed by the shaded voxels. The depiction is here simplified to a 2D tract reconstruction, for simplicity. It can be seen how the trajectory deviates from the true trajectory when a discrete field is considered, and how this is minimized when using a continuous tracking space.

The fiber trajectory can be described as a 3D curve, its evolution can be described by the Frenet equation [97]:

$$\frac{d\mathbf{r}(s)}{ds} = \mathbf{t}(s), \tag{3.2}$$

where $\mathbf{r}$ is said 3D trajectory, s is the arc length and $\mathbf{t}(s)$ is the tangent vector to $\mathbf{r}(s)$ at the point s. As stated earlier, the assumption that is made is that the principal fiber of the estimated tensor $\mathbf{D}$ is parallel to the white matter tract direction. An important difference with the approach earlier described and presented in [29] is that $\mathbf{D}$ is now calculated at every considered point, in a continuous field. Thus, the eigenvector and eigenvalues are not just calculated for every voxel, but the tensor field is interpolated and they are calculated at

every needed point. This considered, the eq. 3.2 becomes

$$\frac{d\mathbf{r}(s)}{ds} = \mathbf{t}(s) = \mathbf{v}_1(\mathbf{r}(s)), \tag{3.3}$$

where $\mathbf{v}_1(\mathbf{r}(s))$ is the principal eigenvector calculated in the position $\mathbf{r}(s)$. A graphical interpretation of this concept is given in figure 3.2. The differential equation system in eq. 3.3 can then be solved using the initial condition $\mathbf{r}_0$:

$$\mathbf{r}(0) = \mathbf{r}_0. \tag{3.4}$$

Eq. 3.3 can be solved numerically using 3.4, using Euler or Runge-Kutta methods, described in the next sections. A tract is terminated if:

1. it reaches the end of the brain
2. it crosses a region with low anisotropy, so that the diffusion direction is too undetermined
3. the angle of the fiber trajectory exceeds a given threshold.

The angle between two tracking steps i and $i+1$ is computed as

$$\theta = \arccos\left(\mathbf{v}_{1i} \cdot \mathbf{v}_{1(i+1)}\right) \tag{3.5}$$

and the tract is terminated based on its value on the assumption that white matter bundles follow smooth trajectories [98].

Lazar et al in [99] proposed an alternative approach, called tensor deflection (TD), for tracking white matter fibers using DTI data. With this technique, the whole information contained in the tensor $\mathbf{D}$ is used instead of just considering the first eigenvector. At the i-th step, the new direction of the trajectory, $\mathbf{v}_{out}^{i}$, is obtained by multiplying the direction $\mathbf{v}_{in}^{(i-1)}$ of the tract at the previous step by the tensor $\mathbf{D}$ at the current point:

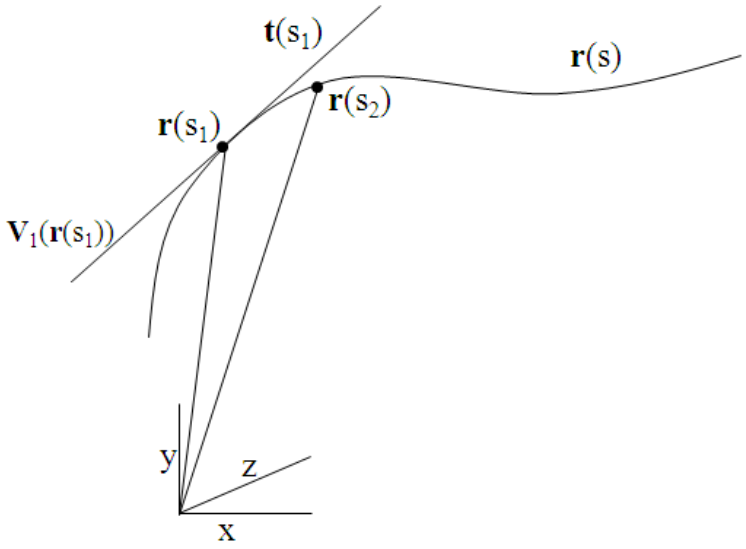

Figure 3.2: Figure modified from [97]. $\mathbf{r}(s)$ is the 3D curve representing a white matter fibre trajectory. The tangent $\mathbf{t}(s_1)$ to $\mathbf{r}(s)$ at s_1 equals the vector $\mathbf{v}_1(\mathbf{r}(s))$, which is the principal eigenvector of the tensor $\mathbf{D}$ calculated at $\mathbf{r}(s_1)$.

$$\mathbf{v}_{out}^{i} = \mathbf{D} \cdot \mathbf{v}_{in}^{(i-1)}, \tag{3.6}$$

The vector $\mathbf{v}_{in}^{(i-1)}$ can be described as a linear combination of the three eigenvalues of $\mathbf{D}$, as $\mathbf{v}_{in}^{(i-1)} = \alpha_1\mathbf{v}_1^i + \alpha_2\mathbf{v}_2^i + \alpha_3\mathbf{v}_3^i$, thus the eq. 3.6 becomes

$$\mathbf{v}_{out}^{i} = \lambda_1\alpha_1\mathbf{v}_1^i + \lambda_2\alpha_2\mathbf{v}_2^i + \lambda_3\alpha_3\mathbf{v}_3^i = \lambda_1\left(\alpha_1\mathbf{v}_1^i + \frac{\lambda_2}{\lambda_1}\alpha_2\mathbf{v}_2^i + \frac{\lambda_3}{\lambda_1}\alpha_3\mathbf{v}_3^i\right). \tag{3.7}$$

If $\mathbf{v}_{in}^{(i-1)}$ has the same direction as the first eigenvector $\mathbf{v}_1^i$, the outgoing direction will coincide with the incoming direction. If $\mathbf{v}_{in}^{(i-1)} \neq \mathbf{v}_1^i$ the tract trajectory deviates, and the amount of deviation is weighted according to the predominance of the first eigenvalues on the others, i.e. by the anisotropy of the tensor, as illustrated in figure 3.3.

In fact, if $\lambda_1 >> \lambda_2$ and λ_3, $\mathbf{v}_{out}^{i}$ will be deviated towards $\mathbf{v}_1^i$, of an amount that depends on the weights α_1, α_2 and α_3 of $\mathbf{v}_{in}^{(i-1)}$. If α_1 is very small compared to α_2 and α_3, the amount of deviation from $\mathbf{v}_{in}^{(i-1)}$ will be negligible even if the

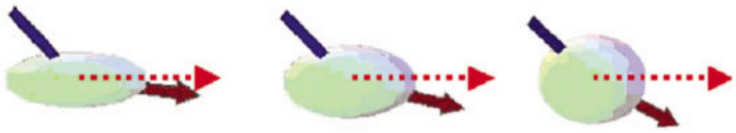

Figure 3.3: Figure from [99]. In the tensor deflection approach, the direction of a reconstructed fiber will be deviated from the incoming direction $\mathbf{v}_{in}$ of an amount that depends not only on the intensity of the principal eigenvector $\mathbf{v}_1$ but also on the shape of the tensor $\mathbf{D}$.

tensor has a very elongated shape. In the extreme case, i.e. $\mathbf{v}_{in}^{(i-1)}$ perpendicular to $\mathbf{v}_1^i$, the trajectory of the reconstructed tract won't be deviated. If the tensor is completely isotropic, the direction won't be deviated as well.

This behavior makes the method less sensitive to noise in respect to the FACT algorithm. Noise inherently affects DTI data and results in higher uncertainty in the process of fitting the tensor to the data. Since in this approach the deviation of the tract is weighted by the shape of the tensor, thus by the certainty of the predominance of one direction, the effect of the noise is mitigated, with the result of producing better results in areas of low anisotropy, in respect to the FACT algorithm [99]. This characteristic of the tensor deflection method can also bring to underestimation of the real curvature of the tract, in curved pathways.

3.2.1 Trajectory estimation with Euler's method

Euler's method allows the numerical solution of differential equations. In this case, the equation to be solved is eq. 3.3, coupled with the initial condition 3.4. Although the tensor field is considered continuous, the numerical solving needs a discretization of the domain of the function, so that the space of possible values of the independent variable becomes $S = \left\{ s_0, s_1, s_2, ... \quad s_n \right\}$. The numerical solution to the 3.3 then is found using a first order Taylor series expansion, considering two near points s_0 and s_1, where

$$\mathbf{r}(s_1) = \mathbf{r}(s_0) + \mathbf{r}^{'}(s_0)(s_1 - s_0). \tag{3.8}$$

Since the tangent to $\mathbf{r}(s)$ at s_0 is assumed to be parallel to $\mathbf{v}_1(\mathbf{r}(s))$, the 3.8 becomes

$$\mathbf{r}(s_1) = \mathbf{r}(s_0) + h\mathbf{v}_1(\mathbf{r}(s_0)), \tag{3.9}$$

once the integration step h has been chosen, usually smaller than a half voxel, so that $\mathbf{r}^{'}(s_0)(s_1 - s_0) \approx h\mathbf{v_1}(\mathbf{r}(s_0))$.

The trajectory of the tract is then given by the solution to the equations

$$\begin{aligned} \mathbf{r}(s_1) &= \mathbf{r}(s_0) + h\mathbf{v_1} \cdot (\mathbf{r}(s_0)) \\ \mathbf{r}(s_2) &= \mathbf{r}(s_1) + h\mathbf{v_1} \cdot (\mathbf{r}(s_1)) \\ &... \\ \mathbf{r}(s_{n+1}) &= \mathbf{r}(s_n) + h\mathbf{v_1} \cdot (\mathbf{r}(s_n)) \end{aligned} \tag{3.10}$$

that will give an approximate solution to the differential equation 3.3.

3.2.2 Trajectory estimation with Runge-Kutta method

Euler's method is easy to implement but since it takes into account only the first order, it could cause accumulation of errors along the tract propagation [97], of the order of $O(h^2)$. Moreover, it is sensitive to noise, that could cause propagation of errors and, in the considered case of tractography, erroneous estimation of the tracts trajectories. A more reliable solution is to adopt the fourth-order Runge-Kutta method, after the same steps of discretization and choice of h adopted in Euler's method:

$$\mathbf{r}(s_{n+1}) = \mathbf{r}(s_n) + \frac{h}{6}(k_1 + 2k_2 + 2k_3 + k_4), \tag{3.11}$$

where

$$\begin{aligned} k_1 &= \mathbf{v_1}(\mathbf{r}(s_n)) \\ k_2 &= \mathbf{v_1}\left(\mathbf{r}\left(s_n + \tfrac{h}{2}k_1\right)\right) \\ k_3 &= \mathbf{v_1}\left(\mathbf{r}\left(s_n + \tfrac{h}{2}k_2\right)\right) \\ k_4 &= \mathbf{v_1}\left(\mathbf{r}\left(s_n + hk_3\right)\right) \end{aligned} . \tag{3.12}$$

This method is however much more demanding computationally. It can be noted that the first step, that involves the computation of k_1, is in fact equivalent to the first-order approximation computed with Euler's method.

3.3 Probabilistic Tractography

As anticipated in section 3.1, tractography methods can be divided into two categories, deterministic and probabilistic algorithms. While the deterministic approaches described in the previous section only take into account the measured data, probabilistic algorithms also give a representation of the noise that corrupts DTI data, thus of the uncertainty that inherently affect the fiber direction estimation.

Jones and colleagues in [100] visualized this uncertainty as cones, estimated using the bootstrap technique. For every voxel, 1000 estimates of the first eigenvector $\mathbf{v}_1$ are estimated. This is obtained by linear fitting of the data to the tensor as shown in chapter 1, where the data are obtained drawing a sample, with replacement, from the acquired data. The angle between the i-th estimate of $\mathbf{v}_1$, ${\mathbf{v}_1}^i$, and the average principal eigenvector $\bar{v}_1$ is computed as

$$\theta_i = \arccos(\mathbf{v}_1^i \cdot \bar{\mathbf{v}}_1). \tag{3.13}$$

where $\bar{\mathbf{v}}_1$ is the mean principal eigenvector of all the bootstrap estimates.
To visualize the uncertainty estimated using this technique, for each voxel a cone is constructed, with an angle corresponding to the 95th percentile, computed

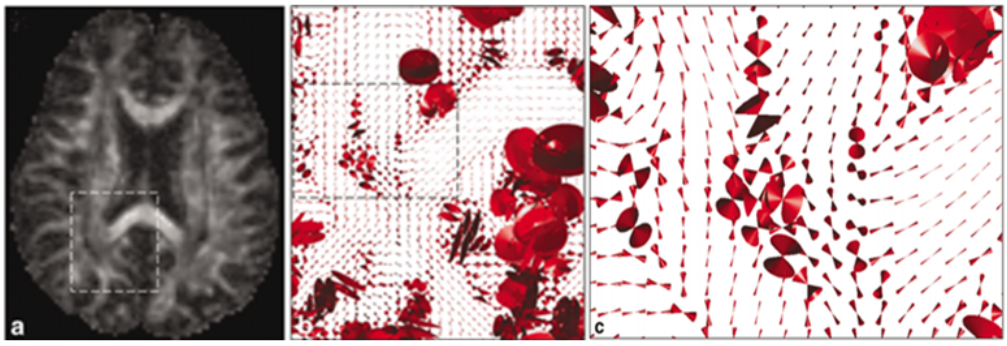

Figure 3.4: Figure from [100]. a) FA map for the considered healthy subject; b) cones on uncertainty of the direction of the diffusion for the region highlighted in a); c) the same region with further enlargement. As can be noted, the shape of the cones is more spread when the FA is lower, while it is narrower where the uncertainty in the fiber direction is negligible, as in the corpus callosum.

using all the bootstrap estimations. The major axis of the cone corresponds to $\bar{v}_1$, and the cone is then oriented in both the possible directions, since the vectors estimated from DTI data are not oriented. As can be seen in figure 3.4, the precision of the estimates is higher in areas with high anisotropy, as the corpus callosum, and drops in area with low anisotropy, as gray matter, regions of crossing fibers and CSF. It is to be noted that aim of this method is not to follow fiber trajectories, but to estimate the uncertainty related to the estimation of said trajectories.

Also in [101] the uncertainty in the diffusion direction is depicted as directional uncertainty. Here, it is estimated using a Monte-Carlo approach, where a modified principal eigenvector, $\mathbf{v}_{1,mod}$ is estimated, at the location x, as $\mathbf{v}_{1,\,\mathrm{mod}}\,(x,n) = \mathbf{v}_1(x) + \delta\mathbf{v}_1(x,n)$, where n refers to the n-th iteration of the Monte-Carlo process. $\delta\mathbf{v}_1$ is estimated from the PDF of possible fiber orientations: the spread of the distribution from which the principal vector direction is drawn is related to the fractional anisotropy of the tensor or to the relative weight of the two minor eigenvalues, in both cases weighted by a sigmoidal function, depicted for FA in figure 3.5. In this way, for example, voxel with low FA are characterized by high

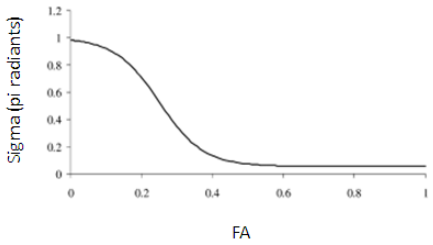

Figure 3.5: Figure from [101]. Sigmodal function for the estimation of $\delta\mathbf{v}_1$

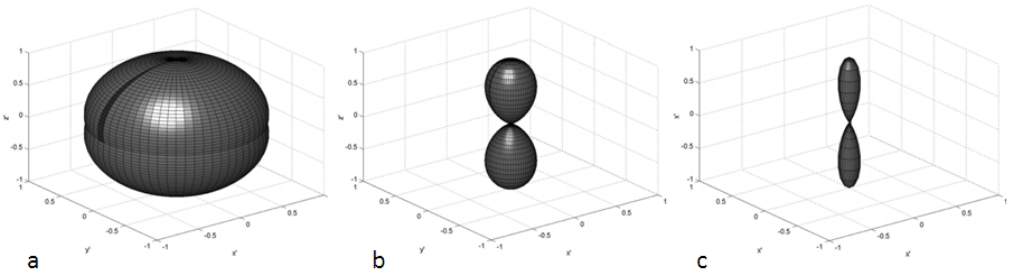

Figure 3.6: Figure modified from [101]. Three examples of PDF profiles estimated using FA for the characterization of uncertainty: a) FA = 0; b) FA = 0.4; c) FA = 0.7.

uncertainty, and vice versa. The so obtained directions of the principal eigenvector define a probability density function (PDF) of possible orientations at each point. An example of these PDF for different values of FA is given in figure 3.6. After the estimation of the PDF, a streamline algorithm is then run from every chosen starting point multiple times following a Monte-Carlo approach again. The number of times a streamline crosses a voxel defines the degree of connection that voxel has with the starting points, and defines a quantity called connectivity. In their approach, Parker and colleagues terminate the tracking when the transition between two points exceeds a threshold angle, fixed at $\pi/2$. When this approach is used, it gives maps of connectivity that are more spread than the streamlines obtained with deterministic tractography. It is not an easy task to identify if this is due to real connections that are not followed with deterministic methods, or to the lack of information in those areas, that results in low and

widespread connectivity.

Similar considerations about the spread of the connectivity maps can be made for the approach presented in [102] and subsequently extended in [25]. In their work, Behrens and colleagues give a complete probabilistic characterization of the connections in white matter. The uncertainty in the estimation of diffusion directions is not derived by the tensor model, but it is obtained in a completely stochastic framework. The probability density functions of the diffusion directions are obtained a posteriori, using bayesian estimation. The Bayes theorem states that, given a model M, a set of measured data Y and a set of parameters ω, the a posteriori probability density function that represents the probability, given the data and the model, of observing the particular set of parameters ω, can be calculated as

$$P(\omega\,|Y, M) = \frac{P(Y\,|\omega, M)\,P(\omega\,|M)}{P(Y\,|M)} \tag{3.14}$$

where $P(Y\,|M)$ is the probability of observing the data given the model and the parameters, and $P(\omega\,|M)$ is the a-priori (i.e. having no information about Y) probability of observing the particular set of parameters given the model. The denominator describes the probability of observing the measured data given a model M, and is calculated as follows:

$$P(Y\,|M) = \int_{\Omega} P(Y\,|\omega, M)\,P(\omega\,|M)d\omega, \tag{3.15}$$

where Ω is the space of parameters. This integral is not solvable analytically. A Markov Chain Monte-Carlo (MCMC) approach has been chosen by Behrens and colleagues, where samples are drawn from regions of the space with high probability, providing a *pdf* in relatively short times.

In their work, that has been implemented in FSL software (`http://www.fmrib.ox.ac.uk/fsl/` [103, 104]), two models have been used: the tensor model (explained in section 1.4)and a partial volume model, where the signal is modeled using two compartments: an isotropic one, that describes the diffusion occurring in free water inside a considered voxel, and an anisotropic one, that describes directionally organized diffusion in the fiber direction. This model is described as:

$$y_i = S_0 \left((1-f)\, e^{-b_i d} \right) + f e^{-b_i d \mathbf{r_i^T R A R^T r}_i}, \tag{3.16}$$

where y_i is the data measured in the voxel, S_0 the signal without diffusion-weighting, d is the diffusivity, f the fraction of volume with anisotropic diffusion inside the voxel, b_i and $\mathbf{r_i}$ are the b-value and the gradient relative to the $i-th$ direction of acquisition. The value $\mathbf{RAR^T}$ represents the tensor along the direction of the fibers. In fact, $\mathbf{R}$ rotates the $\mathbf{A}$, fixed at

$$A = \begin{pmatrix} 1 & 0 & 0 \\ 0 & 0 & 0 \\ 0 & 0 & 0 \end{pmatrix} \tag{3.17}$$

to the predominant direction of diffusion, defined by the three angles (θ,ϕ,ψ). The matrix $\mathbf{A}$ is composed of null elements, except for the first, because in the anisotropic compartment only completely anisotropic diffusion along the estimated direction is allowed, while diffusion is null in the other directions.

In both models used, the noise is modeled as independent and identically distributed (*iid*) and gaussian, with zero mean and standard deviation σ. The priors used for the set of parameters ω (comprising the angles θ,ϕ and ψ that define the diffusion direction, the value of S_0, the SD of the noise and, in the case of the partial volume model, the fraction f) are chosen as completely non-informative, apart from positivity constraints. In particular, the priors for the

angles θ, ϕ and ψ are proportional to the sine of θ. The other priors are defined as follows:

$$P(S_0) \sim \mathrm{U}(0,\infty)$$
$$P(\lambda_1, \lambda_2, \lambda_3) \sim \Gamma(a_\lambda, b_\lambda)$$
$$P\left(\tfrac{1}{\sigma^2}\right) \sim \Gamma(a_\sigma, b_\sigma)$$

where a_λ, b_λ and a_σ, b_σ are chosen to give to the Gamma distribution high variances, so that they are kept non-informative and have a small effect on the posterior distributions.

This model has been later extended in [25], where the diffusivity has not been constrained to happen in a single direction for every voxel. In this case, the case of crossing fibers inside a voxel has been taken into consideration. In this case, the model becomes

$$y_i = S_0 \left(\left(1 - \sum_{j=1}^{N} f_j \right) e^{-b_i d} + \sum_{j=1}^{N} f_j e^{-b_i d r_i^T R_j A R_j^T r_i} \right), \tag{3.18}$$

which is analogous to the 3.16, but now a compartment is assigned to each diffusion direction estimated to be present in a voxel. In the equation 3.18, N is the number of direction of diffusion that fit the measured data y_i. The signal y_i is the sum of all the signals given by the different directions populations. The number of populations of fibers inside a voxel is estimated with a bayesian method. In particular, automatic relevance determination (ARD) is used, where the most complex model is fit, and where parameters don't show to be relevant, they are forced to zero. Both in the case of single fiber and in the case of multiple fibers, the actual tractography is done drawing samples from the *pdf* (or from one of the *pdf*s in the multiple orientations case) and then advancing in that direction, in an approach similar to the streamline deterministic algorithms. As in [101] the connectivity is calculated counting the number of stramlines that fall into a specific voxel. The multi-fiber approach described by Behrens and colleagues 3.18 has been demonstrated to be more sensitive to non-dominant projections, that

are lost with a single fiber approach. Moreover, the probabilistic approach allows the consideration of areas of low anisotropy, in respect to deterministic tractography: since the uncertainty is completely described, it is no longer necessary to interrupt the fiber tracking. Since probabilistic methods, as stated earlier, give as outputs spread maps of probability of connections, it is necessary to threshold the results in order to identify tracts connecting different brain regions, so to exclude voxels with low probability [98].

3.4 Discussion

In the previous sections, the most known algorithms for the estimation of white matter connections have been taken into consideration. The described deterministic and probabilistic approaches have different advantages and drawbacks, and are usually exploited with different aims. Deterministic algorithms have the benefit of allowing the analysis of specific connections: white matter bundles trajectories of interest are tracked along their courses. This can be useful when the interest is specific in the shape or properties of single tracts. Another advantage of deterministic methods is the rapidity of the computation. Deterministic approaches also suffer from some limitations: since deterministic methods rely completely on the measured data, usually the tracking algorithms are terminated when the information obtained from the measures becomes too corrupted by noise for a precise diffusion direction estimation. Moreover, these methods need some parameters, used for the termination of the tracking process, that have to be defined by the user. Probabilistic methods don't discard the noise, inherently present for every DTI acquisition, and model it together with water diffusion. This allows the investigation of brain connections also when the information given by the data is corrupted by noise. In this way, connections that can not be tracked with deterministic approaches because of limited size or weaker directional organization can often be estimated. On the other hand, these methods are more computa-

tionally demanding than deterministic approaches and give outputs that are not easily interpreted: usually the results of the estimation process are connectivity maps, or voxel-wise representations of the probability of tract directions, that need further analysis before being associated with the structural connections between brain areas. Because of these differences, it is not possible to determine if a technique performs better than the other and both methods are currently object of research both clinical and methodological, with the aim of gaining more insight on structural brain connections.

Chapter 4

Structural connectivity in healthy and disease

4.1 Estimation of brain structure with tractography in healthy

Over the last years, both deterministic and probabilistic tractography have been used to investigate brain structure in vivo. Results of tractography are characterized by a good intra and inter-operator reproducibility [105]. Applications of tractography include the tracking of specific white matter tracts, the generation of atlas or templates of connections, and the parcellation of white matter and gray matter, coupled with and the investigation of the general interconnection of brain areas, often denominated structural connectivity.

Deterministic tractography has been extensively used for the detection of specific white matter connections. Using definite ROIs, the tracts of interest are isolated from the rest of the tractography outputs, and used to investigate inter-subject variability, or to define typical brain connections and their diffusion characteristics. One application of this is the investigation of the brain lateralization, i.e.

the dominance of an hemisphere on the other. In [106] the structure of the cingulum (one of the main white matter bundles, involved in emotion processing) was investigated, using a ROI-based deterministic algorithm. A left-right asymmetry was found in healthy subjects for FA values, also confirmed by [107]. This defines a general white matter characteristic not detectable with any other technique and that can give more insight on brain structure. Barrick and colleagues [108] studied asymmetries between the two hemispheres utilizing a streamline algorithm in healthy volunteers, finding that there are consistent left-right asymmetries in the pathways that connect the temporal to the parietal and the temporal to the parietal lobes. An example from this work is reported in figure 4.1, where asymmetries in the tracts are represented using different colors in the two hemispheres, and symmetrical connections have the same color. In particular, two white matter bundles are clearly visible: arcuate fasciculus, that is known to connect the temporoparietal junction with the frontal cortex, and the uncinate fasciculus, that connects the temporal lobe with the orbitofrontal cortex. Asymmetries in the arcuate fasciculus were reported also by [109], and related to findings from phonologic studies and models that describe language processing. This shows that DTI can help in disclosing the relationship between structure and function in the brain. Asymmetries in the white matter circuits related to auditory and phonologic processing, with stronger connections in the dominant hemisphere, were already found in [110], thus have been confirmed with the previously mentioned study.

Another example can be done considering the visual network: in [111] the connections in the occipital lobe are estimated, with a particular focus on the white matter bundles that cross the corpus callosum, as can be seen in figure 4.2. In a later work of the same group [112] the optic radiation, that connects the thalamus with the visual cortex, has been investigated. Its location can be precisely defined using DTI tractography: this could be of great importance in the case of

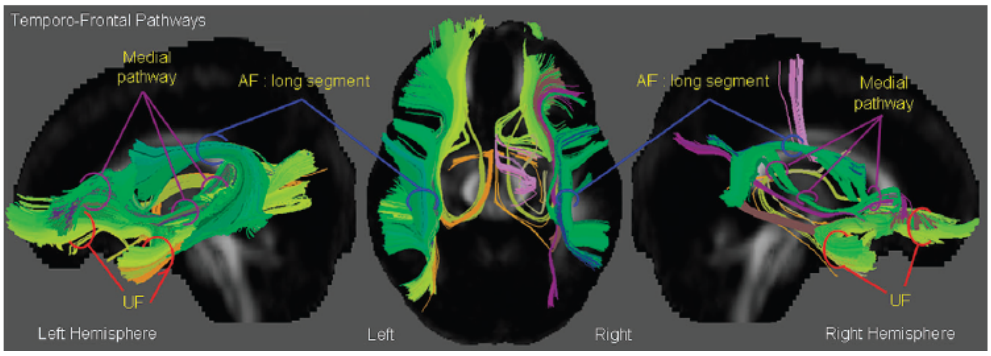

Figure 4.1: Figure from [108]. Reconstructed pathways from temporal to parietal lobes. Symmetric tracts have the same color in both hemispheres, asymmetric pathways are depicted with different colors. AF = arcuate fasciculus; UF = uncinate fasciculus.

neurological surgery procedures. Tracking of the bundles belonging to a network can also be used to estimate possible white matter damage in patients affected by various pathologies. For example, in [113] white matter tractography has been used to evaluate the connections in the visual lobe for early blinds: a lower degree of connectivity has been found for patients in respect to healthy individuals. In this case, it can be noted how tractography reflects the changes in the brain organization following disease. In the work described in [114] probabilistic tractography was applied to a data set of healthy volunteers, and the presence of tracts that connect directly the auditory to the visual cortex was shown, thus suggesting the presence of a direct connection between these two areas.

The ability of locating white matter fiber bundles allows the definition of how the typical brain structure and organization is. This information can be used to form atlases, or templates, that can be utilized to investigate inter-subject variability or pathological changes in structure or diffusivity. In [110] five white matter tracts have been evaluated, in a cohort of healthy individuals: the authors obtained maps that define the location of the considered bundles in the healthy population. In this way, it has been possible to evaluate the variability inherent to the considered population, as can be seen in figure 4.3.

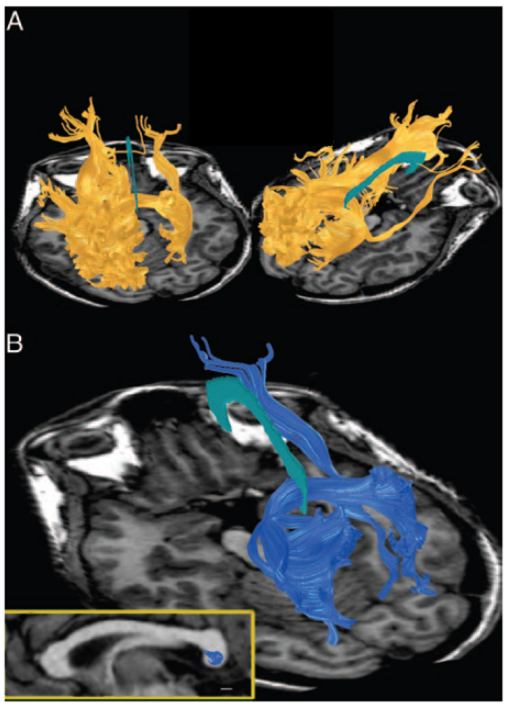

Figure 4.2: Figure modified from [111]. White matter bundles located in the occipital left lobe, estimated with tractography (a). In (b) a subset of those fibers is depicted, in particular the fibers that cross the corpus callosum in the highlighted ROI. The light blue structure is the corpus callosum, superimposed to a T1 slice.

In [115] an atlas of tracts has been created from healthy subjects, to be then used, once coregistered to patients brains, to evaluate damage in connectivity. The probabilistic maps obtained from the results in healthy volunteers allowed the investigation of diffusion characteristics in a MS patient in the presence of white matter lesions, that prevented the tractography from working properly. The same approach has been used in [116] in a group of MS patients. Deterministic tractography has also been used in [117] to reconstruct the major white matter tracts. Results have been proved to be in accordance with post-mortem dissection studies, and allowed to inferring information on lateralization, gender effects and inter-subjects variability, that reflects the natural anatomical differences in healthy population. A white matter tracts template has also been proposed by Peng and colleagues [118]: several white matter bundle were traced from a diffu-

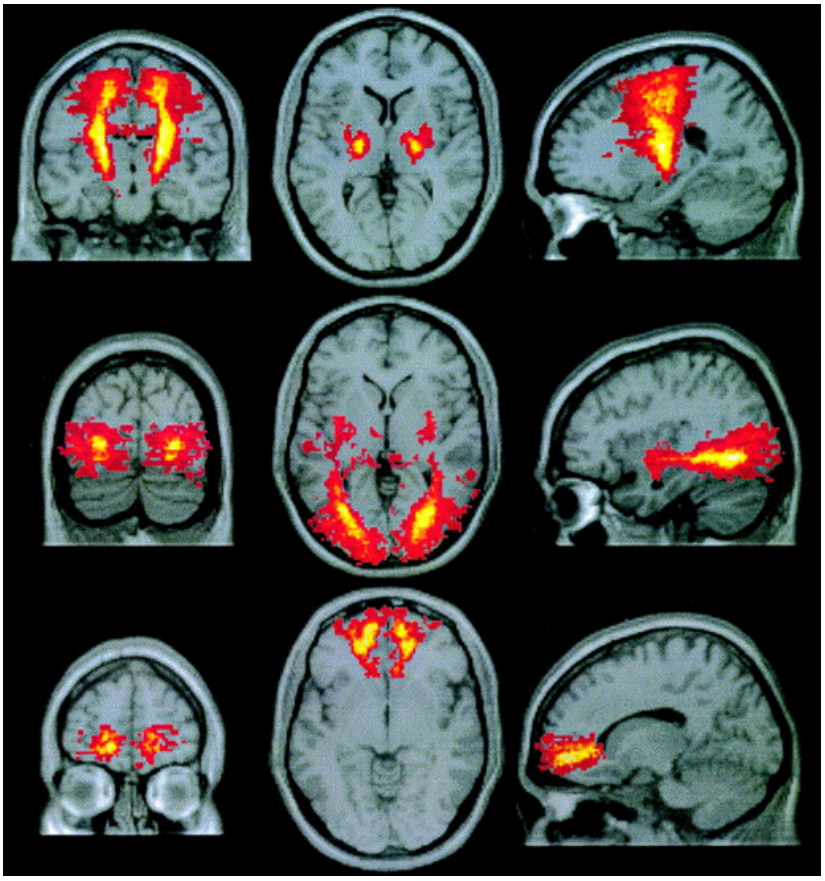

Figure 4.3: Figure modified from 4.3. Inter-subject variability in tract location has been represented by overlap maps: the color is brighter where the degree of overlap between subjects is higher.

sion tensor data template obtained by healthy volunteers, using a deterministic streamline approach. The use of a DT template allows the evaluation of individual characteristics in comparison to those of a whole healthy population. A similar approach was used in [119], where a total of 15 tract masks obtained from tracking in the DTI atlas were used to investigate the diffusion properties of brain tissues during childhood and development.

Often the interest, instead of in the location or on the shape of a fiber bundle, is in the identification of which brain areas are structurally connected. To infer this information, tracts are estimated with a tractography process and voxels are

classified on the basis of the degree of connection with the starting points (denominated connectivity value). An example of this can be seen in [120]. In their work, Behrens and colleagues segmented the gray matter in regions corresponding to areas connected to the thalamus, which is a central deep gray matter structure that is involved in many brain functions. Probabilistic tractography was run starting from these regions, and then the value of connectivity to the different cortical areas was computed for each thalamic voxel. As can be seen in figure 4.4, the thalamus was segmented in different clusters, corresponding to the thalamic nuclei. This result was confirmed in [121], where it was shown that structural connectivity also correlated with functional connectivity between thalamus and cortical areas, and was consistent with histology. Thalamus parcellation results were found to have a high reproducibility, both inter- and intra-subject [122]. The same procedure has also been applied to other brain structures, and demonstrated to be reliable. For example, using a similar procedure, in [123] connections between Broca's area (a cortical area involved in language processing) and the medial cortex are investigated, allowing a connectivity-based parcellation of Broca's area. Another example is represented from [124], where the amygdala (a gray matter structure involved in emotions processing) was segmented in its four nuclei using connectivity values obtained with probabilistic tractography.

The aforementioned relation with functional studies has been taken into consideration multiple times, because of the great insight it could provide on the integration between structure and functionality in the brain. This can be achieved both integrating structural and functional measures and guiding the evaluation of functional connectivity using the knowledge derived from structural connectivity studies [125]. For example, in [126] the parietal cortex was parcellated using probabilistic tractography in several different areas, then functional connectivity of the so-obtained regions was investigated, demonstrating that functional connectivity reflects to a certain degree the underlying structural connections. Another way

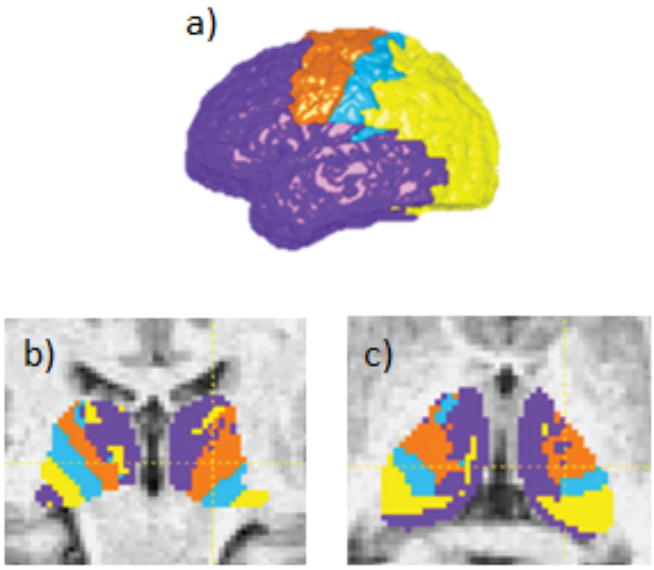

Figure 4.4: Figure modified from [120]. Segmentation of cerebral cortex in four cortical zones corresponding to thalamic connection areas (prefrontal/temporal, motor, somatosensory and parieto-occipital zones (a). Voxels of the thalamus are classified according to the highest probability of connection with the cortical areas in a) and color-coded with the same colors.(b,c).

to define the relationship between structural and functional connectivity is to use as seeds for tractography the clusters of voxels that show functional connections. An example of this technique can be seen in [127], where ROIs selected in activation areas obtained from a resting state fMRI experiment were used as seeds and targets for tractography. Structural connectivity showed to reflect functional connectivity, as can be seen in figure 4.5.

A more advanced way to deal with cerebral connectivity is to consider the whole brain and analyze the connections between all voxels belonging to the cortex, with the aim of defining the general anatomical connectivity networks. In these analyses, usually the brain is parcellated in regions, whose interconnections, in terms of structural linkage, are then investigated. Then a connection matrix, or a graph, is computed from these measurements [128]. For example, in [129] connectivity

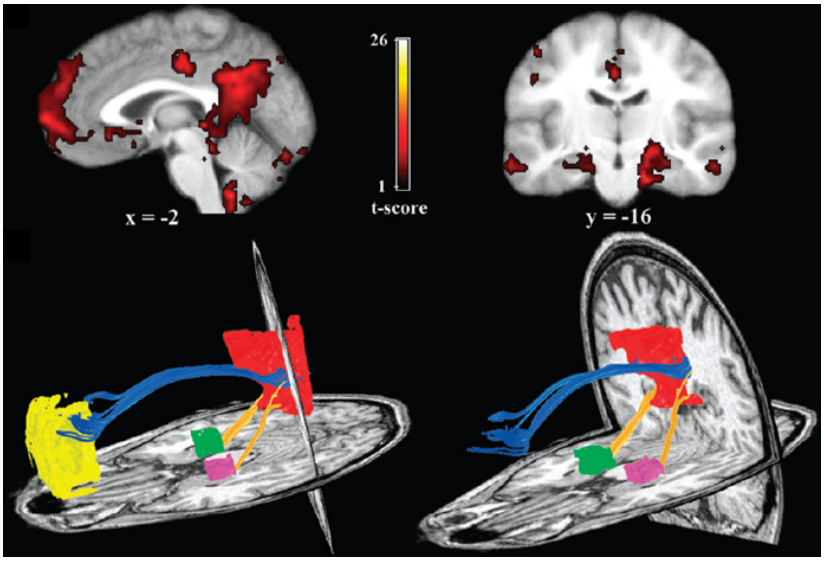

Figure 4.5: Figure from [127]. Top row: functional activation areas obtained from a resting state fMRI experiment. Bottom row: results from deterministic tractography, where the ROIs derived from functional analyses were used as seeds and targets. Left and right figures show the same tracts from different angles.

between 78 cortical regions has been evaluated, using graph properties.Cortex parcellations were used as nodes, and tracts estimated with tractography as the graph edges. It's been found that the brain has some small world properties, meaning that the connections don't follow a random behavior, but short clustered links are preferred across brain areas. Also in this case, the ultimate goal is to link function and structure to gain more insight on the brain inner mechanisms.

In the next section, applications of tractography regarding the three pathologies considered in this thesis are outlined.

4.2 Estimation of structural damage in pathological brains

4.2.1 Tractography in multiple sclerosis

Because of the presence of white matter demyelinating lesions, where, as seen in section 2.2.1, fractional anisotropy values decrease, tractography in multiple sclerosis is a critical process. Tissue disruption underlying changes in diffusivity in lesions makes the tracking through white matter lesions difficult [130, 131], as can be seen in figure 4.6. This problem can be overcome avoiding tractography directly in patients, and using tract templates derived from healthy subjects [132, 133, 115]. These methods make it impossible to analyze the individual changes to the tracts shape or volume caused by the disease, but allow the evaluation of diffusion indeces values along the tracts, or in areas where the tracts are for healthy. In this way, tract-specific abnormalities can be detected even if the tracking is in fact impossible for patients. The method described in [115] has been applied to a population of MS patients in [116], and it has been proven to be reliable in the evaluation of MS white matter tracts. Also applying an atlas of white matter tracts followed to a registration to individual patients spaces, Kezele and colleagues [134] found a decrease in volume, i.e. athrophy, over time, in ten white matter bundles in MS patients.

Nevertheless, in several cases (e.g. in [135, 136, 137, 138]) it has been demonstrated, with particular focus on pyramidal tract (i.e. a corticospinal tract) and corpus callosum, that individual-based tractography discriminates efficiently between MS patients and healthy volunteers, even if patients with a great lesion burden beneficiate from an atlas approach. In general, in patients tracts the directionality of diffusion results disrupted, as is highlighted by low FA values, and its magnitude increases (MD values are high). A disruption in the tract recon-

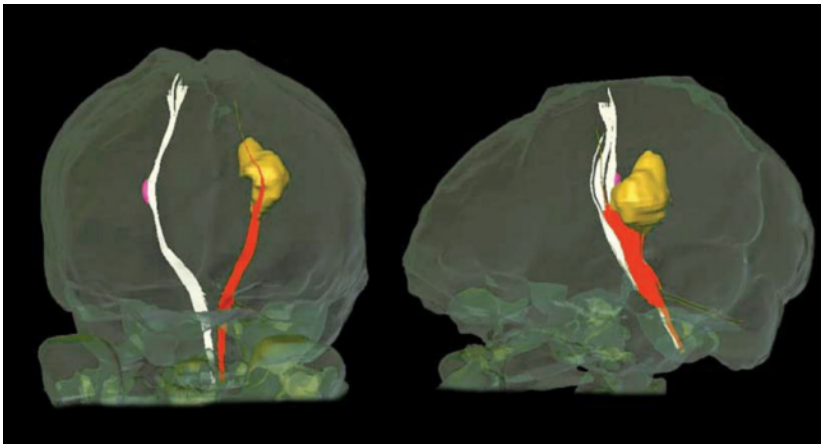

Figure 4.6: Figure from [115]. Tract reconstruction for a MS patient. The lesion, indicated in yellow, prevents the tracking of the whole considered tract.

struction is always detectable in patients (see figure 4.7), but that doesn't affect negatively the differentiation of patients from healthy individuals.

Also structural connectivity in MS has been investigated. For example, in [139] a disruption of the memory network was found in early MS patients, in particular results show a weakening of the connections in the frontal cortex. In another example, using graph theory, reduced efficiency of connections were found in various network, including the sensory-motor system and the visual system [140], with a certain degree of correlation with clinical signs, evaluated with the EDSS scores.

4.2.2 Tractography in traumatic brain injury

Tractography has also been applied to traumatic brain injury patients DTI data. The sensitivity of DTI to white matter damage in absence of visible lesions is particularly important in the case of diffuse axonal injury (DAI), as noted in section 2.2.2. This holds true also when the evaluation of brain integrity is done with tractography. For instance, in conjunction with the abnormalities in diffusion indices already discussed in section 2.2.2, disruption was found in the white matter

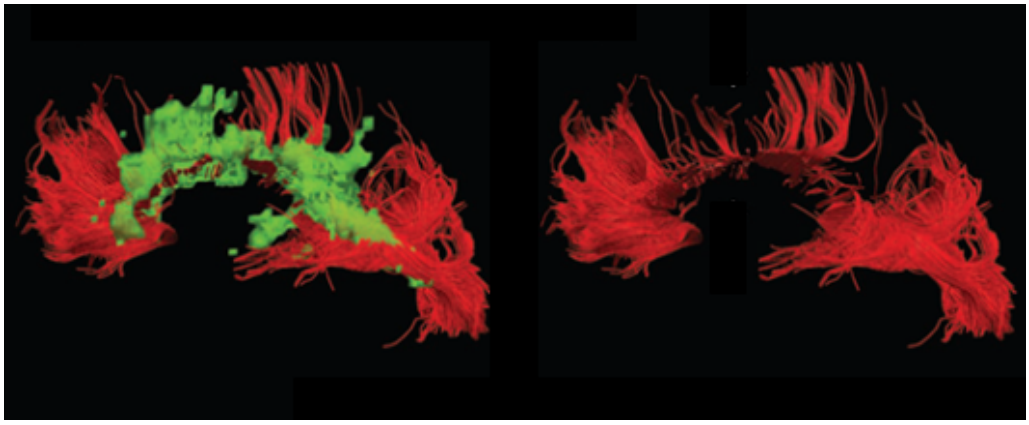

Figure 4.7: Figure from [138]. Reconstruction of the corpus callosum with deterministic tractography for a MS patient. Demyelinating lesions (depicted in green) prevent the algorithm to follow the tract. Left: reconstructed fibers and white matter lesions. Right: the same tracts without the superimposed lesion.

fiber tracts. For example, in [75, 141, 142] reconstruction of fibers from corpus callosum with deterministic tractography resulted abnormal if visually compared with tracts obtained in healthy (figure 4.8), even if there wasn't any detectable abnormality or lesion in the conventional MR images. The same finding proved its clinical usefulness in [143, 144], where DTI tractography helped in the definition of a diagnosis for two TBI patients, clarifying the damage that the injury brought to brain interconnections and functionality. The comparison between patients and healthy was done not only qualitatively, but also quantitatively in [145]: the number of fibers crossing the corpus callosum was counted and compared; it was found that TBI patients had less fibers, in number, through the callosum and that this number related with traumatic injury degree. The number of fibers reconstructed by deterministic tractography has been used also in [146] to analyze the damage caused by trauma. Patients also showed reduced FA, mean length, fiber count, fiber volume, and fiber density, and increased MD [147], correlated with disease outcome. The authors of this work also followed changes in structural connectivity over time, demonstrating that these changes reflect clinical outcome and recovery of patients.

Figure 4.8: Figure modified from [75]. Top row: deterministic tractography of corpus callosum in a healthy volunteer. Bottom row: for comparison, deterministic tractography of corpus callosum in a TBI patient.

4.2.3 Tractography in schizophrenia and bipolar disorder

One of the widely accepted theory on the causes of schizophrenia is the disconnection hypothesis. Postmortem studies, fMRI and electrophysiological experiments support the idea that schizophrenia arises from abnormal connections between prefrontal cortex and other structures [148]. A very similar theory has been proposed also for bipolar disorder (BD). Supporting this theory, the authors investigated structural connectivity with probabilistic tractography in BD and schizophrenia patients, in particular for uncinate fasciculus and anterior thalamic radiation, finding weaker connections both for schizophrenia and for BD.

In schizophrenia, a similar result was found using deterministic tractography in the inferior longitudinal fasciculus, that connects the occipital with the temporal cortex [149, 150]. White matter damage leading to disruption of connections was also found in other structures, such as arcuate fasciculus [150], fornix [151, 152],

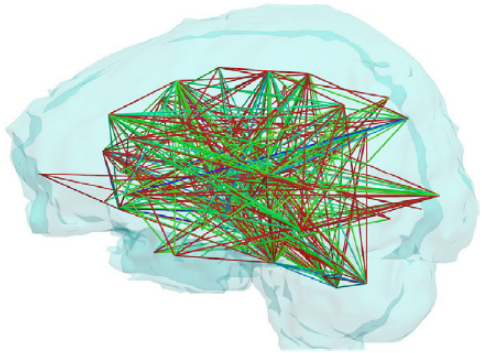

Figure 4.9: Figure from [157]. Depiction of connections that show statistical differences between schizophrenic patients and healthy. The higher statistical difference is depicted in green, the lower in red.

anterior commissura [153] and corpus callosum [154, 155].

Also brain connectivity has been taken into consideration, both analyzing specific connection and taking into account general connectivity difference with healthy. For example, connectivity between inferior frontal gyrus and superior temporal gyrus was investigated in [156] with probabilistic tractography, finding abnormality in pathways. Rathi and colleagues [157], with a slighly different model for DTI data, found a whole set of connections to be altered (fig 4.9), a result that was found also in [158] using graph theory: impaired connections were found especially involving frontal, parietal and temporal lobes. Also thalamo-cortical connections were found to be impaired in schizophrenia [159], as well as general organization of connections [160].

In bipolar disorder, although diffusion characteristics are less investigated than in schizophrenia, some relevant results have been found. Deterministic tractography revealed increased connectivity between the hippocampus and the amygdala [161], in a white matter area corresponding to the uncinate fasciculus, that could be related to hyperactivity that characterizes bipolar behavior. Disrupted diffusion was found in uncinate fasciculus, anterior thalamic radiation and superior

longitudinal fasciculus [162], which can all be related to frontal cortex. These results, along with more widespread white matter damage, was confirmed using probabilistic tractography in [84].

Chapter 5

A novel method to evaluate white matter MS lesions with deterministic tractography

5.1 Introduction

As described in section 2.2.1, multiple sclerosis is characterized by damage to the white matter, in terms of demyelinated plaques. These lesions, where FA value drops because of structural damage, alter the course of tractography in white matter of patients affected by MS. Nonetheless, investigating the degree of damage to connections and to white matter tracts is of primary importance for the evaluation of the disease and its consequences on the integrity of the brain.

In 5.3 a method of deterministic tractography is presented. An existent deterministic tractography algorithm has been modified to make it more reliable in the presence of reduced FA, and the results obtained in the presence of lesions with those obtained in contralateral normal-appearing white matter (NAWM) areas were compared. Conventional deterministic algorithms often interrupt the track-

ing in the case of lowered FA or changes in fiber directionality. Although this behavior is desirable because it makes reconstruction very conservative, the drawback is that some information gets lost. With the technique utilized in this work, the reconstruction is taken a little further than with conventional techniques, because the algorithm that has been used for tracking the fibers in locations where the directionality is not strongly determined is robust to noise and allows data that would otherwise be discarded to be taken into account.

Using the conventional streamline method [29], the presence of a lesion could precociously interrupt the reconstruction of the tract, because of low FA [115]. The possibility of the presence of noise is completely discarded and the reconstruction is abruptly terminated. With the method here proposed, the value of FA to be used to terminate the tract is lowered, because the considered algorithm is more robust to noise than conventional streamline. Moreover, in section 5.3.1, the interpolation applied in the algorithm that has been developed is explained in detail, because the choice of an interpolation technique over others is critical.

5.2 Dataset

For this study, 12 relapsing-remitting multiple sclerosis (RRMS) patients have been considered (8 males, 4 females, age 35 $\pm$11 years, mean EDSS 3 $\pm$ 1). They underwent MRI acquisition, with a 1.5T Philips Achieva scan. 32 non-collinear directions were applied, TR and TE were 11730 and 6 ms respectively, and the voxel resolution was 2mm isovoxel (i.e. identical size in the three dimensions) (matrix 112x112x60). Two additional non-diffusion weighted volumes (B0) were also acquired. To identify white matter lesions, also a FLAIR volume was acquired (TE = 120 ms, TR = 10000 ms, TI = 2500 ms, matrix 288 x 288 x 50). MRI scans were conducted in Euganea Medica, Padova, Italy in collaboration with the Multiple Sclerosis Centre of Veneto region, Dept. of Neurosciences, Uni-

versity Hospital of Padova, Italy.

For the comparison of the interpolation methods, two additional DTI volumes were used: a volume acquired at the hospital of Verona at 3T (TR = 5000 ms, TE = 118ms, b-value = 1000s/mm^2, matrix 128 x 128 x 23 and voxels with dimensions 1.7188 x 1.7188 x 6 mm^3) with 30 non-collinear diffusion directions and 5 additional B0 acquisitions, of a healthy volunteer, and a volume acquired at 1.5T, with 15 non-collinear diffusion directions (TR = 15634 ms, TE = 25ms, b-value = 800s/mm^2, matrix 256 x 256 x 50 voxels and voxel size 0.9375 x 0.9375 x 3 mm^3), of a MS patient who underwent a MR scan at Euganea Medica.

5.3 Methods

5.3.1 Interpolation of the tensor field

DTI images were corrected for distortions caused by eddy currents using FSL - FMRIB's Diffusion Toolbox (FDT) (`www.fmrib.ox.ac.uk/fsl`). To assess the interpolation technique that could give the best results, interpolation results have been evaluated on a DTI volume of a MS patient, acquired with 15 directions at 1.5T, and on a volume of a healthy volunteer, acquired at 3T with 30 directions. This was done to better analyze possible differences in the results given by the interpolation technique. In particular, it is of particular interest how the interpolation affects the results in the case of a voxel with strongly different dimensions.

Interpolation is necessary because both with continuous tracking and with tensor deflection, the computation of the tract trajectory is done considering a continuous tensor field, and the integration step is always smaller than the size of a voxel. If all the voxel neighboring the voxel containing the actual position in which the tensor is evaluated are considered, interpolation acts on 27 voxels. The tensor $\mathbf{D}_i$ evaluated at the position $\mathbf{r}(\mathbf{s}_i)$ is computed as a weighted sum of the contributions from all 27 voxels:

$$D_i = \frac{\sum_{j=1}^{27} p_j D_j}{\sum_{j=1}^{27} p_j}. \tag{5.1}$$

The weights p_js are defined as the linear function of the difference between the maximum distance from $\mathbf{r}(\mathbf{s}_i)$ that can be obtained for a point in the 27 neighboring voxel, that is 1.5 times the diagonal of the voxel, and the distance between $\mathbf{r}(\mathbf{s}_i)$ and the center of the voxel $\mathbf{c}_j$. With this definition, non-negative weights are obtained, and the nearer voxels have more weight in the computation of the interpolated tensor field. If the diagonal of the voxel is called d, the above definition can be summarized as follows:

$$p_j = 1.5 \cdot d - |\mathbf{c}_j - \mathbf{r}(\mathbf{s}_i)|\,. \tag{5.2}$$

This way of interpolating the tensor field has been compared with gaussian interpolation, where the weights are defined using a gaussian distribution, centered in the position $\mathbf{r}(\mathbf{s}_i)$ and with variable standard deviation, in this work chosen to be equal to the inverse of the diagonal of the voxel d.

$$p_j = \frac{d}{\sqrt{2\pi}} e^{-d^2 \frac{\left(\mathbf{c}_j - \mathbf{r}(\mathbf{s}_i)\right)^2}{2}}. \tag{5.3}$$

For the evaluation of interpolation, two ROIs have been considered, both located on the splenium of the corpus callosum, as can be seen in figure 5.1.

5.3.2 Propagation of the tract and evaluation of MS lesions

Tractography has been implemented integrating the FACT method firstly described by [97] and illustrated in section 3.2, combined with the tensor deflection (TD) method, presented in [99] and also described in 3.2.

Since the tensor deflection method is proven to be less sensitive to noise and low

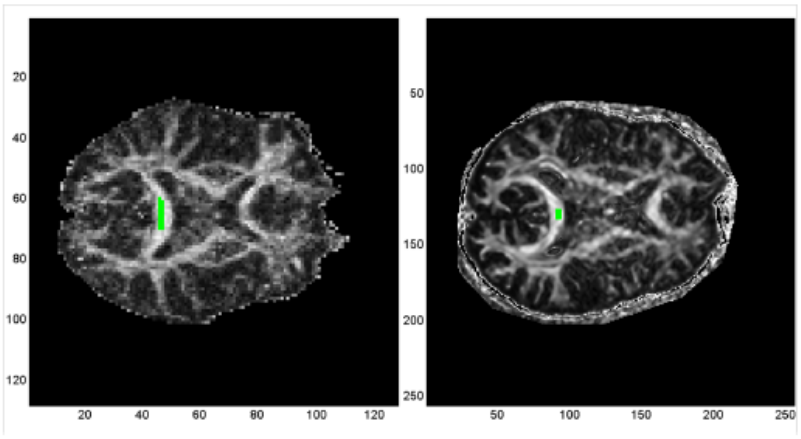

Figure 5.1: ROIs defined for the comparison of interpolation of the tensor field. For both datasets the ROI was located on the splenium of the corpus callosum. Left: Reconstructed FA for the 3T volume (voxel size 1.7188 x 1.7188 x 6 mm^3) and superimposed ROI. Right: reconstructed FA and superimposed ROI for the volume acquired at 1.5T (voxel size 0.9375 x 0.9375 x 3 mm^3.)

FA, but more computationally demanding, the algorithm switches from conventional tractography solved with Eulero method, to tensor deflection, following the rule:

$$\mathbf{r}(s_{n+1}) = \mathbf{r}(s_n) + \alpha \cdot \mathbf{v}_{out}, \tag{5.4}$$

where

$$\mathbf{v}_{out} = \begin{cases} \mathbf{v}_1 & FA > threshold \\ \\ \mathbf{D} \cdot \mathbf{v}_{in} & FA < threshold \end{cases} \tag{5.5}$$

where $\mathbf{D}$ is the tensor evaluated at the n-th step in the tracking process, and $\mathbf{v}_1$ its first eigenvector. $\mathbf{v}_{in}$ is the direction of the tract evaluated at the n-th step as well. α is the integration step, and is a parameter that can be tuned in accordance with the tracking method that is being used. It has beed defined as follows:

$$\alpha = \begin{cases} h & FA > threshold \\ \\ \frac{h}{k} & FA < threshold, k > 1 \end{cases} \tag{5.6}$$

In this case, the threshold has been set for a FA value of 0.2, and α is fixed at 0.4 voxels. k has values > 1, since tensor deflection works best with smaller integration steps, given that it tends to underestimate the tract curvature. In the rest of this work, k has been set to 5. The algorithm is terminated when FA reaches a value of 0.16. Another termination criterion is the angle that the trajectory covers in a voxel: it has been set to a value of 40 degrees.

This algorithm was applied to the patients data, and used to evaluate the damage in terms of reconstructed white matter tracts. All voxels with FA > 0.6, which is a value for which the white matter is formed by well-defined fibers, were used as starting points, thus obtaining a whole brain tractography. From the obtained tracts, those of interest have been selected using predefined ROIs located on white matter MS lesions identified on FLAIR images. To compare the tractography outputs in pathological areas to that in normal appearing white matter, we manually delineated contralateral ROIs, paying close attention that the surrounding region didn't present MS plaques. The lesions were identified on T2-weighted images, and then registered to the DTI space using FSL FLIRT [163]. An example showing the considered ROIs is presented in figure 5.2 Finally, we compared the density of reconstructed fibers and their mean length in the pathological and in the normal appearing ROIs. The distribution of lengths in the ROIs were also statistically compared using the Wilcoxon rank-sum test (p=0.05).

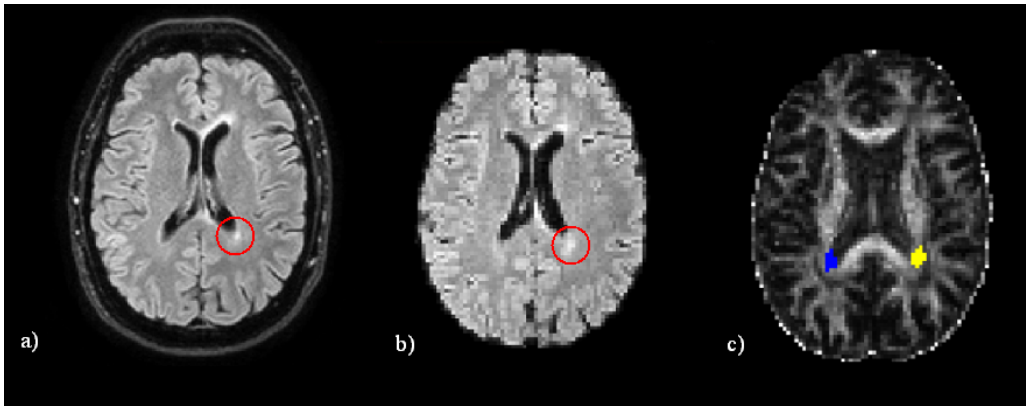

Figure 5.2: ROIs for the evaluation of tracts in MS white matter lesions. a) peri-ventricular lesion identified in T2 space; b) T2 image registered to DTI patient space: the lesion is visible also in this space; c) lesion and contralateral ROI, obtained from b), superimposed to the FA map.

5.4 Results

5.4.1 Interpolation of the tensor field

Interpolations with linear and gaussian weights have been compared, selecting fibers that cross a corpus callosum ROI. This ROI, shown in figure 5.1, is located in an area of high anisotropy, where tractography results are well-defined. It has been chosen because of the high reproducibility of results. In figure 5.3 an example of the results of tractography with both interpolation techniques are reported. As can be seen, tracts show a good degree of overlap with the exception of some small tracts that don't interfere with the reconstruction.

The performance of the two interpolation methods has been compared also quantitatively. In table 5.1 results, in terms of number and length of reconstructed tract (i.e. the number of integration steps of size α), are reported for the data with resolution 1.7188 x 1.7188 x 6 mm^3 . As can be noted, the interpolation with gaussian weights results in around 16% less reconstructed tract, in number, than with linear weights. Also their length is smaller, and results reduced of 20% in respect to linear weights. This can be explained because voxels have a low

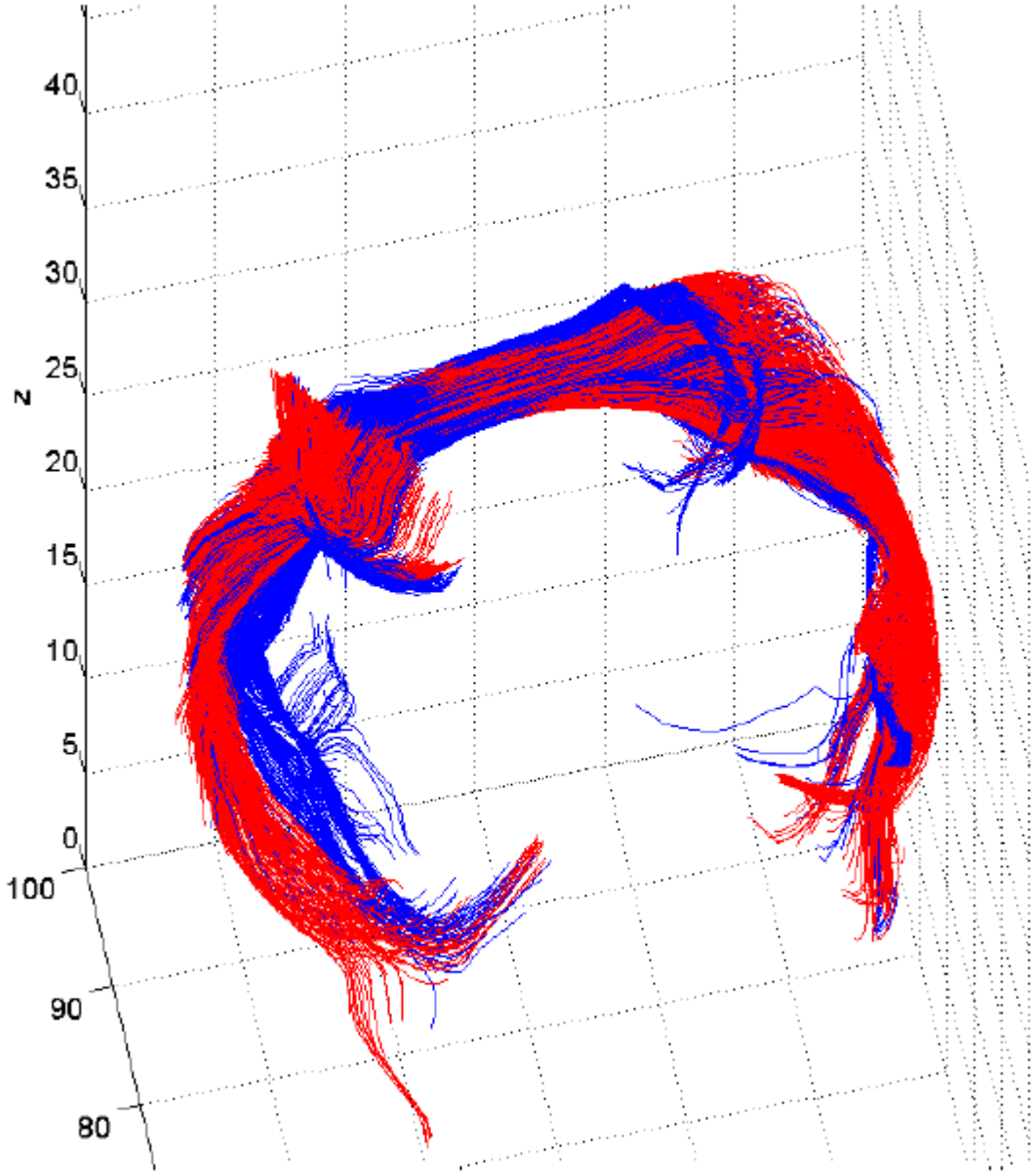

Figure 5.3: Reconstruction of corpus callosum fibers for the dataset at 1.5T with resolution 0.9375 x 0.9375 x 3 mm^3. Tracking was done interpolating the tensor field with linear weights (red lines) and gaussian weights (blue lines).

	number of tracts	mean length of tracts
linear weights	268	90
gaussian weights	225	72

Table 5.1: Comparison of interpolation with linear or gaussian weights, for the DTI volume acquired at 3T, with 30 non-collinear diffusion directions and resolution of 1.7188 x 1.7188 x 6 mm^3

	number of tracts	mean length of tracts
linear weights	1960	170
gaussian weights	1636	167

Table 5.2: Comparison of interpolation with linear or gaussian weights, for the DTI volume acquired at 1.5T, with 15 non-collinear diffusion directions and resolution of 0.9375 x 0.9375 x 3 mm^3

resolution in the third dimension, z. This causes the term d^2 in equation 5.3 to get high values, thus weights for voxels different from the one containing $\mathbf{r}(\mathbf{s}_i)$ become very small, making the interpolation less effective than with linear weights and obtaining a less smooth tensor field. In this way, abrupt transitions of directions are more likely to happen than utilizing linear weights, and the whole tractography process becomes more conservative. For the data with resolution 0.9375 x 0.9375 x 3 mm^3 the effects of different interpolations don't show such consistent differences, especially in the estimated length of tracts. Since the standard deviation of the gaussian distribution of weights is larger, the interpolation obtained with gaussian weights is more similar to that obtained with linearly weighted coefficients, as can be noted in table 5.2. With gaussian distributed weights, the estimated number of tracts was still reduced of around 16%, but the length was reduced just of 2%. For the reconstruction of tracts in MS patients brains, whose results are shown in section 5.4.2, the more conservative approach has been chosen.

	Lesion ROI		Controlateral ROI		Rank-sum results	
	length	density	length	density	h	p
Subject 1	123	0.12	147	0.35	1	<0.0001
Subject 2	119	0.01	140	0.02	1	<0.0001
Subject 3	162	0.42	157	0.31	0	0.10
Subject 4	147	0.13	154	0.39	1	0.03
Subject 5	138	0.05	147	0.12	0	0.09
Subject 6	126	0.12	145	0.41	1	0.02
Subject 7	122	0.14	136	0.16	0	0.09
Subject 8	143	0.18	151	0.52	1	0.02
Subject 9	149	0.18	155	0.46	0	0.14
Subject 10	148	0.06	148	0.18	0	0.45
Subject 11	118	0.05	143	0.11	1	<0.0001
Subject 12	107	0.01	139	0.08	1	<0.0001

Table 5.3: Deterministic tractograpy for MS patients. Length and density of tracts in MS plaques and in normal-appearing contralateral white matter are reported, as well as the output of a rank-sum test between the lengths in lesion and in contralateral ROIs.

5.4.2 Evaluation of tracts in presence of white matter MS lesions

Tracts length and density in pathological ROIs resulted consistently smaller than in NAWM ROIs. In particular, we found that there is a mean decrease of 9% in tract length and of 52% in fibers density in ROIs containing MS plaques. Remarkably, the presence of lesions didn't interrupt the tracking algorithm, but affected the integrity of the reconstructed tracts. In one subject we found a small increase in length (3%). Using the rank-sum statistical tests we found that the majority of distributions of tracts lengths are different in lesions and NAWM ROIs, with 7 out of 11 ROIs presenting different statistical distributions. When the difference in length didn't reach statistical significance, an effect of the presence of the lesion is still visible in the density of tracts. All quantitative results are reported in table 5.3.

5.5 Discussion

In this chapter, two algorithms for the tracking of white matter fibers are combined and, integrated with an evaluation of the methods for the tensor field interpolation, used to track fibers in the white matter of MS patients. The tracking is continued also for voxels where conventional streamline algorithms interrupt the reconstruction, because the tensor deflection method, used where the FA goes below the threshold of 0.2, is robust to noise. This avoids blunt terminations for tracts affected by lesions. It is to be noted that the value of 0.16, used for the termination of the algorithm, defines voxels, even if with a lower value of FA, belonging to the white matter. This has been proven considering a white matter segmentation obtained with SPM (`http://www.fil.ion.ucl.ac.uk/spm/`) and considering the voxels belonging to the white matter where the FA ranges from 0.2 to 0.16, thus the voxels where tensor deflection is used. As can be seen in figure 5.4, there are a non negligible number of voxel belonging to white matter characterized by those values of FA. With this technique, it has been possible to quantitatively evaluate the disruption to the tracts caused by white matter MS lesions. These lesions could be identified from the rest of the white matter on the basis of the estimated density of fibers that go through them.

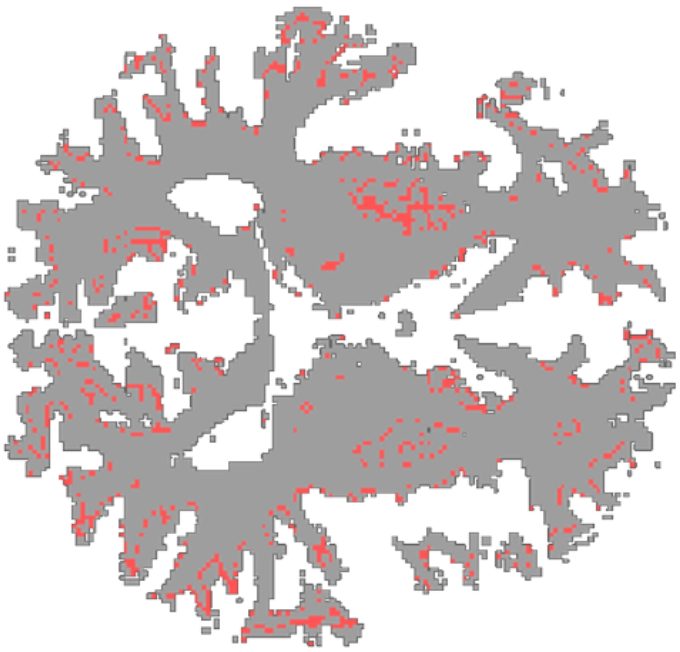

Figure 5.4: Segmentation of white matter for a MS patient considered in this study obtained with SPM (only voxels with probability of belonging to white matter ≥ 0.8 are considered) with superimposed (in red) voxels of white matter with a FA value ranging from 0.16 to 0.20. The segmentation has been done for the T1 image, then registered to DTI space.

Chapter 6

A novel method for the evaluation of structural connectivity in pathological brains

6.1 Introduction

The thalamus is a central deep gray matter structure, involved in sensory function and in regulating the level of consciousness, and is a relay for information directed to different cortex areas. The integrity of the connections from thalamus to cortex is of great importance, and any change in diffusivity along fiber tracts can be a sign of deterioration or damage. It is a key node in many of brain networks [164, 165, 120]. Damage to this key subcortical structure and its connections is an important determinant of outcome after TBI [166].

The best method for defining the location of a particular tract in patient groups with white matter damage is unclear and is topic of current research [115, 146].

The standard approach in the uninjured brain is to perform tractography in individual space to produce tracts in subject-specific space. This method can be performed in patients, but abnormalities in tract structure can be difficult to interpret. Tractography can evidentiate, in TBI patients, parts of the tract that appear to be absent [143, 145, 167] or a reduced number of tract fibers compared to controls [146]. However, abnormalities in tract structure might also result from a technical failure of the deterministic tractography algorithm because of low FA in parts of the white matter and, similarly, because of too high uncertainty in damaged areas for probabilistic tractography. Therefore, metrics extracted from tracts obtained directly in patients might be mis-leading, because severely damaged areas could be completely discarded from the tractographic reconstruction.

These issues have led to alternative proposals for ways to investigate the structure of specific white matter tracts in patient groups. For example, Hua and colleagues use deterministic tractography to define the structure of a number of large white matter tracts in healthy controls [115]. This information was combined across subjects and used to define mean tract locations in standard space, before transforming them back into individual space to study a MS patient with white matter damage.

On the basis of the previous findings, in this chapter an approach to investigate thalamo-cortical connectivity following TBI is proposed, without applying tractography directly on patients, to avoid misinterpretation of unsure results. In contrast to Hua and colleagues probabilistic tractography has been used in a young group of controls to define the location of a number of thalamo-cortical connections. These are then combined across subjects to derive a template of mean thalamo-cortical connectivity, which is used to investigate white matter structure along these tracts. To prove the feasibility of the use of such a template instead of individual tractography, the values of diffusion indices on healthy

obtained applying the template were evaluated, comparing them with values obtained using individual tractography. In the patients the advantages of taking the template approach are illustrated by comparing template results to the individual tractography. Differently from [115] and [116] white matter damage was evaluated quantitatively, in terms of number of voxels which result to be damaged in comparison to healthy individuals.

Unlike previous approaches, this method is independent from user defined parameters, as the FA threshold at which to terminate the tracking algorithm, thanks to the use of probabilistic tractography, which is not dependent on the FA value, and it is also not necessary to place specific ROIs in the patients space, since tractography in pathological brains is completely avoided. Also partial volume and registration problems discussed in [116] are addressed, using non-linear registration and excluding the possible presence of cerebrospinal fluid (CBF), using a masking technique.

This study was conducted in collaboration with the Computational, Cognitive and Clinical Neuroimaging Laboratory of Imperial College (Hammersmith Hospital), London, UK.

6.2 Dataset

The dataset was composed by 22 TBI patients (age 39 $\pm$ 11 years, 17 males, 5 females) and 21 age-matched healthy control subjects (age 35 $\pm$ 12 years, 10 males, 11 females). Patients were all recruited at least two months post injury (23 $\pm$ 17 months). Based on the Mayo classification system for TBI severity [64] there were 14 moderate/severe, and 8 mild (probable) cases of TBI. Injury was secondary to road traffic accidents (50%), falls (29%) and assaults (21%). Exclusion criteria were as follows: neurosurgery, except for invasive intracranial pressure monitoring (one patient); history of psychiatric or neurological illness prior to their head injury; history of significant previous TBI; anti-epileptic medication;

current or previous drug or alcohol abuse; or contraindication to MRI. The study was approved by the Hammersmith and Queen Charlotte's and Chelsea Research ethics committee, and all participants gave written informed consent.

6.3 Methods

6.3.1 MRI acquisition

MRI data were obtained using a Philips (Best, The Netherlands) Intera 3.0 Tesla MRI scanner using Nova Dual gradients, a phased array head coil, and sensitivity encoding (SENSE) with an under-sampling factor of 2. High-resolution images (T1-weighted MPRAGE) were acquired with the following acquisition parameters: matrix size 208 × 208; slice thickness=1.2 mm, 0.94 mm × 0.94 mm in plane resolution, 150 slices; TR=9.6 ms; TE=4.5 ms; flip angle 8°. Diffusion-weighted volumes with gradients applied in 64 non-collinear directions were collected. The following parameters were used: 73 contiguous slices, slice thickness = 2 mm, field of view (FOV) 224 mm, matrix 128 x 128 (voxel size = 1.75 x 1.75 x 2 mm^3), b value = 1000. Four images with no diffusion weighting (b = 0 s/mm^2) were also acquired.

6.3.2 Data processing

A high level overview of the methodology used is provided in figure 6.1. The approach here presented comprised the following steps: 1) data preprocessing; 2) definition of anatomical regions-of-interest in the control group to use as the starting point for tractography; 3) probabilistic tractography in the control group; 4) generation of mean thalamo-cortical tract templates; 5) validation of the tract templates in two control groups; 6) application of the template in patients for the investigation of white matter structure in the TBI group.

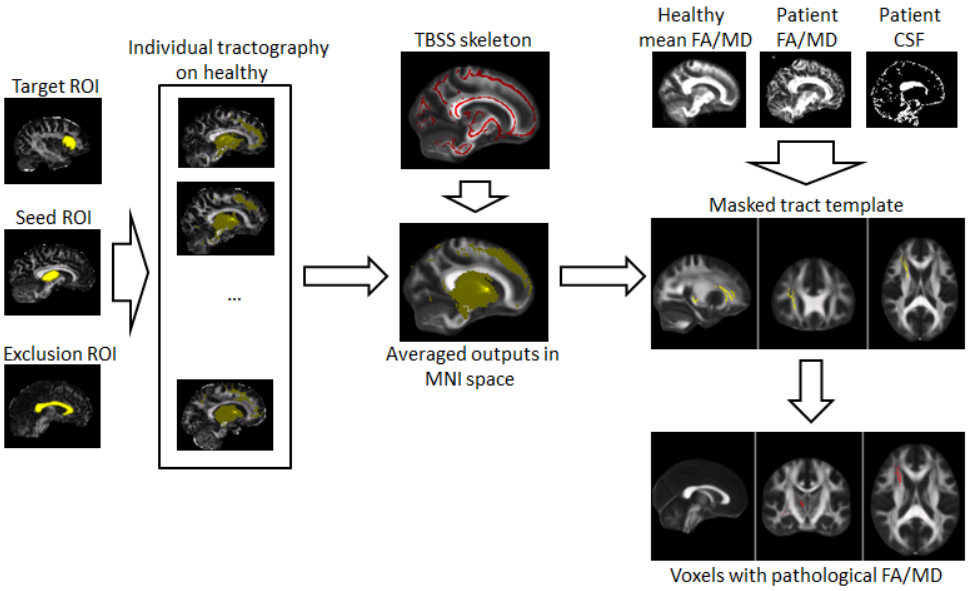

Figure 6.1: Summary of processing steps. Seed, target and exclusion ROI for tractography are identified in subject space for all healthy controls. Individual tractography is run for all healthy. The output is non-linearly registered to MNI 1 mm^2 standard space, averaged and binarized to get a mean white matter thalamo-cortical connectivity template for every considered tract. The obtained maps are then masked with a TBSS white matter skeleton. For every patient, the template is masked with a CSF mask, to avoid partial volume effects. Then, patients FA and MD values are compared to healthy mean FA and MD within the specified tracts, and voxels with abnormal values are counted.

Diffusion tensor imaging preprocessing

Diffusion-weighted images were registered to the b = 0 image by affine transformations to minimize distortion due to motion and eddy currents and then brain-extracted using BET [168], part of the FSL image processing toolbox [103, 104]. Voxelwise fractional anisotropy (FA) and mean diffusivity (MD) maps were generated using FDT in FSL [102, 120, 25].

Brain segmentation and region of interest definition

The MAPER (multi-atlas propagation with enhanced registration) procedure was used to generate the start and target points for tractography. Anatomical regions of interest were defined in native space from high-resolution T1 images. The procedure has previously been shown to yield accurate and robust segmentation results and to minimize the potential sampling error associated with misregistration [169, 170]. Bilateral thalamic regions were defined to provide the starting point of tractography. A number of cortical regions were then defined to provide the termination points of thalamo-cortical tracts likely to be damaged by TBI: bilateral anterior cingulate cortices, superior frontal, inferior frontal, superior temporal gyri and superior parietal lobe regions.

Probabilistic tractography

Probabilistic tractography was used to define thalamo-cortical connections in the control group [102, 25]. Ten tracts were generated for every subject. To limit inter-hemispheric connections, a corpus callosum ROI also obtained from the MAPER procedure was used as exclusion mask. Tractography was performed in DTI subject space. Therefore, DTI b = 0 images were linearly registered to T1 images and the inverted transformation matrix was applied to the T1 segmentation to bring the regions of interest into DTI space. The probabilistic tractography algorithm considered a maximum of two fibers per voxel. A curva-

ture threshold of 0.2 was employed, with 5000 samples producing the estimated fiber distribution for each seed voxel.

Mean connectivity template creation

Data from the 10 control subjects were then combined to create the thalamo-cortical connectivity template. Individual FA maps were non-linearly warped and registered to the 1x1x1 mm^3 FMRIB MNI FA template using FSL FNIRT tool [171, 172]. The transformation matrix obtained was then applied to the individual tractography outputs. Thalamo-cortical tract templates were generated by averaging the individual warped connectivity values in standard space, and retaining only the voxels whose intensity exceeded a specified threshold. The applied threshold was defined as the 5% of voxels with highest connectivity values. The obtained maps were then binarised. This identified voxels with a high likelihood of falling within a tract of interest across all controls.

Comparison with individual tractography

The validity of using a tract template to sample white matter integrity measures was investigated in the control subjects. To test if it is possible to obtain similar results using the mean tract template and individual tractography, mean FA and MD values and their distributions derived from tracts generated by both individual tractography and the tract templates were compared.

The rough output of individual probabilistic tractography is a spread map of values of connectivity, not comparable in terms of spatial extent with the template tracts, that consist in the voxels with the highest connectivity values across subject. Given that the number of voxels with a connectivity value different from zero obtained from the tractography algorithm is different for every individual, a 5% or fixed threshold would give a different volume for every subject, different from the volume obtained with the tract maps. Therefore, the same volume of voxels is kept, in terms of mm^3, both in the template tracts in standard space

and in individual DTI space. To do so, the number of voxels to be kept was calculated using the following relationship:

$$\text{Voxels to be retained} = \tag{6.1}$$

$$\text{voxels retained in standard space} \cdot \frac{\text{dimensions of individual space}}{\text{dimensions of standard space}} \tag{6.2}$$

The registration process involved in producing the tract templates can introduce partial volume errors, particularly around the edge of white matter tracts [173]. As part of the validation procedure the best way to minimize this problem has been investigated using two types of masking. Firstly, the white matter skeleton produced by TBSS was used as a mask. This 'skeleton' defines the center points of large white matter tracts and, by doing this, greatly limits the impact of partial volume effects. Secondly, a CSF mask produced by FSL FAST [174] and the gray matter masks of start and target regions were masked out of the assessment. The DTI metrics from the individual tractography and tract template approaches were then compared in three situations:

1. no masking;

2. white matter 'skeleton' masking;

3. 'skeleton' + CSF + ROIs masking.

Spearman's correlation statistics were used for mean MD and FA values and Wilcoxon rank-sum test ($p = 0.01$) for statistical distributions. Importantly, we performed the same set of analyses on a further group of 11 controls, who were not used to generate the template tracts. This was done to prove if the tract templates could be applied outside the original group, and still gives estimates of DTI metrics that correlated highly with those generated by individual tractography.

Tractography in the patients group

Then it was directly tested whether individual tractography in the patients group was problematic. To evaluate differences with the individual tractography algorithm, the FSL algorithm has been run also for the TBI patients, and the same comparisons of values of diffusion indices done for controls have been made for the patients. The FSL tractography has been run with the same procedure used for healthy during the generation of the template. In addition to considering the diffusion indices, also the evaluated dispersion of the estimates of the principal and second diffusion direction were taken into account. The dispersion values give a measure of the noise, thus of the uncertainty, of the estimation of the diffusion direction during the sampling from its probability density function. The dispersion values within the template tracts to the mean dispersion values obtained from healthy controls were compared.

Investigation of white matter damage in the patients

DTI metrics (FA and MD) were sampled from the patients using the tract templates defined in the control group. FA and MD maps were non-linearly registered into MNI space using FSL FNIRT. DTI measures in the patients were compared voxel-wise to the mean distribution obtained from all 21 controls. The percentage of voxels within each mask with FA and MD values more than 3 standard deviations away from the mean was calculated, to provide a measure of the severity of tract damage.

6.4 Results

6.4.1 Validation of a novel template for thalamo-cortical connectivity

A representation of the tracts comprised in the template is shown in figure 6.2.

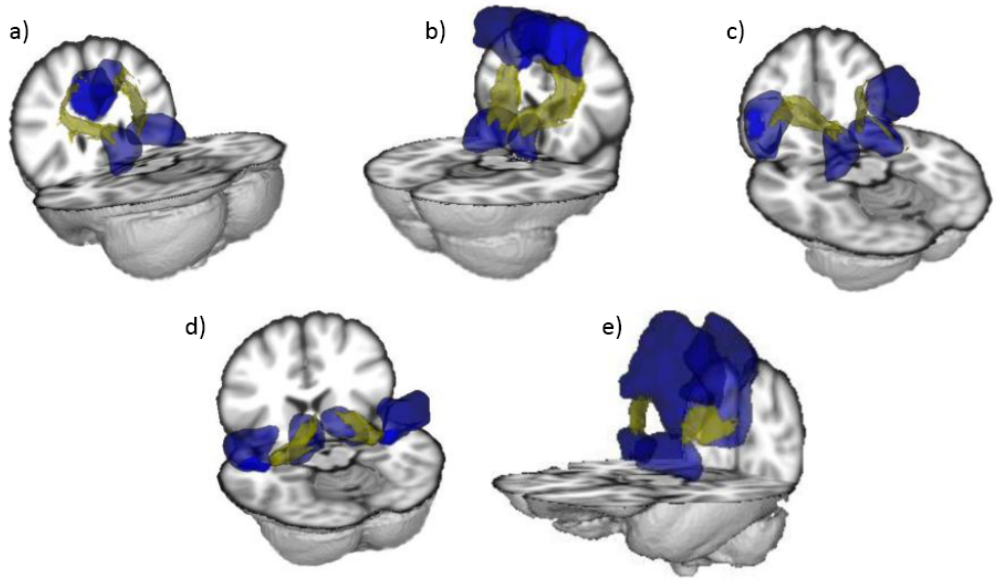

Figure 6.2: Averaged tracts in MNI standard space. ROIs are in blue, averaged tracts in yellow. Tracts from thalamus to anterior cingulate cortex (a), superior frontal gyrus (b), inferior frontal gyrus (c), superior temporal gyrus (d), superior parietal lobe (e).

Estimates of FA and MD were extracted from individual DTI data using both the tract templates and the individual probabilistic tractography. Visual inspection of the two tract estimates revealed a reasonable correspondence in their location. To quantify this correspondence, mean FA and MD were calculated for both approaches applying the two masking methods (TBSS skeleton with or without CSF and target ROIs exclusion). Then it was tested whether the two sets of values were correlated and whether they were from the same or different distributions. In general the masking procedure improved the number of tracts showing significant correlations of FA and MD. We first extracted DTI metrics from the group of subjects used to define the templates (N=10). In the case of FA only 2 tracts showed a significant correlation between the two approaches when no masking was used, with a Spearman correlation coefficient ρ of 0.88. 7 tracts significantly correlated when the TBSS skeleton was used to constrain the search area, with ρ ranging from 0.60 to 0.96. When the skeleton plus additional masking approach

Tract	*No masking* *Spearman ρ* (p)	*Mask I* *Spearman ρ (p)*	*Mask II* *Spearman ρ (p)*
Left TH − left ACC	0.51 (0.13)	0.60 (0.07)	0.89(<0.01)
Left TH − left IFG	0.34 (0.33)	0.82(<0.01)	0.90(<0.01)
Left TH − left SFG	0.58 (0.08)	0.59(0.08)	0.94(<0.01)
Left TH − left PL	0.28 (0.43)	0.54(0.11)	0.53(0.12)
Left TH − left TG	0.87 (0.002)	0.72(0.02)	0.59(0.08)
Right TH − right ACC	0.27 (0.45)	0.96(<0.01)	0.84(0.004)
Right TH − right IFG	0.42 (0.23)	0.81(<0.01)	0.89(<0.01)
Right TH − right SFG	0.88 (<0.01)	0.79(<0.01)	0.43(0.21)
Right TH − right PL	0, 52(0.13)	0.95(<0.01)	0.85(<0.01)
Right TH − right TG	0.21 (0.55)	0.60(0.07)	0.73(0.02)

Table 6.1: Spearman correlation coefficient for the mean FA values of all the considered thalamo-cortical tracts, using both masking approaches, for the healthy subjects from which the template has been derived

was used 7 tracts showed significant correlations, with coefficients ranging from 0.84 to 0.94. For MD, with no masking 4 tracts significantly correlated, with Spearman ρ from 0.66 to 0.73. Applying both masking techniques, all tracts correlated significantly, with coefficients ranging from 0.61 to 0.97. All correlation results are reported in tables 6.1 and 6.2.

The same metrics from a second group of controls (N=11), not involved with the template creation, were extracted. In this case, for FA, 5 tracts showed significant correlation with no masking, with ρ ranging from 0.72 to 0.82. Applying the TBSS mask, 7 tracts significantly correlated, with coefficients from 0.71 to 0.91. 7 tracts resulted to show significant correlation also masking for CBF, where the ρ ranged from 0.68 to 0.98. For MD, 7 tracts correlated significantly with no masking, with ρ values from 0.63 to 0.88. With the two masking approaches, all tracts showed a significant correlation, with coefficients from 0.65 to 0.98. Correlation coefficient in the three cases are reported in tables 6.3 and 6.4.

Next it has been tested whether the DTI metrics produced by the different approaches belonged to different statistical distributions. Convergence of the ap-

Tract	*No masking* *Spearman ρ* (p)	*Mask I* *Spearman ρ (p)*	*Mask II* *Spearman ρ (p)*
Left TH − left ACC	0.66 (0.04)	0.94 (<0.01)	0.90 (<0.01)
Left TH − left IFG	0.49 (0.15)	0.90 (<0.01)	0.86 (<0.01)
Left TH − left SFG	0.60 (0.07)	0.90 (<0.01)	0.87 (<0.01)
Left TH − left PL	0.64 (0.05)	0.75 (<0.01)	0.76 (0.01)
Left TH − left TG	0.66 (0.04)	0.78 (0.01)	0.61 (0.05)
Right TH − right ACC	0.28 (0.43)	0.85 (<0.01)	0.93 (<0.01)
Right TH − right IFG	0.73 (0.02)	0.90 (<0.01)	0.90 (<0.01)
Right TH − right SFG	0.72 (0.02)	0.95 (<0.01)	0.88 (<0.01)
Right TH − right PL	0.36 (0.31)	0.96 (<0.01)	0.85 (<0.01)
Right TH − right TG	0.26 (0.47)	0.97 (<0.01)	0.82 (<0.01)

Table 6.2: Spearman correlation coefficient for the mean MD values of all the considered thalamo-cortical tracts, using both masking approaches, for the healthy subjects from which the template has been derived

Tract	*No masking* *Spearman ρ* (p)	*Mask I* *Spearman ρ (p)*	*Mask II* *Spearman ρ (p)*
Left TH − left ACC	0.82 (<0.01)	0.89 (<0.01)	0.92(<0.01)
Left TH − left IFG	0.06 (0.86)	0.91(<0.01)	0.56(0.07)
Left TH − left SFG	0.82 (<0.01)	0.57(0.09)	0.73(<0.01)
Left TH − left PL	0.79 (<0.01)	0.78(<0.01)	0.28(<0.40)
Left TH − left TG	0.57 (0.07)	0.88(<0.01)	0.98(<0.01)
Right TH − right ACC	0.77 (<0.01)	0.77(<0.01)	0.74(0.01)
Right TH − right IFG	0.32 (<0.01)	0.87(<0.01)	0.78(<0.01)
Right TH − right SFG	0.72 (<0.01)	0.71(0.02)	0.81(<0.01)
Right TH − right PL	0.35(0.28)	0.73(0.02)	0.81(<0.01)
Right TH − right TG	0.49 (0.12)	0.56(0.08)	0.68(0.02)

Table 6.3: Correlation coefficient for the mean FA values of all the considered thalamo-cortical tracts, using all masking approaches, for 11 healthy subjects not involved in the template creation

Tract	*No masking* *Spearman ρ* (p)	*Mask I* *Spearman ρ (p)*	*Mask II* *Spearman ρ (p)*
Left TH − left ACC	0.88 (<0.01)	0.90 (<0.01)	0.90 (<0.01)
Left TH − left IFG	0.52 (0.1)	0.86 (<0.01)	0.90 (<0.01)
Left TH − left SFG	0.63 (0.04)	0.88 (<0.01)	0.97 (<0.01)
Left TH − left PL	0.63 (0.04)	0.98 (<0.01)	0.92 (<0.01)
Left TH − left TG	0.44 (0.18)	0.69 (0.02)	0.91 (<0.01)
Right TH − right ACC	0.74 (<0.01)	0.65 (0.03)	0.95 (<0.01)
Right TH − right IFG	0.73 (0.01)	0.78 (<0.01)	0.75 (<0.01)
Right TH − right SFG	0.69 (0.02)	0.85 (<0.01)	0.95 (<0.01)
Right TH − right PL	0.79 (<0.01)	0.86 (<0.01)	0.92 (<0.01)
Right TH − right TG	0.11 (0.43)	0.77 (<0.01)	0.79 (<0.01)

Table 6.4: Correlation coefficient for the mean MD values of all the considered thalamo-cortical tracts, using both masking approaches, for 11 healthy subjects not involved in the template creation

proach would result in samples from the same distribution, so this provides a measure of how closely aligned the tract regions were from a statistical point of view. For FA in the group used to define the tract templates, with no masking 62% of the studied tracts came from statistically different statistical distributions. This decreased to 17% with the first masking technique and 8% when the second was used. For the separate group, with no masking, 74% had different distributions. This fell to 14% for the first masking technique and 13% using the second technique. Figure 6.3 shows a representative example of the FA values distributions from a healthy subject. No specific tracts have been identified that consistently showed values to come from different distributions with all different masking approaches or across different subjects.

Similar results were found with MD, although more tracts were found where the distributions were distinct. In the group used to define the templates 74% or tracts showed results from different distributions. This fell to 41% for the first masking technique and 37% for the second. For subjects not involved in the atlas creation, 72% of tracts had values from distinct statistical distributions, falling to 34% and to 30% for the two masking techniques. These results demonstrate that

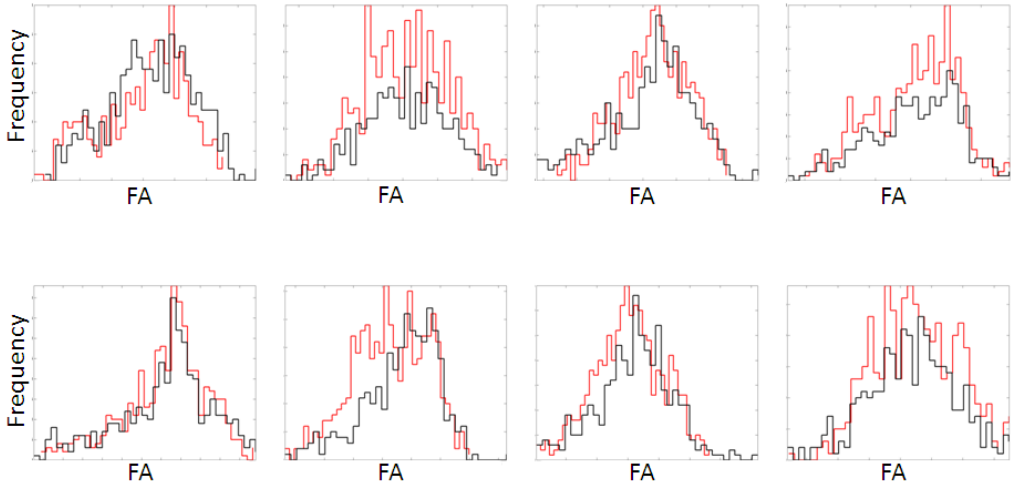

Figure 6.3: Distribution of FA in the right thalamus to parietal lobe . Overlaid histograms of FA values for every voxel belonging to the individual tractography output (black line) and to the mean projected tract (red line). This is demonstrated for TBSS skeleton plus gray matter masking . Distributions depicted for four healthy controls not involved in the atlas creation (top row) and for four belonging to the group from which the atlas was derived (bottom row).

focusing the analysis of white matter to regions at the centre of each tract produces results that converge between the approaches. This supports the proposal that a mean tract template can be used in most cases to robustly sample DTI metrics from large white matter tracts, and that this approach can be generalized to subjects not used to define the original tract templates.

6.4.2 Application of a thalamo-cortical connectivity template in traumatic brain injury patients

The percentage of voxels with abnormal MD and FA values within the tracts maps and within the maps obtained with individual tractography was investigated. Abnormality was defined as voxels where the considered diffusion parameter value was more than 3 standard deviations away from the mean value of the whole normal group. This technique was sensitive to demonstrating damage within the tracts examined. The hypotesis, regarding the individual tractography results, was that where large amounts of white matter damage was present, the output of tractography would be disrupted. We tested this by performing probabilistic

tractography between in patients as stated in 6.3.2.

The potential problems are illustrated by considering patients with and without extensive damage to the tract connecting the right thalamus to right anterior cingulate cortex (figure 6.4). In a patient with a low amount of abnormal voxels (patient 1 - 1.17% MD, 0% FA) tractography produces a similar result to that found for the mean tract template in the normal subjects. However, for a patient with a large amount of damage (patient 5 - 28.81% MD, 7,19 %FA) tractography produces a very atypical tract. This extends far outside the likely location of this tract and is likely to be a spurious result of the tractography algorithm failing to cope with the effects of the white matter damage, as there are no gross abnormalities visible on standard structural imaging in this area. A similar finding is illustrated for the thalamic to inferior frontal gyrus tract (figure 6.5), in a patient that shows extensive damage in the white matter. Patient 1 (0.69% MD, 0% FA) and patient 6 (47.96% MD, 27.35% FA) are shown. Here, the tractography fails almost completely in the patient's brain and it would be not possible to sample diffusion indices in that area using individual algorithm. Using the template, the analysis of diffusion can be extended to that area, that in normals belongs to a well-defined white matter tract.
To better highlight the potential problems given by running the probabilistic tractography in patients, the estimated dispersion relative to the principal and the secondary diffusion direction have been taken into consideration. It is to be expected that for patients the dispersion, that is a quantification of the uncertainty in the estimation of the diffusion direction, has higher values than for controls, where the tractography in the white matter deals with normal, healthy tissue. Results for this analysis can be seen in figure 6.6 and figure 6.7. It can be seen that for patients the dispersion is consistently higher in respect to healthy.

We next compared the estimates of damage produced by using the patients' trac-

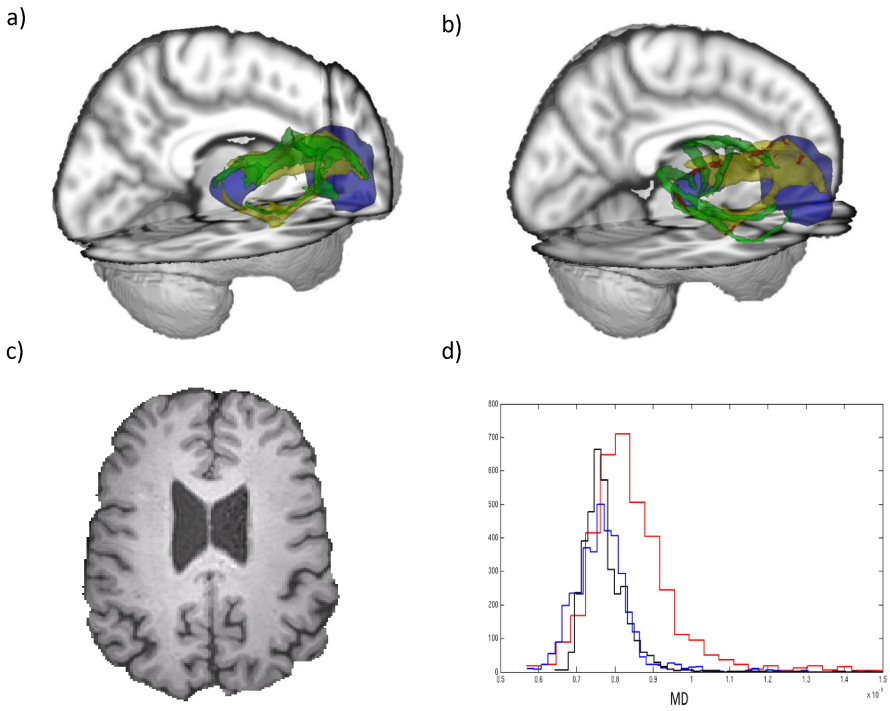

Figure 6.4: 3D representation of tract from right thalamus to right anterior cingulate cortex. Blue ROIs: right thalamus and right anterior cingulate cortex. Yellow tract: template averaged tract. Green tract: Individual tractography output. Red areas: voxels with MD > MDmean + 3sd. A patient with a low percentage of damaged voxels (a) and a patient with a high percentage of voxels with high MD (b) are depicted. c)) T1 slice for the same subject depicted in b). The structural image does not show gross damage. d) Histogram of MD values in the same tract depicted above. Black: mean atlas MD. Blue: MD values for patient depicted in a) (patient 1). Red: MD values for patient depicted in b) (patient 5).)

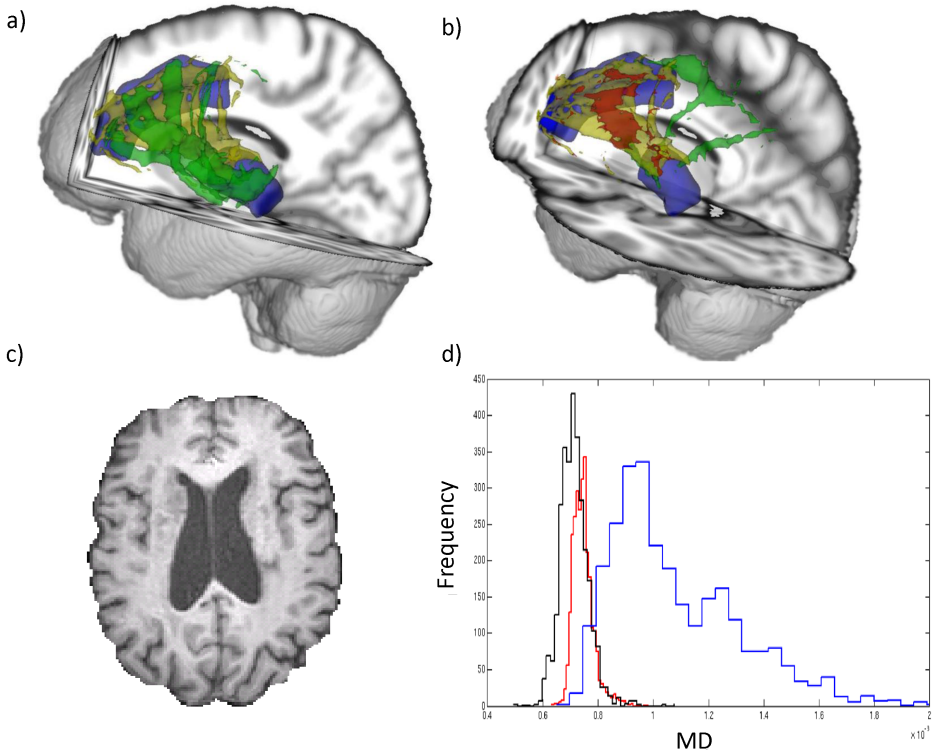

Figure 6.5: 3D representation of tract from left thalamus to left inferior frontal gyrus. Blue ROIs: left thalamus and left inferior frontal gyrus. Yellow tract: atlas tract. Green tract: individual tractography output. Red areas: voxels with MD > MDmean + 3sd. A patient with a low percentage of damaged voxels (a) and a patient with a high percentage of voxels with high MD (b) are depicted. c) T1 slice for the same subject depicted in b). The structural image does not show, especially on the left side, a load of damage that prevents the presence of a white matter tract. That tract is not detected by tractography. d) Histogram of MD values in the same tract depicted above. Black: mean atlas MD. Blue: MD values for patient 1. Red: MD values for patient 6.

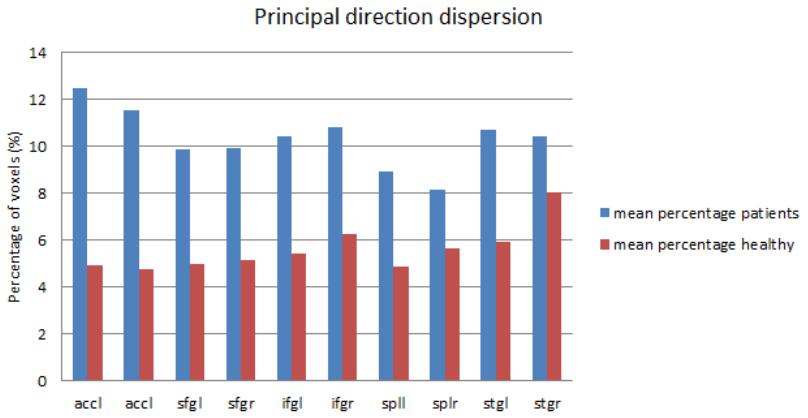

Figure 6.6: Mean percentage across subjects of the number of voxels with dispersion higher than the mean healthy dispersion + 3SD for the principal diffusion direction. Patients have a higher percentage of voxels with high dispersion in the analysed tracts, with values significantly different from those of healthy in 8 out of 10 tracts.

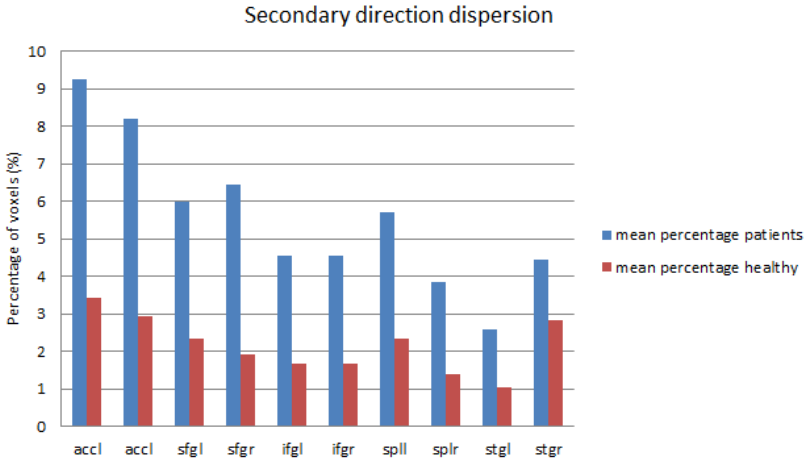

Figure 6.7: Mean percentage across subjects of the number of voxels with dispersion higher than the mean healthy dispersion + 3SD for the secondary diffusion direction. Patients have a higher percentage of voxels with high dispersion in the analysed tracts, with values significantly different from those of healthy in 8 out of 10 tracts.

tography and the tract template assessment. Mean FA and MD were extracted using both approaches, with the second masking approach used to maximize sensitivity to damage and exclude CSF, that is often present in large quantities in patients. Using the template, the number of voxels with abnormal diffusion charachteristics was in general higher than using the output of tractography, especially for patients with a high level of damage (see tables 6.5, 6.6, 6.7, 6.8).

6.5 Discussion

Thalamic dysfunction appears to be a key determinant of clinical outcome after TBI e. g. [175]. Therefore, the ability to robustly define the impact of TBI on thalamo-cortical connections is important. The key finding is that areas of low FA resulting from traumatic axonal injury after TBI disrupt the reconstruction of individual tracts. This results in uncertainty about the validity of the tracts produced in individual patients, and makes DTI metrics extracted from these tracts difficult to interpret. This is an important problem as DTI is increasingly being used to study the pathological effects of TBI e.g.[176, 177, 178], and it is important to quantify the amount of damage within particular tracts of interest [146]. The use of probability maps coupled with careful registration provides an alternative to tractography performed in individual patients. It is shown how this can be used in TBI patients to estimate the amount of damage in a particular tract.

Probability maps of large tracts have previously been shown to provide an efficient tool for investigating white matter structure that bypass some of the problems of performing tractography in patient populations [115]. In this study maps for 11 large white matter tracts were generated from control DTI data. The method described in this thesis addresses two problems cited in [115, 116], i.e. difficult registration and partial volume effects. The registration between DTI individual

Tract	Percentages (%)																					
	1	2	3	4	5	6	7	8	9	10	11	12	13	14	15	16	17	18	19	20	21	22
Left TH - left ACC	0.64	0.68	2.53	2.85	10.53	63.17	2.63	1.99	3.52	0.89	1.42	1.99	0.07	1.99	0.53	3.13	7.37	0.39	14.13	0.46	12.78	0.39
Right TH - right ACC	1.17	2.89	0.49	16.06	28.81	71.84	2.76	6.27	5.31	6.60	7.92	4.79	0.31	2.12	0.09	12.81	21.90	0.25	15.23	1.78	6.36	0.28
Left TH - left IFG	0.69	0.38	1.02	4.80	10.84	47.96	2.22	2.36	5.68	1.02	4.55	2.88	0.22	2.91	0.41	4.53	6.36	0.38	17.97	0.63	14.79	1.10
Right TH - right IFG	1.12	2.28	1.36	17.82	19.92	53.92	1.56	5.67	6.22	7.88	5.48	3.05	0.67	4.24	0.22	19.15	20.12	0.25	15.04	4.11	9.89	1.12
Left TH - left SFG	0.55	0.35	0.39	3.38	14.32	59.13	2.74	2.35	7.46	1.13	2.23	3.36	0.14	4.33	0.32	5.00	5.64	0.30	16.79	0.58	13.33	0.25
Right TH - right SFG	1.76	2.60	0.95	16.17	23.89	62.07	1.83	6.73	5.61	7.74	7.37	5.59	0.18	6.56	0.13	17.25	16.92	0.26	18.09	3.19	7.48	0.31
Left TH - left PL	0.28	0.18	0.28	2.20	20.79	37.80	0.30	0.58	3.31	2.12	2.02	8.91	0.13	2.85	0.56	8.02	12.47	0.18	10.75	0.45	11.00	2.07
Right TH - right PL	0.95	1.69	1.18	2.41	26.71	38.48	0.90	2.27	2.13	9.81	3.49	16.72	0.95	1.76	0.12	7.84	11.91	0.02	18.04	5.74	11.12	0.93
Left TH - left TG	0.33	0.37	1.47	1.76	11.42	15.32	0.53	0.87	5.23	1.53	1.07	5.23	0.37	1.67	0.23	7.19	11.86	0.07	6.36	2.30	10.12	1.80
Right TH - right TG	1.43	4.25	2.76	3.67	23.20	18.30	2.08	2.21	2.53	10.61	3.47	12.36	1.07	3.02	0.32	13.86	13.40	0.00	12.56	9.28	11.65	0.75

Table 6.5: Percentage of voxels with MD higher than healthy mean MD for 22 TBI patients. Percentages computed using the tracts obtained from the atlas.

	Percentages (%)																					
Tract	1	2	3	4	5	6	7	8	9	10	11	12	13	14	15	16	17	18	19	20	21	22
Left TH - left ACC	0.36	0.39	1.60	1.32	0.00	1.03	0.00	0.25	0.46	0.50	0.75	1.49	0.00	0.00	0.00	0.64	0.00	0.00	5.05	0.00	7.69	0.25
Right TH - right ACC	0.06	1.17	0.37	2.83	0.00	21.78	0.03	1.11	2.09	2.06	1.97	3.47	0.06	1.17	0.09	5.22	7.22	0.18	6.45	1.57	5.04	0.12
Left TH - left IFG	0.27	0.27	0.49	3.07	3.54	6.26	0.05	0.14	1.04	0.60	1.76	2.63	0.03	1.32	0.19	0.00	0.91	0.22	10.59	0.03	12.15	0.16
Right TH - right IFG	0.42	0.79	0.20	9.24	3.99	28.94	0.27	0.25	3.30	1.07	2.33	1.91	0.42	1.39	0.12	10.41	9.34	0.10	7.68	2.92	5.33	0.77
Left TH - left SFG	0.39	0.28	0.30	2.07	3.55	20.15	0.39	0.71	1.73	0.44	0.78	2.46	0.07	0.41	0.00	0.21	0.12	0.00	10.52	0.07	9.92	0.21
Right TH - right SFG	0.26	1.25	0.42	3.96	2.40	32.81	0.26	1.85	3.72	3.15	2.07	5.21	0.09	3.17	0.15	7.66	9.35	0.26	11.79	2.95	5.17	0.13
Left TH - left PL	0.25	0.08	0.05	1.64	16.50	31.04	0.08	0.18	1.97	1.89	0.43	8.88	0.00	0.88	0.03	2.80	3.41	0.10	9.21	0.08	10.45	1.67
Right TH - right PL	0.81	0.74	0.37	1.83	23.29	24.26	0.14	1.41	1.09	5.76	2.27	14.89	0.44	1.30	0.07	6.11	11.12	0.00	13.02	3.58	8.79	0.65
Left TH - left TG	0.23	0.33	1.13	1.43	7.89	11.72	0.07	0.30	4.20	0.40	0.37	5.00	0.00	0.70	0.07	1.17	3.40	0.07	3.73	0.23	9.12	1.37
Right TH - right TG	1.33	3.05	2.34	3.05	19.99	13.34	0.71	1.91	2.34	4.74	1.98	9.80	0.75	1.85	0.29	10.09	12.56	0.00	9.09	6.07	6.20	0.78

Table 6.6: Percentage of voxels with MD higher than healthy mean MD for 22 TBI patients. Percentages computed using the individual tractography outputs.

Tract	Percentages (%)																					
	1	2	3	4	5	6	7	8	9	10	11	12	13	14	15	16	17	18	19	20	21	22
Left TH - left ACC	0,00	0,23	0,63	1,06	7,84	28,68	3,34	0,30	2,18	2,58	0,23	2,08	0,10	1,46	0,04	1,26	1,42	0,33	4,05	0,22	2,52	0,96
Right TH - right ACC	0,00	0,18	0,70	7,19	6,11	39,42	1,70	1,41	1,37	0,53	0,21	2,02	0,00	0,10	0,00	0,97	1,08	0,35	5,23	0,35	1,03	0,64
Left TH - left IFG	0,00	0,16	0,16	1,44	7,90	27,35	2,19	0,82	2,94	3,98	0,19	2,53	0,24	4,03	0,09	2,09	1,31	0,29	4,52	0,27	3,86	1,19
Right TH - right IFG	0,00	0,17	0,61	12,35	6,70	36,78	2,23	2,15	1,37	4,11	0,20	2,71	0,11	1,48	0,00	4,71	2,98	0,27	4,16	0,56	2,61	0,80
Left TH - left SFG	0,00	0,24	0,09	2,40	7,15	27,71	2,09	0,91	3,22	2,66	0,40	2,52	0,11	3,87	0,05	2,47	1,67	0,31	4,72	0,48	2,94	1,06
Right TH - right SFG	0,00	0,24	0,09	2,40	7,15	27,71	2,09	0,91	3,22	2,66	0,40	2,52	0,11	1,90	0,13	2,47	1,67	0,31	4,72	0,48	2,94	1,06
Left TH - left PL	0,00	0,17	0,25	0,20	4,71	14,89	0,10	0,03	0,68	1,01	2,19	1,68	0,03	0,13	0,03	1,23	2,08	0,15	1,68	0,37	0,87	1,32
Right TH - right PL	0,02	0,17	0,05	0,21	3,68	12,21	0,17	0,00	0,74	1,82	0,76	3,67	0,17	0,10	0,08	3,30	3,53	0,11	5,67	0,49	1,38	0,30
Left TH - left TG	0,13	0,20	0,07	0,40	6,48	10,12	0,00	0,32	0,62	2,93	0,59	0,65	0,14	0,23	0,00	2,09	2,17	0,00	0,49	0,81	1,54	0,53
Right TH - right TG	0,03	0,06	0,03	0,20	6,25	9,23	0,35	0,00	0,10	4,96	0,16	3,71	0,14	0,35	0,00	3,77	3,31	0,00	0,86	0,96	2,30	0,64

Table 6.7: Percentage of voxels with FA lower than healthy mean FA for 22 TBI patients. Percentages computed using the thalamo-cortical template.

Tract	Percentages (%)																					
	1	2	3	4	5	6	7	8	9	10	11	12	13	14	15	16	17	18	19	20	21	22
Left TH - left ACC	0,00	0,21	0,28	0,87	0,09	10,82	1,20	0,33	0,12	0,43	0,17	2,04	0,00	0,09	0,04	0,49	1,02	10,82	6,46	0,49	2,40	1,76
Right TH - right ACC	0,04	0,20	0,08	0,85	4,58	7,32	1,35	0,24	0,00	0,00	0,00	1,89	0,00	1,64	0,15	0,00	0,67	19,67	7,69	0,00	6,79	2,40
Left TH - left IFG	0,04	0,26	0,22	20,35	4,01	13,98	0,95	0,88	0,05	0,62	0,03	1,47	0,99	0,83	0,05	5,30	5,15	12,68	4,35	1,50	3,60	2,56
Right TH - right IFG	0,01	0,21	0,08	0,92	5,18	6,96	1,13	0,57	0,00	0,00	0,00	1,80	0,08	0,84	0,00	2,82	0,66	12,31	6,23	0,02	5,12	2,68
Left TH - left SFG	0,02	0,33	0,20	2,13	1,63	12,72	1,56	0,77	0,25	0,64	0,85	1,02	0,02	0,83	0,05	1,35	1,49	12,93	6,24	0,92	3,77	1,80
Right TH - right SFG	0,00	0,09	0,04	0,15	1,53	4,10	0,09	0,02	0,00	0,00	0,00	0,90	0,00	0,09	0,00	0,51	0,90	7,41	3,31	0,08	2,13	1,84
Left TH - left PL	0,05	0,20	0,08	0,16	1,49	4,70	0,13	0,05	0,39	0,05	0,23	1,65	0,57	0,18	0,07	3,88	5,09	8,71	5,42	1,11	2,07	0,79
Right TH - right PL	0,03	0,07	0,02	0,19	2,19	2,38	0,06	0,03	0,00	0,00	0,00	0,37	0,00	0,34	0,00	1,37	0,76	10,28	1,09	0,27	2,82	0,91
Left TH - left TG	0,06	0,16	0,07	0,11	2,32	3,56	0,35	0,03	0,00	0,00	0,11	1,65	0,87	0,10	0,02	3,78	5,16	4,81	1,50	1,89	2,80	0,84
Right TH - right TG	0,00	0,21	0,28	0,87	0,09	10,82	1,20	0,33	0,12	0,43	0,17	2,04	0,00	0,09	0,04	0,49	1,02	10,82	6,46	0,49	2,40	1,76

Table 6.8: Percentage of voxels with FA lower than healthy mean FA for 12 TBI patients. Percentages computed using the individual tractography outputs.

spaces and the MNI template has been made using nonlinear techniques, to account for deformations and to provide a more precise alignment with standard space. In fact, transformation to a standard space must account also for deformations that can not be covered with a linear transformation, whereas when the alignment is made between images acquired with different imaging methods, or in different times, for the same subject, linear registration can provide all the necessary information. Moreover, the use of a nonlinear method is a powerful way to achieve the best alignment for pathological brains. After a thorough visual assessment of the registrations, it has been possible to note that the use of nonlinear algorithms can give more accurate mapping from individual to MNI space in the case of the here considered TBI patients.
To avoid partial volume effects, only the center of the selected tracts are considered, using a white matter skeleton obtained using the TBSS procedure, and also masked out the CSF, that is enlarged in patients, utilizing an individual CSF segmentation obtained with FSL. This is particularly important in the case of the most severely affected patients, because the CSF is massively present also in areas normally not affected by partial volume, and obviously the inclusion of CSF in the evaluation of damage could lead to erroneous considerations.

Using probabilistic tractography has some advantages over deterministic tractography, particularly when one wants to investigate tracts that involve deep gray matter structures. Moreover, probabilistic tractography relies less than deterministic on user-dependent parameters as the FA thresholds. The benefits of masking the probability maps are specifically addressed, and it is shown that focusing investigation to the center of white matter tracts, as expected, produces a better convergence of results between the probability templates and the individual tractography approaches in the control group.

As with any in vivo human tractography study there is no 'gold standard' for

identifying the location of white matter tracts. Probabilistic tractography in an individual can produce idiosyncratic and noisy estimates of tract location, which may complicate the comparison of results across individuals and across groups of subjects. The goal of using the template tracts was to provide a more robust way of estimating white matter integrity from areas of white matter that in general are contained within a particular tract of interest. A complete correspondence between the two approaches is not to be expected, but comparing them provides a way of studying how much they converge on similar answers. An inter-subject variation in tractography outputs is to be expected. [116] showed that, although the overlap between individual results and a tracts template is not expected to be perfect, the use of a template, obtained for particular white matter tracts and using deterministic tractography, can be considered to give results comparable to those obtained with individual tractography. Not only diffusion indices obtained with the two methods strongly correlate, but it is also not possible to find a statistical difference between the distribution of values of these indices obtained from the template and from individual results in the majority of cases. This result is confirmed when these correspondences have been tested in healthy subjects not involved in the template creation, in addition to those from which the template tracts have been derived.

Chapter 7

Evaluation of diffusion indices in patients

7.1 Introduction

As seen in chapter 2, water diffusion characteristics can help in the interpretation of disease and in particular of microstructural damage, which is often present in neurological and psychiatric pathologies. In the course of this chapter, three pathologies will be taken into consideration: multiple sclerosis, schizophrenia and bipolar disorder. These two last diseases will be accounted for in conjunction, because the interest was in finding structural differences between the two pathologies. Aim of this part of the thesis is to find structural abnormalities, in terms of diffusion indices, in particular FA, in patients.

In the case of multiple sclerosis, the analysis described in next sections focuses on gray matter damage. As already introduced, multiple sclerosis patients often show gray matter lesions, that in the past weren't extensively considered. More recently, it has been demonstrated that conventional MRI only shows a minimal part of the real lesion load in gray matter [179, 180]. Moreover, these lesions seem to be related to the clinical cognitive impairment in patients [181, 182] and

they have been demonstrated to be present since the early stages of disease for example in [183, 184]. Cortical pathology is histologically different from white matter [180], in example massive demyelination of gray matter is found, as well as less inflammation in respect to white matter lesions. Cortical pathology is to date still not clear, thus it is of importance to gain information about the structural changes that occur for this tissue. Aim of this study was to determine if the diffusion characteristics of gray matter lesions are different from the normal-appearing gray matter, and if they change over time.

In 7.3.2 a whole brain analysis [173] for FA values of patients affected by schizophrenia or bipolar disorder is presented. As described in section 2.2.3, white matter abnormalities in these pathologies, in terms of fractional anisotropy (FA), are reported by several studies investigating the neuropathology of these disorders. The study here presented is the first that compares directly these two pathologies in term of diffusion whole-brain analysis.

7.2 Datasets

7.2.1 Dataset 1: MS patients for the evaluation of cortical lesions

In this study, 34 patients (12 males, 22 females, age 38 $\pm$ 12 years , duration of disease 11 $\pm$ 9 years, EDSS 3.3 $\pm$ 1.8) affected by relapsing-remitting multiple sclerosis were considered. Patients underwent MRI acquisitions with a 1.5T scanner (Philips Achieva, Philips Medical Systems, Best, the Netherlands) twice, in a 9-months period. The acquisition scheme comprised a high-resolution T1 sequence (TR = 25 ms, TE = 4.6, 256 x 256 x 120 matrix), a DTI sequence with 15 non-collinear directions of acquisition (TR = 15634 ms, TE = 25 ms, TI = 3400 ms, 256 x 256 x 50 matrix, 15 gradient directions, B0 = 800 s x mm^2), and a DIR (TR = 7974 ms, TE = 74 ms, 256 x 256 x 50 matrix) sequence. All patients were examinated in Euganea Medica, Padova, Italy. This study was conducted

in collaboration with the Multiple Sclerosis Centre of Veneto region, Dept. of Neurosciences, University Hospital of Padova, Italy.

7.2.2 Dataset 2: schizophrenia and bipolar disorder patients

61 healthy controls, 17 schizophrenic patients and 9 patients affected by bipolar disorder underwent MRI scans using a 3T Siemens Allegra scanner. DTI data were acquired along 30 directions, with parameters B0 = 1000 s x mm^2 and matrix 128 x 128 x 23, TR = 5000 ms, TE = 118 ms. This study was done in collaboration with the Section of Psychiatry and Psychological Medicine, Inter-University Center for Behavioural Neurosciences, University of Verona, Verona, Italy.

7.3 Methods

7.3.1 ROI-based studies of multiple sclerosis patients

Patients DTI images were corrected for distortions caused by eddy currents using FSL - FMRIB's Diffusion Toolbox (FDT) (`www.fmrib.ox.ac.uk/fsl`). All volumes of the DTI sequence were registered to the first volume without diffusion weighting, with a combination of scaling and translation [185].

FA maps were obtained with the linearized model [17] using the same software (FSL). T1 images were registered to the DTI using a linear transformation with FSL-FLIRT [163]. Thereafter, DIR images were registered to the previously registered T1 images, so that both DIR and T1 images were in subjects DTI space. GM lesions at the two time points were manually segmented on the DIR images and registered to the DTI using the same transformation used for the DIR images. Only lesions containing more than 5 voxels were considered. Cerebral GM was segmented using SPM (`http://www.fil.ion.ucl.ac.uk/spm/`) from the T1 images. Voxels with a probability greater than 0.8 to belong to gray matter were considered. . Mean FA and SD were calculated for the whole gray matter and

for the gray matter MS lesions.

The values of FA were compared in the two time points, and gray matter FA was compared with lesion FA (ranksum test, p = 0.05). Results of this study were combined with those of a study involving cerebral perfusion in the same patients and lesions.

7.3.2 Whole brain studies of schizophrenia and bipolar disorder patients

Also for this study, image processing was done using FMRIB-FSL software. Eddy currents correction was applied and FA maps were calculated using the linearized model. Using the tract-based spatial statistics (TBSS) procedure [173], all FA maps were non-linearly registered to the Montreal Neurological Institute (MNI) standard space, using the FMRIB-58_FA standard space(created from the FA maps of 58 healthy adult subjects brought in MNI space) with a resolution of 1 x 1 x 1 mm. All images were visually checked to ensure that the normalization process didn't cause misalignment or abnormal deformations. A FA skeleton was then obtained, thinning the mean FA map and keeping only the center of the white matter tracts. Then, to avoid residual misalignment, for all subjects the appropriate voxels were projected into the skeleton, by choosing the voxel with the highest FA along the perpendicular to the skeleton structure. Voxelwise statistics were then performed using permutation-based nonparametric inference, using randomize FSL tool. Schizophrenic patients - controls, bipolar patients - controls and bipolar - schizophrenic patients contrasts were tested, taking into consideration only a subset of healthy, to match the patients for age. Multiple comparisons were corrected using threshold-free cluster enhancement (TFCE), with a level of significance of p = 0.05. The analyses were conducted considering age as a nuisance covariate to avoid confounding effects due to age differences between the groups.

7.4 Results

7.4.1 ROI-based studies of multiple sclerosis patients

Mean and standard deviation (SD) of the FA of the voxels belonging to lesions were computed, using manually drawn ROIs on the DIR images, brought using linear registration into individual DTI spaces. Each parameter was computed both considering the mean value across all CLs together, and taking each lesion separately, with consistent results. FA values of CLs resulted higher (Wilcoxon rank-sum test, p=0.05)than the mean NAGM FA value, and their values mostly don't change significantly over the time span we considered. All subjects show, in the two time points, elevated FA for the lesion voxels, even if the mean FA of some lesions doesn't differ with statistical significance (p=0.05) from the mean of NAGM FA. The percentage difference between mean FA of the lesions and mean FA of the GM ranges from 9.04% to 63.81%, with a mean of 35% at the first time point (T0), while at the second time point (T9) the percentage difference was from a minimum of 8.57% to a maximum of 59.34% with a mean of 32%. Five illustrative examples are reported, for clarity, in figure 7.1.

It was possible to identify some lesions that had FA mean value significantly (rank-sum test, p=0.05) lower than the mean NAGM FA. In all subjects, seven of these lesions, called outliers because of theirs particular behavior, were found. Their value over time is represented in figure 7.2. As can be seen, after nine months these lesions didn't show abnormal behavior in respect to the others. Results obtained with DSC-MRI confirmed that these lesions showed values that were different from the other GM lesions. In particular, these particular areas showed high cerebral blood flow (CBF), in contrast to lower CBF in respect to the NAGM detected in the other lesions. This could be explained hypothesizing that these were at T0 active lesions, thus hyperperfused, that lose this activity during the nine months occurred between the two scans. This can also be ex-

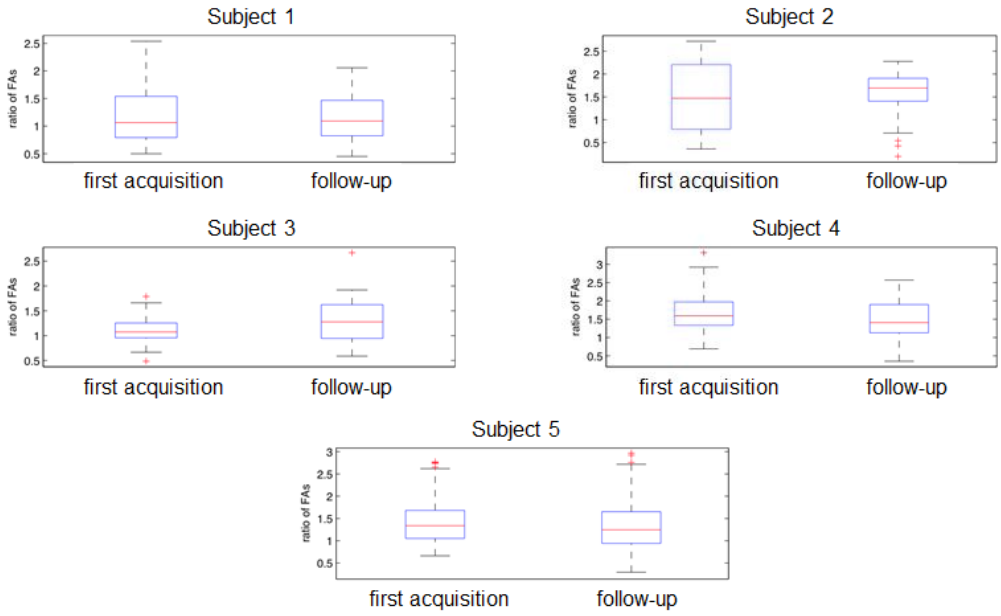

Figure 7.1: Boxplots of the ratio of the mean cortical lesions FA on the mean gray matter FA. All five patients showed as example show higher values of FA in the cortical lesions in both time points. The value of the represented ratio doesn't change sigificantly over time.

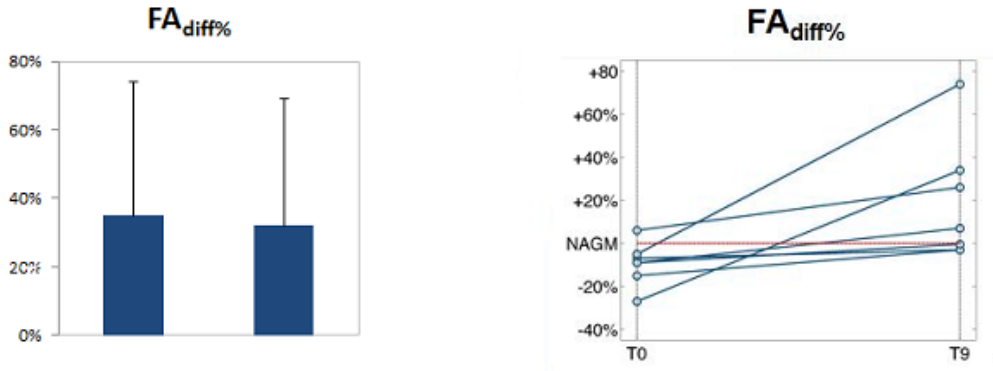

Figure 7.2: Left: mean value of the difference between mean FA in cortical lesions and in NAGM. Right: behavior over of the seven outliers that showed a FA lower than the mean NAGM FA at T0.

plained with FA values. A decrease in FA followed by a subsequent increase could indicate a period in which demyelination and inflammation is active, followed by a period during which the lesion becomes chronic.

Although FA in gray matter hasn't been evaluated in the past, in this study differences in FA values have been found to be reliable and consistent over time. Moreover, the precision of FA estimation in gray matter was not lower than the precision in white matter. This increase in FA in lesions in respect to gray matter could suggest that the pathologic process involves microstructural reorganization, in particular microglial activation: microglial cells that change toward a more elongated shape could explain from a biological point of view these findings obtained with DTI.

7.4.2 Whole brain studies of schizophrenia and bipolar disorder patients

Using the TBSS procedure illustrated in section 7.3.2, differences in FA were investigated for three different combinations of groups: bipolar disorder patients and healthy controls, schizophrenia patients and healthy controls, and bipolar and schizophrenia patients directly. In agreement with literature, the comparison between bipolar disorder and healthy demonstrated widespread FA differences. Decreased FA can be noted in various white matter tracts, as corpus callosum, corona radiata and superior longitudinal fasciculus, as can be seen in figure 7.3. These differences resulted statistically significant (p=0.05) after TFCE correction for multiple comparisons and correction for age effects.

The comparison between schizophrenia and healthy revealed, among other structures, significantly reduced FA (p=0.05, TFCE correction, correction for age effects) in corpus callosum and corona radiata, clearly affected by the disease. Results are illustrated in figure 7.4.

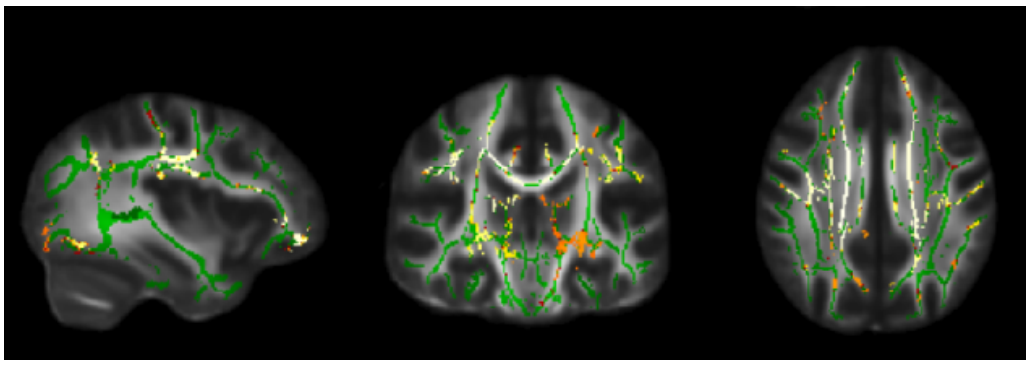

Figure 7.3: Results of TBSS voxel-wise analysis for 9 patients affected by bipolar disorder versus 17 age-matched healthy controls. Voxel in green represent the TBSS white matter skeleton. Voxel in red-yellow are the voxel where FA for patients is statistically lower than for healthy, after TFCE multiple comparisons correction ($p = 0.05$). Widespread white matter damage was found, especially in corpus callosum and longitudinal fasciculus (statistical significance is higher where the color assigned to the voxel is brighter)

Then, patients affected by the two diseases were compared directly. This direct comparison of voxel-wise FA has never been published, thus here are reported both uncorrected and TFCE corrected results.

Lower FA for bipolar patients than for schizophrenia patients was found, as can be seen in figures 7.5 and 7.6, in the corpus callosum and in the right and left longitudinal fasciculus. These differences didn't reach statistical significance when corrected for multiple comparisons. It is to be noted, though, that in two clusters of voxels located within the superior left superior longitudinal fasciculus tract and the corpus callosum, a difference can be found between the two group, not much below the level of significance ($p = 0.09$), as can be seen in figure 7.6. Abnormality in the diffusion parameters in the longitudinal fasciculus in bipolar disorder patients, in respect to healthy, have been previously been reported, e.g. in [162]. A comparison between bipolar disorder and schizophrenia, in terms of diffusion, has been done in [186], utilizing voxel-based morphometry (VBM). TBSS has the great advantage, over VBM, of restricting the analysis to the centre of white matter tracts. This allows potential partial volume effects to be reduced, and to focus the attention on the possible disruption of connections, that is of

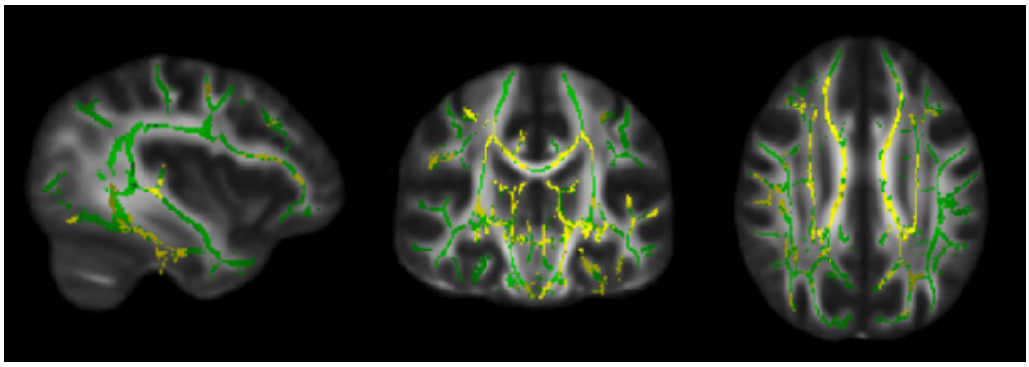

Figure 7.4: Results of TBSS voxel-wise analysis for 17 patients affected by schizophrenia versus 17 age-matched healthy controls. Voxel in green represent the TBSS white matter skeleton. Voxel in red-yellow are the voxel where FA for patients is statistically lower than for healthy, after TFCE multiple comparisons correction ($p = 0.05$). White matter tracts damage was found, especially in corpus callosum and corona radiata (statistical significance is higher where the color assigned to the voxel is brighter

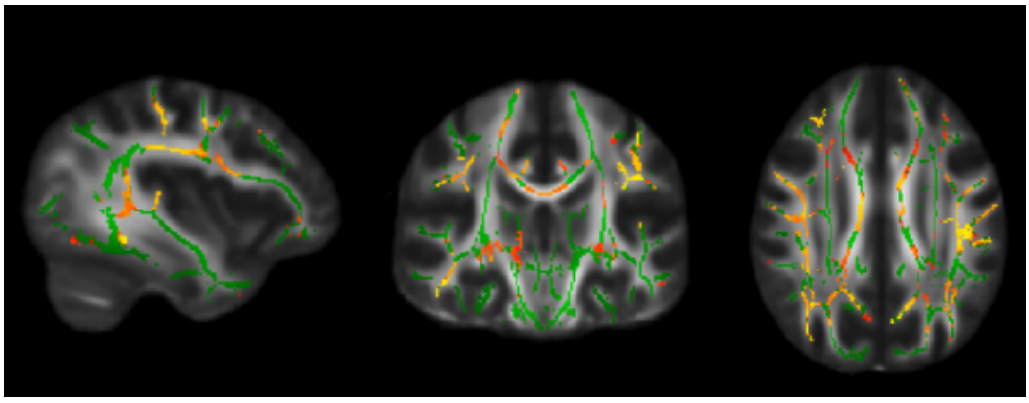

Figure 7.5: Results of TBSS voxel-wise analysis for 9 patients affected by bipolar disorder versus 17 patients affected by schizophrenia. Voxel in green represent the TBSS white matter skeleton. Voxel in red-yellow are the voxel where FA for patients is statistically lower than for healthy, uncorrected ($p = 0.05$). White matter tracts damage was found, especially in corpus callosum and corona radiata (statistical significance is higher where the color assigned to the voxel is brighter.) Results here reported are not corrected for multiple comparisons.

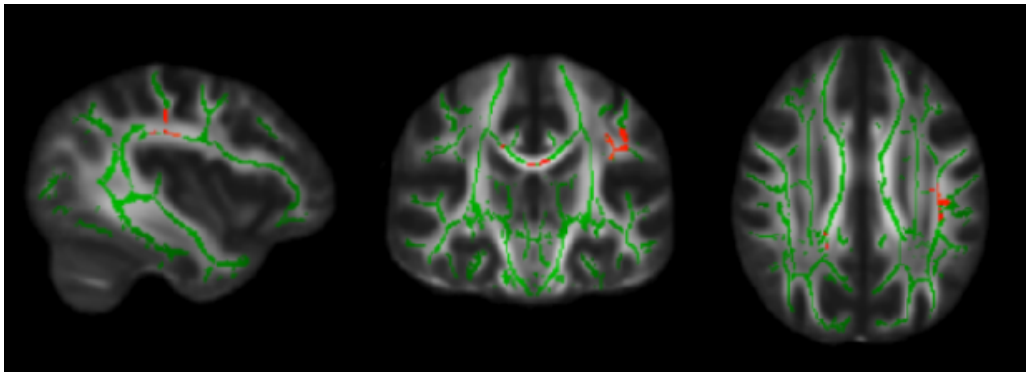

Figure 7.6: Results of TBSS voxel-wise analysis for 9 patients affected by bipolar disorder versus 17 patients affected by schizophrenia. Voxel in green represent the TBSS white matter skeleton. Voxel in red-yellow are the voxel where FA for patients is statistically lower than for healthy, after TFCE multiple comparisons correction ($p = 0.09$). There are two clusters of voxels, in corpus callosum and left superior longitudinal fasciculus that show difference between the two groups, although statistical significance is not reached.

primary importance in psychiatric diseases. Given the promising results of this exploratory study, an increase in the number of patients could help in better understanding the diffusion characteristics present in these two groups of patients, also by strengthening the results statistical value.

Chapter 8

Conclusions

In this thesis, a novel approach for the evaluation of brain structure and integrity has been proposed. In particular, a novel method for tractography and a novel method for the evaluation of structural thalamo-cortical connectivity have been presented.

The tractography algorithm presented in chapter 5 has been developed especially for the evaluation of white matter lesions in multiple sclerosis. To do so, particular attention has been posed on the best way to track fibers that are affected by the presence of demyelinated lesions. The method is a combination of two techniques: the fiber-assignment by continuous tracking (FACT) and the tensor deflection (TD) algorithms. In this way, it has been possible to combine the simplicity and rapidity of the FACT algorithm, used when diffusion directionality is well defined, and the robustness to noise of the tensor deflection method, that allowed the tracking also through the white matter lesions. This is a great advantage on the conventional methods of tractography, that often interrupts the tracking bluntly when encountering a lesion, losing the possibility of investigating its diffusion properties. Future work regardig this method will involve the integration of the method from a stochastic point of view, that could allow a more in-depth evaluation of diffusion inside white matter demyelinating MS lesions.

For the evaluation of thalamo-cortical connectivity, a method based on the use of a template has been proposed in chapter 6. From a cohort of healthy volunteers, thalamo-cortical connections have been derived using probabilistic tractography, run from left and right thalamus to ten different cortical areas. This template has been validated in healthy, and then applied in traumatic brain injury (TBI) patients. Using the template, various damaged tracts have been identified, and it has also been possible to investigate quantitatively the amount of damage for each patient and each considered tract. This method has several advantage on conventional tractography done directly on patients: it is less time consuming than estimating the tracts for every patient and it is completely automatic, eliminating the need of supervision by expert clinicians. More importantly, it allows the determination of diffusion characteristics in tracts where the tractography in patients fails, because of the damage provoked by trauma. This is of primary importance, because in this way white matter disruption can be identified and evaluated, comparing it with the behavior of diffusion in healthy, even if the tissue microstructure is compromised. In respect to the other few methods that apply a template of connectivity, this here presented has the advantage of focalising in the thalamic connections, particularly important in the case of TBI patients. A natural future expansion for this work will be the integration of this technique with fMRI, to analyze the interconnection of structure and function, regarding the connections between the thalamus and the cortex, both in healthy and for TBI patients.

In chapter 7, diffusion indices have been evaluated for multiple sclerosis, bipolar disorder and schizophrenia patients. Diffusion anisotropy of gray matter lesions has been taken into consideration. The obtained results, described in section 7.4.1, revealed a modification of diffusion behavior in gray matter plaques. This evidentiates that the disease causes a reorganization of brain microstructure. This

is one of the first studies that considers diffusion properties of gray matter MS lesions and, to date, the first to have followed diffusion changes over time, with a longitudinal study. Results obtained with tract-based spatial statistics (TBSS) for the populations of healthy, bipolar disorder patients and schizophrenia patients, presented in section 7.4.2 are promising, especially the direct comparison between bipolar and schizophrenic patients, never investigated before in terms of whole brain diffusion properties, and will be integrated with a dataset of SUV-PET that is already being acquired.

In conclusion, in this thesis an overview on DTI is presented, as well as some novel algorithms and applications with the aim of better investigating and understanding microstructural brain charachteristics and organization in vivo.

Bibliography

[1] E. L. Hahn. Spin echoes. *Phys. Rev.*, 80:580–594, Nov 1950.

[2] H. Y. Carr and E. M. Purcell. Effects of diffusion on free precession in nuclear magnetic resonance experiments. *Phys. Rev.*, 94:630–638, May 1954.

[3] E. O. Stejskal and J. E. Tanner. Spin Diffusion Measurements: Spin Echoes in the Presence of a Time-Dependent Field Gradient. *The Journal of Chemical Physics*, 42(1):288, Jan 1965.

[4] M. E. Moseley, Y. Cohen, J. Kucharczyk, J. Mintorovitch, H. S. Asgari, M. F. Wendland, J. Tsuruda, and D. Norman. Diffusion-weighted MR imaging of anisotropic water diffusion in cat central nervous system. *Radiology*, 176:439–445, Aug 1990.

[5] D. Le Bihan. Diffusion/perfusion MR imaging of the brain: from structure to function. *Radiology*, 177:328–329, Nov 1990.

[6] P. J. Basser, J. Mattiello, and D. LeBihan. Estimation of the effective self-diffusion tensor from the NMR spin echo. *J Magn Reson B*, 103:247–254, Mar 1994.

[7] S. C. Jones, A. D. Perez-Trepichio, M. Xue, A. J. Furlan, and I. A. Awad. Magnetic resonance diffusion-weighted imaging: sensitivity and apparent diffusion constant in stroke. *Acta Neurochir Suppl (Wien)*, 60:207–210, 1994.

[8] M. A. Horsfield, M. Lai, S. L. Webb, G. J. Barker, P. S. Tofts, R. Turner, P. Rudge, and D. H. Miller. Apparent diffusion coefficients in benign and secondary progressive multiple sclerosis by nuclear magnetic resonance. *Magn Reson Med*, 36:393–400, Sep 1996.

[9] M. S. Buchsbaum, C. Y. Tang, S. Peled, H. Gudbjartsson, D. Lu, E. A. Hazlett, J. Downhill, M. Haznedar, J. H. Fallon, and S. W. Atlas. MRI white matter diffusion anisotropy and PET metabolic rate in schizophrenia. *Neuroreport*, 9:425–430, Feb 1998.

[10] M. E. Thomason and P. M. Thompson. Diffusion imaging, white matter, and psychopathology. *Annu Rev Clin Psychol*, 7:63–85, Apr 2011.

[11] C. Beaulieu and P. S. Allen. Determinants of anisotropic water diffusion in nerves. *Magn Reson Med*, 31:394–400, Apr 1994.

[12] S. Rengachary and R. Ellenbogen. *Principles of Neurosurgery*. Mosby, 2004.

[13] H. Johansen-Berg and T.E.J. Behrens. *Diffusion MRI from quantitative measurement to in-vivo neuroanatomy*. Academic Press, Amsterdam Boston, 2009.

[14] D. Le Bihan. Molecular diffusion nuclear magnetic resonance imaging. *Magnetic resonance quarterly*, 7(1):1–30, Jan 1991.

[15] D. Le Bihan, E. Breton, D. Lallemand, P. Grenier, E. Cabanis, and M. Laval-Jeantet. MR imaging of intravoxel incoherent motions: application to diffusion and perfusion in neurologic disorders. *Radiology*, 161:401–407, Nov 1986.

[16] S. Wang, S. Kim, Y. Zhang, L. Wang, E. B. Lee, P. Syre, H. Poptani, E. R. Melhem, and J. Y. Lee. Determination of Grade and Subtype of Meningiomas by Using Histogram Analysis of Diffusion-Tensor Imaging Metrics. *Radiology*, Nov 2011.

[17] C. Pierpaoli, P. Jezzard, P. J. Basser, A. Barnett, and G. Di Chiro. Diffusion tensor MR imaging of the human brain. *Radiology*, 201:637–648, Dec 1996.

[18] G. K. Rohde, A. S. Barnett, P. J. Basser, S. Marenco, and C. Pierpaoli. Comprehensive approach for correction of motion and distortion in diffusion-weighted MRI. *Magn Reson Med*, 51:103–114, Jan 2004.

[19] D. K. Jones and C. Pierpaoli. Confidence mapping in diffusion tensor magnetic resonance imaging tractography using a bootstrap approach. *Magn Reson Med*, 53:1143–1149, May 2005.

[20] J. D. Tournier, S. Mori, and A. Leemans. Diffusion tensor imaging and beyond. *Magn Reson Med*, 65:1532–1556, Jun 2011.

[21] V. J. Wedeen, P. Hagmann, W. Y. Tseng, T. G. Reese, and R. M. Weisskoff. Mapping complex tissue architecture with diffusion spectrum magnetic resonance imaging. *Magn Reson Med*, 54:1377–1386, Dec 2005.

[22] D. S. Tuch, T. G. Reese, M. R. Wiegell, N. Makris, J. W. Belliveau, and V. J. Wedeen. High angular resolution diffusion imaging reveals intravoxel white matter fiber heterogeneity. *Magn Reson Med*, 48:577–582, Oct 2002.

[23] D. S. Tuch. Q-ball imaging. *Magn Reson Med*, 52:1358–1372, Dec 2004.

[24] T. Hosey, G. Williams, and R. Ansorge. Inference of multiple fiber orientations in high angular resolution diffusion imaging. *Magn Reson Med*, 54:1480–1489, Dec 2005.

[25] T. E. Behrens, H. J. Berg, S. Jbabdi, M. F. Rushworth, and M. W. Woolrich. Probabilistic diffusion tractography with multiple fibre orientations: What can we gain? *Neuroimage*, 34:144–155, Jan 2007.

[26] Y. Assaf, R. Z. Freidlin, G. K. Rohde, and P. J. Basser. New modeling and experimental framework to characterize hindered and restricted water diffusion in brain white matter. *Magn Reson Med*, 52:965–978, Nov 2004.

[27] J. S. Shimony, R. C. McKinstry, E. Akbudak, J. A. Aronovitz, A. Z. Snyder, N. F. Lori, T. S. Cull, and T. E. Conturo. Quantitative diffusion-tensor anisotropy brain MR imaging: normative human data and anatomic analysis. *Radiology*, 212:770–784, Sep 1999.

[28] A. Pfefferbaum, E. Adalsteinsson, and E. V. Sullivan. Replicability of diffusion tensor imaging measurements of fractional anisotropy and trace in brain. *J Magn Reson Imaging*, 18:427–433, Oct 2003.

[29] S. Mori, B. J. Crain, V. P. Chacko, and P. C. van Zijl. Three-dimensional tracking of axonal projections in the brain by magnetic resonance imaging. *Ann. Neurol.*, 45:265–269, Feb 1999.

[30] T. A. Huisman, T. Loenneker, G. Barta, M. E. Bellemann, J. Hennig, J. E. Fischer, and K. A. Il'yasov. Quantitative diffusion tensor MR imaging of the brain: field strength related variance of apparent diffusion coefficient (ADC) and fractional anisotropy (FA) scalars. *Eur Radiol*, 16:1651–1658, Aug 2006.

[31] S. Bisdas, D. E. Bohning, N. Besenski, J. S. Nicholas, and Z. Rumboldt. Reproducibility, interrater agreement, and age-related changes of fractional anisotropy measures at 3T in healthy subjects: effect of the applied b-value. *AJNR Am J Neuroradiol*, 29:1128–1133, Jun 2008.

[32] A. Brander, A. Kataja, A. Saastamoinen, P. Ryymin, H. Huhtala, J. Ohman, S. Soimakallio, and P. Dastidar. Diffusion tensor imaging of the brain in a healthy adult population: Normative values and measurement reproducibility at 3 T and 1.5 T. *Acta Radiol*, 51:800–807, Sep 2010.

[33] P. C. Sundgren, Q. Dong, D. Gomez-Hassan, S. K. Mukherji, P. Maly, and R. Welsh. Diffusion tensor imaging of the brain: review of clinical applications. *Neuroradiology*, 46:339–350, May 2004.

[34] H. L. Lutsep, G. W. Albers, A. DeCrespigny, G. N. Kamat, M. P. Marks, and M. E. Moseley. Clinical utility of diffusion-weighted magnetic resonance imaging in the assessment of ischemic stroke. *Ann. Neurol.*, 41:574–580, May 1997.

[35] A. Pfefferbaum, E. V. Sullivan, M. Hedehus, K. O. Lim, E. Adalsteinsson, and M. Moseley. Age-related decline in brain white matter anisotropy measured with spatially corrected echo-planar diffusion tensor imaging. *Magn Reson Med*, 44:259–268, Aug 2000.

[36] P. Mukherjee, J. H. Miller, J. S. Shimony, T. E. Conturo, B. C. Lee, C. R. Almli, and R. C. McKinstry. Normal brain maturation during childhood: developmental trends characterized with diffusion-tensor MR imaging. *Radiology*, 221:349–358, Nov 2001.

[37] P. Gideon, C. Thomsen, and O. Henriksen. Increased self-diffusion of brain water in normal aging. *J Magn Reson Imaging*, 4:185–188, 1994.

[38] H. Hanyu, H. Sakurai, T. Iwamoto, M. Takasaki, H. Shindo, and K. Abe. Diffusion-weighted MR imaging of the hippocampus and temporal white matter in Alzheimer's disease. *J. Neurol. Sci.*, 156:195–200, Apr 1998.

[39] S. E. Rose, F. Chen, J. B. Chalk, F. O. Zelaya, W. E. Strugnell, M. Benson, J. Semple, and D. M. Doddrell. Loss of connectivity in Alzheimer's disease: an evaluation of white matter tract integrity with colour coded MR diffusion tensor imaging. *J. Neurol. Neurosurg. Psychiatr.*, 69:528–530, Oct 2000.

[40] S. Sinha, M. E. Bastin, I. R. Whittle, and J. M. Wardlaw. Diffusion tensor MR imaging of high-grade cerebral gliomas. *AJNR Am J Neuroradiol*, 23:520–527, Apr 2002.

[41] T. W. Stadnik, C. Chaskis, A. Michotte, W. M. Shabana, K. van Rompaey, R. Luypaert, L. Budinsky, V. Jellus, and M. Osteaux. Diffusion-weighted MR imaging of intracerebral masses: comparison with conventional MR imaging and histologic findings. *AJNR Am J Neuroradiol*, 22:969–976, May 2001.

[42] L. Testaverde, L. Caporali, E. Venditti, G. Grillea, and C. Colonnese. Diffusion tensor imaging applications in multiple sclerosis patients using 3T magnetic resonance: a preliminary study. *Eur Radiol*, Dec 2011.

[43] J. F. Kurtzke. Rating neurologic impairment in multiple sclerosis: an expanded disability status scale (EDSS). *Neurology*, 33:1444–1452, Nov 1983.

[44] A. Castriota Scanderbeg, F. Tomaiuolo, U. Sabatini, U. Nocentini, M. G. Grasso, and C. Caltagirone. Demyelinating plaques in relapsing-remitting and secondary-progressive multiple sclerosis: assessment with diffusion MR imaging. *AJNR Am J Neuroradiol*, 21:862–868, May 2000.

[45] M. Filippi, M. Cercignani, M. Inglese, M. A. Horsfield, and G. Comi. Diffusion tensor magnetic resonance imaging in multiple sclerosis. *Neurology*, 56:304–311, Feb 2001.

[46] D. J. Werring, C. A. Clark, G. J. Barker, A. J. Thompson, and D. H. Miller. Diffusion tensor imaging of lesions and normal-appearing white matter in multiple sclerosis. *Neurology*, 52:1626–1632, May 1999.

[47] A. L. Tievsky, T. Ptak, and J. Farkas. Investigation of apparent diffusion coefficient and diffusion tensor anisotrophy in acute and chronic multiple sclerosis lesions. *AJNR Am J Neuroradiol*, 20:1491–1499, Sep 1999.

[48] A. Castriota-Scanderbeg, U. Sabatini, F. Fasano, R. Floris, L. Fraracci, M. D. Mario, U. Nocentini, and C. Caltagirone. Diffusion of water in large demyelinating lesions: a follow-up study. *Neuroradiology*, 44:764–767, Sep 2002.

[49] R. Bammer, M. Augustin, S. Strasser-Fuchs, T. Seifert, P. Kapeller, R. Stollberger, F. Ebner, H. P. Hartung, and F. Fazekas. Magnetic resonance diffusion tensor

imaging for characterizing diffuse and focal white matter abnormalities in multiple sclerosis. *Magn Reson Med*, 44:583–591, Oct 2000.

[50] C. Till, A. Deotto, V. Tipu, J. G. Sled, A. Bethune, S. Narayanan, D. L. Arnold, and B. L. Banwell. White matter integrity and math performance in pediatric multiple sclerosis: a diffusion tensor imaging study. *Neuroreport*, 22:1005–1009, Dec 2011.

[51] A. Bethune, V. Tipu, J. G. Sled, S. Narayanan, D. L. Arnold, D. Mabbott, C. Rockel, R. Ghassemi, C. Till, and B. Banwell. Diffusion tensor imaging and cognitive speed in children with multiple sclerosis. *J. Neurol. Sci.*, 309:68–74, Oct 2011.

[52] M. Rovaris, A. Gass, R. Bammer, S. J. Hickman, O. Ciccarelli, D. H. Miller, and M. Filippi. Diffusion MRI in multiple sclerosis. *Neurology*, 65:1526–1532, Nov 2005.

[53] S. D. Roosendaal, J. J. Geurts, H. Vrenken, H. E. Hulst, K. S. Cover, J. A. Castelijns, P. J. Pouwels, and F. Barkhof. Regional DTI differences in multiple sclerosis patients. *Neuroimage*, 44:1397–1403, Feb 2009.

[54] R. A. Dineen, J. Vilisaar, J. Hlinka, C. M. Bradshaw, P. S. Morgan, C. S. Constantinescu, and D. P. Auer. Disconnection as a mechanism for cognitive dysfunction in multiple sclerosis. *Brain*, 132:239–249, Jan 2009.

[55] Y. Liu, Y. Duan, Y. He, C. Yu, J. Wang, J. Huang, J. Ye, P. M. Parizel, K. Li, and N. Shu. Whole brain white matter changes revealed by multiple diffusion metrics in multiple sclerosis: A TBSS study. *Eur J Radiol*, Dec 2011.

[56] M. Cercignani, M. Bozzali, G. Iannucci, G. Comi, and M. Filippi. Magnetisation transfer ratio and mean diffusivity of normal appearing white and grey matter from patients with multiple sclerosis. *J. Neurol. Neurosurg. Psychiatr.*, 70:311–317, Mar 2001.

[57] M. Rovaris, M. Bozzali, G. Iannucci, A. Ghezzi, D. Caputo, E. Montanari, A. Bertolotto, R. Bergamaschi, R. Capra, G. L. Mancardi, V. Martinelli, G. Comi, and M. Filippi. Assessment of normal-appearing white and gray matter in patients with primary progressive multiple sclerosis: a diffusion-tensor magnetic resonance imaging study. *Arch. Neurol.*, 59:1406–1412, Sep 2002.

[58] M. Bozzali, M. Cercignani, M. P. Sormani, G. Comi, and M. Filippi. Quantification of brain gray matter damage in different MS phenotypes by use of diffusion tensor MR imaging. *AJNR Am J Neuroradiol*, 23:985–988, 2002.

[59] C. Oreja-Guevara, M. Rovaris, G. Iannucci, P. Valsasina, D. Caputo, R. Cavarretta, M. P. Sormani, P. Ferrante, G. Comi, and M. Filippi. Progressive gray matter damage in patients with relapsing-remitting multiple sclerosis: a longitudinal diffusion tensor magnetic resonance imaging study. *Arch. Neurol.*, 62:578–584, Apr 2005.

[60] M. Rovaris, A. Gallo, P. Valsasina, B. Benedetti, D. Caputo, A. Ghezzi, E. Montanari, M. P. Sormani, A. Bertolotto, G. Mancardi, R. Bergamaschi, V. Martinelli, G. Comi, and M. Filippi. Short-term accrual of gray matter pathology in patients with progressive multiple sclerosis: an in vivo study using diffusion tensor MRI. *Neuroimage*, 24:1139–1146, Feb 2005.

[61] F. Zhou, C. S. Zee, H. Gong, M. Shiroishi, and J. Li. Differential changes in deep and cortical gray matters of patients with multiple sclerosis: a quantitative magnetic resonance imaging study. *J Comput Assist Tomogr*, 34:431–436, 2010.

[62] A. H. Poonawalla, K. M. Hasan, R. K. Gupta, C. W. Ahn, F. Nelson, J. S. Wolinsky, and P. A. Narayana. Diffusion-tensor MR imaging of cortical lesions in multiple sclerosis: initial findings. *Radiology*, 246:880–886, Mar 2008.

[63] J. Bruns and W. A. Hauser. The epidemiology of traumatic brain injury: a review. *Epilepsia*, 44 Suppl 10:2–10, 2003.

[64] J. F. Malec, J. A. Testa, B. K. Rush, A. W. Brown, and A. M. Moessner. Self-assessment of impairment, impaired self-awareness, and depression after traumatic brain injury. *J Head Trauma Rehabil*, 22:156–166, 2007.

[65] L. Whitnall, T. M. McMillan, G. D. Murray, and G. M. Teasdale. Disability in young people and adults after head injury: 5-7 year follow up of a prospective cohort study. *J. Neurol. Neurosurg. Psychiatr.*, 77:640–645, May 2006.

[66] P. C. Blumbergs, N. R. Jones, and J. B. North. Diffuse axonal injury in head trauma. *J. Neurol. Neurosurg. Psychiatr.*, 52:838–841, Jul 1989.

[67] R. A. Hurley, J. C. McGowan, K. Arfanakis, and K. H. Taber. Traumatic axonal injury: novel insights into evolution and identification. *J Neuropsychiatry Clin Neurosci*, 16:1–7, 2004.

[68] J. H. Adams, B. Jennett, L. S. Murray, G. M. Teasdale, T. A. Gennarelli, and D. I. Graham. Neuropathological findings in disabled survivors of a head injury. *J. Neurotrauma*, 28:701–709, May 2011.

[69] M. Inglese, S. Makani, G. Johnson, B. A. Cohen, J. A. Silver, O. Gonen, and R. I. Grossman. Diffuse axonal injury in mild traumatic brain injury: a diffusion tensor imaging study. *J. Neurosurg.*, 103:298–303, Aug 2005.

[70] J. M. Meythaler, J. D. Peduzzi, E. Eleftheriou, and T. A. Novack. Current concepts: diffuse axonal injury-associated traumatic brain injury. *Arch Phys Med Rehabil*, 82:1461–1471, Oct 2001.

[71] J. T. Povlishock and D. I. Katz. Update of neuropathology and neurological recovery after traumatic brain injury. *J Head Trauma Rehabil*, 20:76–94, 2005.

[72] D. H. Smith, D. F. Meaney, and W. H. Shull. Diffuse axonal injury in head trauma. *J Head Trauma Rehabil*, 18:307–316, 2003.

[73] F. J. Rugg-Gunn, M. R. Symms, G. J. Barker, R. Greenwood, and J. S. Duncan. Diffusion imaging shows abnormalities after blunt head trauma when conventional magnetic resonance imaging is normal. *J. Neurol. Neurosurg. Psychiatr.*, 70:530–533, Apr 2001.

[74] K. Arfanakis, V. M. Haughton, J. D. Carew, B. P. Rogers, R. J. Dempsey, and M. E. Meyerand. Diffusion tensor MR imaging in diffuse axonal injury. *AJNR Am J Neuroradiol*, 23:794–802, May 2002.

[75] N. Nakayama, A. Okumura, J. Shinoda, Y. T. Yasokawa, K. Miwa, S. I. Yoshimura, and T. Iwama. Evidence for white matter disruption in traumatic brain injury without macroscopic lesions. *J. Neurol. Neurosurg. Psychiatr.*, 77:850–855, Jul 2006.

[76] M. L. Lipton, E. Gellella, C. Lo, T. Gold, B. A. Ardekani, K. Shifteh, J. A. Bello, and C. A. Branch. Multifocal white matter ultrastructural abnormalities in mild

traumatic brain injury with cognitive disability: a voxel-wise analysis of diffusion tensor imaging. *J. Neurotrauma*, 25:1335–1342, Nov 2008.

[77] R. R. Benson, S. A. Meda, S. Vasudevan, Z. Kou, K. A. Govindarajan, R. A. Hanks, S. R. Millis, M. Makki, Z. Latif, W. Coplin, J. Meythaler, and E. M. Haacke. Global white matter analysis of diffusion tensor images is predictive of injury severity in traumatic brain injury. *J. Neurotrauma*, 24:446–459, Mar 2007.

[78] M. Matsushita, K. Hosoda, Y. Naitoh, H. Yamashita, and E. Kohmura. Utility of diffusion tensor imaging in the acute stage of mild to moderate traumatic brain injury for detecting white matter lesions and predicting long-term cognitive function in adults. *J. Neurosurg.*, 115:130–139, Jul 2011.

[79] M. Bellani and P. Brambilla. Diffusion imaging studies of white matter integrity in bipolar disorder. *Epidemiol Psychiatr Sci*, 20:137–140, Jun 2011.

[80] C. M. Adler, S. K. Holland, V. Schmithorst, M. Wilke, K. L. Weiss, H. Pan, and S. M. Strakowski. Abnormal frontal white matter tracts in bipolar disorder: a diffusion tensor imaging study. *Bipolar Disord*, 6:197–203, Jun 2004.

[81] F. Wang, J. H. Kalmar, E. Edmiston, L. G. Chepenik, Z. Bhagwagar, L. Spencer, B. Pittman, M. Jackowski, X. Papademetris, R. T. Constable, and H. P. Blumberg. Abnormal corpus callosum integrity in bipolar disorder: a diffusion tensor imaging study. *Biol. Psychiatry*, 64:730–733, Oct 2008.

[82] S. Bruno, M. Cercignani, and M. A. Ron. White matter abnormalities in bipolar disorder: a voxel-based diffusion tensor imaging study. *Bipolar Disord*, 10:460–468, Jun 2008.

[83] F. Benedetti, P. H. Yeh, M. Bellani, D. Radaelli, M. A. Nicoletti, S. Poletti, A. Falini, S. Dallaspezia, C. Colombo, G. Scotti, E. Smeraldi, J. C. Soares, and P. Brambilla. Disruption of white matter integrity in bipolar depression as a possible structural marker of illness. *Biol. Psychiatry*, 69:309–317, Feb 2011.

[84] F. Benedetti, M. Absinta, M. A. Rocca, D. Radaelli, S. Poletti, A. Bernasconi, S. Dallaspezia, E. Pagani, A. Falini, M. Copetti, C. Colombo, G. Comi, E. Smeraldi, and M. Filippi. Tract-specific white matter structural disruption in patients with bipolar disorder. *Bipolar Disord*, 13:414–424, Jun 2011.

[85] D. A. Yurgelun-Todd, M. M. Silveri, S. A. Gruber, M. L. Rohan, and P. J. Pimentel. White matter abnormalities observed in bipolar disorder: a diffusion tensor imaging study. *Bipolar Disord*, 9:504–512, Aug 2007.

[86] A. Versace, J. R. Almeida, S. Hassel, N. D. Walsh, M. Novelli, C. R. Klein, D. J. Kupfer, and M. L. Phillips. Elevated left and reduced right orbitomedial prefrontal fractional anisotropy in adults with bipolar disorder revealed by tract-based spatial statistics. *Arch. Gen. Psychiatry*, 65:1041–1052, Sep 2008.

[87] R. A. Kanaan, J. S. Kim, W. E. Kaufmann, G. D. Pearlson, G. J. Barker, and P. K. McGuire. Diffusion tensor imaging in schizophrenia. *Biol. Psychiatry*, 58:921–929, Dec 2005.

[88] J. Foong, M. Maier, C. A. Clark, G. J. Barker, D. H. Miller, and M. A. Ron. Neuropathological abnormalities of the corpus callosum in schizophrenia: a diffusion tensor imaging study. *J. Neurol. Neurosurg. Psychiatr.*, 68:242–244, Feb 2000.

[89] Z. Sun, F. Wang, L. Cui, J. Breeze, X. Du, X. Wang, Z. Cong, H. Zhang, B. Li, N. Hong, and D. Zhang. Abnormal anterior cingulum in patients with schizophrenia: a diffusion tensor imaging study. *Neuroreport*, 14:1833–1836, Oct 2003.

[90] M. Kubicki, C. F. Westin, P. G. Nestor, C. G. Wible, M. Frumin, S. E. Maier, R. Kikinis, F. A. Jolesz, R. W. McCarley, and M. E. Shenton. Cingulate fasciculus integrity disruption in schizophrenia: a magnetic resonance diffusion tensor imaging study. *Biol. Psychiatry*, 54:1171–1180, Dec 2003.

[91] G. Okugawa, K. Nobuhara, T. Minami, C. Tamagaki, K. Takase, T. Sugimoto, S. Sawada, and T. Kinoshita. Subtle disruption of the middle cerebellar peduncles in patients with schizophrenia. *Neuropsychobiology*, 50:119–123, 2004.

[92] J. J. Levitt, M. Kubicki, P. G. Nestor, H. Ersner-Hershfield, C. F. Westin, J. L. Alvarado, R. Kikinis, F. A. Jolesz, R. W. McCarley, and M. E. Shenton. A diffusion tensor imaging study of the anterior limb of the internal capsule in schizophrenia. *Psychiatry Res*, 184:143–150, Dec 2010.

[93] M. Kyriakopoulos, T. Bargiotas, G. J. Barker, and S. Frangou. Diffusion tensor imaging in schizophrenia. *Eur. Psychiatry*, 23:255–273, Jun 2008.

[94] Q. Wang, W. Deng, C. Huang, M. Li, X. Ma, Y. Wang, L. Jiang, S. Lui, X. Huang, S. E. Chua, C. Cheung, G. M. McAlonan, P. C. Sham, R. M. Murray, D. A. Collier, Q. Gong, and T. Li. Abnormalities in connectivity of white-matter tracts in patients with familial and non-familial schizophrenia. *Psychol Med*, 41:1691–1700, Aug 2011.

[95] J. Tang, Y. Liao, B. Zhou, C. Tan, T. Liu, W. Hao, D. Hu, and X. Chen. Abnormal anterior cingulum integrity in first episode, early-onset schizophrenia: a diffusion tensor imaging study. *Brain Res.*, 1343:199–205, Jul 2010.

[96] A. Schüz and V. Braitenberg. *The Human Cortical White Matter: Quantitative Aspects of Cortico-Cortical Long-Range Connectivity.* Cortical areas : unity and diversity, Taylor & Francis, London New York, 2002.

[97] P. J. Basser, S. Pajevic, C. Pierpaoli, J. Duda, and A. Aldroubi. In vivo fiber tractography using DT-MRI data. *Magn Reson Med*, 44:625–632, Oct 2000.

[98] M. Lazar. Mapping brain anatomical connectivity using white matter tractography. *NMR Biomed*, 23:821–835, Aug 2010.

[99] M. Lazar, D. M. Weinstein, J. S. Tsuruda, K. M. Hasan, K. Arfanakis, M. E. Meyerand, B. Badie, H. A. Rowley, V. Haughton, A. Field, and A. L. Alexander. White matter tractography using diffusion tensor deflection. *Hum Brain Mapp*, 18:306–321, Apr 2003.

[100] D. K. Jones. Determining and visualizing uncertainty in estimates of fiber orientation from diffusion tensor MRI. *Magn Reson Med*, 49:7–12, Jan 2003.

[101] G. J. Parker, H. A. Haroon, and C. A. Wheeler-Kingshott. A framework for a streamline-based probabilistic index of connectivity (PICo) using a structural interpretation of MRI diffusion measurements. *J Magn Reson Imaging*, 18:242–254, Aug 2003.

[102] T. E. Behrens, M. W. Woolrich, M. Jenkinson, H. Johansen-Berg, R. G. Nunes, S. Clare, P. M. Matthews, J. M. Brady, and S. M. Smith. Characterization and propagation of uncertainty in diffusion-weighted MR imaging. *Magn Reson Med*, 50:1077–1088, Nov 2003.

[103] M. W. Woolrich, S. Jbabdi, B. Patenaude, M. Chappell, S. Makni, T. Behrens, C. Beckmann, M. Jenkinson, and S. M. Smith. Bayesian analysis of neuroimaging data in FSL. *Neuroimage*, 45:S173–186, Mar 2009.

[104] S. M. Smith, M. Jenkinson, M. W. Woolrich, C. F. Beckmann, T. E. Behrens, H. Johansen-Berg, P. R. Bannister, M. De Luca, I. Drobnjak, D. E. Flitney, R. K. Niazy, J. Saunders, J. Vickers, Y. Zhang, N. De Stefano, J. M. Brady, and P. M. Matthews. Advances in functional and structural MR image analysis and implementation as FSL. *Neuroimage*, 23 Suppl 1:S208–219, 2004.

[105] S. Wakana, A. Caprihan, M. M. Panzenboeck, J. H. Fallon, M. Perry, R. L. Gollub, K. Hua, J. Zhang, H. Jiang, P. Dubey, A. Blitz, P. van Zijl, and S. Mori. Reproducibility of quantitative tractography methods applied to cerebral white matter. *Neuroimage*, 36:630–644, Jul 2007.

[106] G. Gong, T. Jiang, C. Zhu, Y. Zang, F. Wang, S. Xie, J. Xiao, and X. Guo. Asymmetry analysis of cingulum based on scale-invariant parameterization by diffusion tensor imaging. *Hum Brain Mapp*, 24:92–98, Feb 2005.

[107] L. Concha, D. W. Gross, and C. Beaulieu. Diffusion tensor tractography of the limbic system. *AJNR Am J Neuroradiol*, 26:2267–2274, Oct 2005.

[108] T. R. Barrick, I. N. Lawes, C. E. Mackay, and C. A. Clark. White matter pathway asymmetry underlies functional lateralization. *Cereb. Cortex*, 17:591–598, Mar 2007.

[109] M. F. Glasser and J. K. Rilling. DTI tractography of the human brain's language pathways. *Cereb. Cortex*, 18:2471–2482, Nov 2008.

[110] O. Ciccarelli, A. T. Toosy, G. J. Parker, C. A. Wheeler-Kingshott, G. J. Barker, D. H. Miller, and A. J. Thompson. Diffusion tractography based group mapping of major white-matter pathways in the human brain. *Neuroimage*, 19:1545–1555, Aug 2003.

[111] R. F. Dougherty, M. Ben-Shachar, R. Bammer, A. A. Brewer, and B. A. Wandell. Functional organization of human occipital-callosal fiber tracts. *Proc. Natl. Acad. Sci. U.S.A.*, 102:7350–7355, May 2005.

[112] A. J. Sherbondy, R. F. Dougherty, S. Napel, and B. A. Wandell. Identifying the human optic radiation using diffusion imaging and fiber tractography. *J Vis*, 8:1–11, 2008.

[113] J. S. Shimony, H. Burton, A. A. Epstein, D. G. McLaren, S. W. Sun, and A. Z. Snyder. Diffusion tensor imaging reveals white matter reorganization in early blind humans. *Cereb. Cortex*, 16:1653–1661, Nov 2006.

[114] A. L. Beer, T. Plank, and M. W. Greenlee. Diffusion tensor imaging shows white matter tracts between human auditory and visual cortex. *Exp Brain Res*, 213:299–308, Sep 2011.

[115] K. Hua, J. Zhang, S. Wakana, H. Jiang, X. Li, D. S. Reich, P. A. Calabresi, J. J. Pekar, P. C. van Zijl, and S. Mori. Tract probability maps in stereotaxic spaces: analyses of white matter anatomy and tract-specific quantification. *Neuroimage*, 39:336–347, Jan 2008.

[116] D. S. Reich, A. Ozturk, P. A. Calabresi, and S. Mori. Automated vs. conventional tractography in multiple sclerosis: variability and correlation with disability. *Neuroimage*, 49:3047–3056, Feb 2010.

[117] M. Thiebaut de Schotten, D. H. Ffytche, A. Bizzi, F. Dell'Acqua, M. Allin, M. Walshe, R. Murray, S. C. Williams, D. G. Murphy, and M. Catani. Atlasing location, asymmetry and inter-subject variability of white matter tracts in the human brain with MR diffusion tractography. *Neuroimage*, 54:49–59, Jan 2011.

[118] H. Peng, A. Orlichenko, R. J. Dawe, G. Agam, S. Zhang, and K. Arfanakis. Development of a human brain diffusion tensor template. *Neuroimage*, 46:967–980, Jul 2009.

[119] J. S. Verhoeven, C. A. Sage, A. Leemans, W. Van Hecke, D. Callaert, R. Peeters, P. De Cock, L. Lagae, and S. Sunaert. Construction of a stereotaxic DTI atlas with full diffusion tensor information for studying white matter maturation from childhood to adolescence using tractography-based segmentations. *Hum Brain Mapp*, 31:470–486, Mar 2010.

[120] T. E. Behrens, H. Johansen-Berg, M. W. Woolrich, S. M. Smith, C. A. Wheeler-Kingshott, P. A. Boulby, G. J. Barker, E. L. Sillery, K. Sheehan, O. Ciccarelli,

A. J. Thompson, J. M. Brady, and P. M. Matthews. Non-invasive mapping of connections between human thalamus and cortex using diffusion imaging. *Nat. Neurosci.*, 6:750–757, Jul 2003.

[121] D. Zhang, A. Z. Snyder, J. S. Shimony, M. D. Fox, and M. E. Raichle. Noninvasive functional and structural connectivity mapping of the human thalamocortical system. *Cereb. Cortex*, 20:1187–1194, May 2010.

[122] C. Traynor, R. A. Heckemann, A. Hammers, J. O'Muircheartaigh, W. R. Crum, G. J. Barker, and M. P. Richardson. Reproducibility of thalamic segmentation based on probabilistic tractography. *Neuroimage*, 52:69–85, Aug 2010.

[123] A. Ford, K. M. McGregor, K. Case, B. Crosson, and K. D. White. Structural connectivity of Broca's area and medial frontal cortex. *Neuroimage*, 52:1230–1237, Oct 2010.

[124] Z. M. Saygin, D. E. Osher, J. Augustinack, B. Fischl, and J. D. Gabrieli. Connectivity-based segmentation of human amygdala nuclei using probabilistic tractography. *Neuroimage*, 56:1353–1361, Jun 2011.

[125] E. Rykhlevskaia, G. Gratton, and M. Fabiani. Combining structural and functional neuroimaging data for studying brain connectivity: a review. *Psychophysiology*, 45:173–187, Mar 2008.

[126] R. B. Mars, S. Jbabdi, J. Sallet, J. X. O'Reilly, P. L. Croxson, E. Olivier, M. P. Noonan, C. Bergmann, A. S. Mitchell, M. G. Baxter, T. E. Behrens, H. Johansen-Berg, V. Tomassini, K. L. Miller, and M. F. Rushworth. Diffusion-weighted imaging tractography-based parcellation of the human parietal cortex and comparison with human and macaque resting-state functional connectivity. *J. Neurosci.*, 31:4087–4100, Mar 2011.

[127] M. D. Greicius, K. Supekar, V. Menon, and R. F. Dougherty. Resting-state functional connectivity reflects structural connectivity in the default mode network. *Cereb. Cortex*, 19:72–78, Jan 2009.

[128] O. Sporns. The human connectome: a complex network. *Ann. N. Y. Acad. Sci.*, 1224:109–125, Apr 2011.

[129] G. Gong, Y. He, L. Concha, C. Lebel, D. W. Gross, A. C. Evans, and C. Beaulieu. Mapping anatomical connectivity patterns of human cerebral cortex using in vivo diffusion tensor imaging tractography. *Cereb. Cortex*, 19:524–536, Mar 2009.

[130] R. Bakshi, A. J. Thompson, M. A. Rocca, D. Pelletier, V. Dousset, F. Barkhof, M. Inglese, C. R. Guttmann, M. A. Horsfield, and M. Filippi. MRI in multiple sclerosis: current status and future prospects. *Lancet Neurol*, 7:615–625, Jul 2008.

[131] Bing Hu, Binbin Ye, Yang Yang, Kangshun Zhu, Zhuang Kang, Sichi Kuang, Lin Luo, and Hong Shan. Quantitative diffusion tensor deterministic and probabilistic fiber tractography in relapsing-remitting multiple sclerosis. *European journal of radiology*, 79(1):101–7, July 2011.

[132] E. Pagani, M. Filippi, M. A. Rocca, and M. A. Horsfield. A method for obtaining tract-specific diffusion tensor MRI measurements in the presence of disease: application to patients with clinically isolated syndromes suggestive of multiple sclerosis. *Neuroimage*, 26:258–265, May 2005.

[133] F. Lin, C. Yu, T. Jiang, K. Li, and P. Chan. Diffusion tensor tractography-based group mapping of the pyramidal tract in relapsing-remitting multiple sclerosis patients. *AJNR Am J Neuroradiol*, 28:278–282, Feb 2007.

[134] I. B. Kezele, D. L. Arnold, and D. L. Collins. Atrophy in white matter fiber tracts in multiple sclerosis is not dependent on tract length or local white matter lesions. *Mult. Scler.*, 14:779–785, Jul 2008.

[135] M. Wilson, C. R. Tench, P. S. Morgan, and L. D. Blumhardt. Pyramidal tract mapping by diffusion tensor magnetic resonance imaging in multiple sclerosis: improving correlations with disability. *J. Neurol. Neurosurg. Psychiatr.*, 74:203–207, Feb 2003.

[136] X. Lin, C. R. Tench, P. S. Morgan, G. Niepel, and C. S. Constantinescu. 'Importance sampling' in MS: use of diffusion tensor tractography to quantify pathology related to specific impairment. *J. Neurol. Sci.*, 237:13–19, Oct 2005.

[137] M. Lagana, M. Rovaris, A. Ceccarelli, C. Venturelli, D. Caputo, P. Cecconi, and G. Baselli. Atlas-based vs. individual-based deterministic tractography of corpus callosum in multiple sclerosis. *Conf Proc IEEE Eng Med Biol Soc*, 2009:2699–2702, 2009.

[138] M. Lagana, A. Ceccarelli, M. Giulia Preti, C. Venturelli, M. Pia Sormani, R. Cavarretta, G. Baselli, P. Cecconi, D. Caputo, and M. Rovaris. Atlas-Based Versus Individual-Based Fiber Tracking of the Corpus Callosum in Patients with Multiple Sclerosis: Reliability and Clinical Correlations. *J Neuroimaging*, Sep 2011.

[139] B. Audoin, M. Guye, F. Reuter, M. V. Au Duong, S. Confort-Gouny, I. Malikova, E. Soulier, P. Viout, A. A. Cherif, P. J. Cozzone, J. Pelletier, and J. P. Ranjeva. Structure of WM bundles constituting the working memory system in early multiple sclerosis: a quantitative DTI tractography study. *Neuroimage*, 36:1324–1330, Jul 2007.

[140] N. Shu, Y. Liu, K. Li, Y. Duan, J. Wang, C. Yu, H. Dong, J. Ye, and Y. He. Diffusion tensor tractography reveals disrupted topological efficiency in white matter structural networks in multiple sclerosis. *Cereb. Cortex*, 21:2565–2577, Nov 2011.

[141] K. Sugiyama, T. Kondo, S. Higano, M. Endo, H. Watanabe, K. Shindo, and S. Izumi. Diffusion tensor imaging fiber tractography for evaluating diffuse axonal injury. *Brain Inj*, 21:413–419, Apr 2007.

[142] K. Sugiyama, T. Kondo, Y. Oouchida, Y. Suzukamo, S. Higano, M. Endo, H. Watanabe, K. Shindo, and S. Izumi. Clinical utility of diffusion tensor imaging for evaluating patients with diffuse axonal injury and cognitive disorders in the chronic stage. *J. Neurotrauma*, 26:1879–1890, Nov 2009.

[143] K. Hashimoto, A. Okumura, J. Shinoda, M. Abo, and T. Nakamura. Tensor magnetic resonance imaging in a case of mild traumatic brain injury with lowered verbal intelligence quotient. *J Rehabil Med*, 39:418–420, May 2007.

[144] J. H. Hong and S. H. Jang. Degeneration of cingulum and fornix in a patient with traumatic brain injury: diffuse tensor tractography study. *J Rehabil Med*, 42:979–981, Nov 2010.

[145] D. R. Rutgers, P. Fillard, G. Paradot, M. Tadie, P. Lasjaunias, and D. Ducreux. Diffusion tensor imaging characteristics of the corpus callosum in mild, moderate, and severe traumatic brain injury. *AJNR Am J Neuroradiol*, 29:1730–1735, Oct 2008.

[146] M. Singh, J. Jeong, D. Hwang, W. Sungkarat, and P. Gruen. Novel diffusion tensor imaging methodology to detect and quantify injured regions and affected

brain pathways in traumatic brain injury. *Magn Reson Imaging*, 28:22–40, Jan 2010.

[147] J. Y. Wang, K. Bakhadirov, H. Abdi, M. D. Devous, C. D. Marquez de la Plata, C. Moore, C. J. Madden, and R. Diaz-Arrastia. Longitudinal changes of structural connectivity in traumatic axonal injury. *Neurology*, 77:818–826, Aug 2011.

[148] A. M. McIntosh, S. Munoz Maniega, G. K. Lymer, J. McKirdy, J. Hall, J. E. Sussmann, M. E. Bastin, J. D. Clayden, E. C. Johnstone, and S. M. Lawrie. White matter tractography in bipolar disorder and schizophrenia. *Biol. Psychiatry*, 64:1088–1092, Dec 2008.

[149] M. Ashtari, J. Cottone, B. A. Ardekani, K. Cervellione, P. R. Szeszko, J. Wu, S. Chen, and S. Kumra. Disruption of white matter integrity in the inferior longitudinal fasciculus in adolescents with schizophrenia as revealed by fiber tractography. *Arch. Gen. Psychiatry*, 64:1270–1280, Nov 2007.

[150] O. R. Phillips, K. H. Nuechterlein, K. A. Clark, L. S. Hamilton, R. F. Asarnow, N. S. Hageman, A. W. Toga, and K. L. Narr. Fiber tractography reveals disruption of temporal lobe white matter tracts in schizophrenia. *Schizophr. Res.*, 107:30–38, Jan 2009.

[151] J. Fitzsimmons, M. Kubicki, K. Smith, G. Bushell, R. S. Estepar, C. F. Westin, P. G. Nestor, M. A. Niznikiewicz, R. Kikinis, R. W. McCarley, and M. E. Shenton. Diffusion tractography of the fornix in schizophrenia. *Schizophr. Res.*, 107:39–46, Jan 2009.

[152] D. Luck, A. K. Malla, R. Joober, and M. Lepage. Disrupted integrity of the fornix in first-episode schizophrenia. *Schizophr. Res.*, 119:61–64, Jun 2010.

[153] H. Choi, M. Kubicki, T. J. Whitford, J. L. Alvarado, D. P. Terry, M. Niznikiewicz, R. W. McCarley, J. S. Kwon, and M. E. Shenton. Diffusion tensor imaging of anterior commissural fibers in patients with schizophrenia. *Schizophr. Res.*, 130:78–85, Aug 2011.

[154] M. Kubicki, M. Styner, S. Bouix, G. Gerig, D. Markant, K. Smith, R. Kikinis, R. W. McCarley, and M. E. Shenton. Reduced interhemispheric connectivity in schizophrenia-tractography based segmentation of the corpus callosum. *Schizophr. Res.*, 106:125–131, Dec 2008.

[155] T. J. Whitford, P. Savadjiev, M. Kubicki, L. J. O'Donnell, D. P. Terry, S. Bouix, C. F. Westin, J. S. Schneiderman, L. Bobrow, A. C. Rausch, M. Niznikiewicz, P. G. Nestor, C. Pantelis, S. J. Wood, R. W. McCarley, and M. E. Shenton. Fiber geometry in the corpus callosum in schizophrenia: evidence for transcallosal misconnection. *Schizophr. Res.*, 132:69–74, Oct 2011.

[156] M. Kubicki, J. L. Alvarado, C. F. Westin, D. F. Tate, D. Markant, D. P. Terry, T. J. Whitford, J. De Siebenthal, S. Bouix, R. W. McCarley, R. Kikinis, and M. E. Shenton. Stochastic tractography study of Inferior Frontal Gyrus anatomical connectivity in schizophrenia. *Neuroimage*, 55:1657–1664, Apr 2011.

[157] Y. Rathi, M. Kubicki, S. Bouix, C. F. Westin, J. Goldstein, L. Seidman, R. Mesholam-Gately, R. W. McCarley, and M. E. Shenton. Statistical analysis of fiber bundles using multi-tensor tractography: application to first-episode schizophrenia. *Magn Reson Imaging*, 29:507–515, May 2011.

[158] A. Zalesky, A. Fornito, M. L. Seal, L. Cocchi, C. F. Westin, E. T. Bullmore, G. F. Egan, and C. Pantelis. Disrupted axonal fiber connectivity in schizophrenia. *Biol. Psychiatry*, 69:80–89, Jan 2011.

[159] S. Marenco, J. L. Stein, A. A. Savostyanova, F. Sambataro, H. Y. Tan, A. L. Goldman, B. A. Verchinski, A. S. Barnett, D. Dickinson, J. A. Apud, J. H. Callicott, A. Meyer-Lindenberg, and D. R. Weinberger. Investigation of anatomical thalamo-cortical connectivity and FMRI activation in schizophrenia. *Neuropsychopharmacology*, 37:499–507, Jan 2012.

[160] Q. Wang, T. P. Su, Y. Zhou, K. H. Chou, I. Y. Chen, T. Jiang, and C. P. Lin. Anatomical insights into disrupted small-world networks in schizophrenia. *Neuroimage*, 59:1085–1093, Jan 2012.

[161] J. Houenou, M. Wessa, G. Douaud, M. Leboyer, S. Chanraud, M. Perrin, C. Poupon, J. L. Martinot, and M. L. Paillere-Martinot. Increased white matter connectivity in euthymic bipolar patients: diffusion tensor tractography between the subgenual cingulate and the amygdalo-hippocampal complex. *Mol. Psychiatry*, 12:1001–1010, Nov 2007.

[162] F. Lin, S. Weng, B. Xie, G. Wu, and H. Lei. Abnormal frontal cortex white matter connections in bipolar disorder: a DTI tractography study. *J Affect Disord*, 131:299–306, Jun 2011.

[163] M. Jenkinson and S. Smith. A global optimisation method for robust affine registration of brain images. *Medical image analysis*, 5(2):143–56, Jun 2001.

[164] B. Alkonyi, C. Juhasz, O. Muzik, M. E. Behen, J. W. Jeong, and H. T. Chugani. Thalamocortical connectivity in healthy children: asymmetries and robust developmental changes between ages 8 and 17 years. *AJNR Am J Neuroradiol*, 32:962–969, May 2011.

[165] B. Alkonyi, H. T. Chugani, M. Behen, S. Halverson, E. Helder, M. I. Makki, and C. Juhasz. The role of the thalamus in neuro-cognitive dysfunction in early unilateral hemispheric injury: a multimodality imaging study of children with Sturge-Weber syndrome. *Eur. J. Paediatr. Neurol.*, 14:425–433, Sep 2010.

[166] J. H. Adams, D. I. Graham, and B. Jennett. The neuropathology of the vegetative state after an acute brain insult. *Brain*, 123 (Pt 7):1327–1338, Jul 2000.

[167] D. R. Rutgers, F. Toulgoat, J. Cazejust, P. Fillard, P. Lasjaunias, and D. Ducreux. White matter abnormalities in mild traumatic brain injury: a diffusion tensor imaging study. *AJNR Am J Neuroradiol*, 29:514–519, Mar 2008.

[168] S. M. Smith. Fast robust automated brain extraction. *Hum Brain Mapp*, 17:143–155, Nov 2002.

[169] R. A. Heckemann, J. V. Hajnal, P. Aljabar, D. Rueckert, and A. Hammers. Automatic anatomical brain MRI segmentation combining label propagation and decision fusion. *Neuroimage*, 33:115–126, Oct 2006.

[170] R. A. Heckemann, S. Keihaninejad, P. Aljabar, D. Rueckert, J. V. Hajnal, and A. Hammers. Improving intersubject image registration using tissue-class information benefits robustness and accuracy of multi-atlas based anatomical segmentation. *Neuroimage*, 51:221–227, May 2010.

[171] J.L.R. Andersson, M. Jenkinson, and S. Smith. Non-linear optimisation. *FMRIB technical report TR07JA1.*

[172] J.L.R. Andersson, M. Jenkinson, and S. Smith. Non-linear registration, aka spatial normalisation. *FMRIB technical report TR07JA2*.

[173] S. M. Smith, M. Jenkinson, H. Johansen-Berg, D. Rueckert, T. E. Nichols, C. E. Mackay, K. E. Watkins, O. Ciccarelli, M. Z. Cader, P. M. Matthews, and T. E. Behrens. Tract-based spatial statistics: voxelwise analysis of multi-subject diffusion data. *Neuroimage*, 31:1487–1505, Jul 2006.

[174] Y. Zhang, M. Brady, and S. Smith. Segmentation of brain MR images through a hidden Markov random field model and the expectation-maximization algorithm. *IEEE Trans Med Imaging*, 20:45–57, Jan 2001.

[175] J Hume Adams, Bryan Jennett, Lilian S Murray, Graham M Teasdale, Thomas A Gennarelli, and David I Graham. Neuropathological findings in disabled survivors of a head injury. *Journal of Neurotrauma*, 28(5):701–709, May 2011. PMID: 21401319.

[176] C. L. Mac Donald, K. Dikranian, P. Bayly, D. Holtzman, and D. Brody. Diffusion tensor imaging reliably detects experimental traumatic axonal injury and indicates approximate time of injury. *J. Neurosci.*, 27:11869–11876, Oct 2007.

[177] K. M. Kinnunen, R. Greenwood, J. H. Powell, R. Leech, P. C. Hawkins, V. Bonnelle, M. C. Patel, S. J. Counsell, and D. J. Sharp. White matter damage and cognitive impairment after traumatic brain injury. *Brain*, 134:449–463, Feb 2011.

[178] A. Sidaros, A. W. Engberg, K. Sidaros, M. G. Liptrot, M. Herning, P. Petersen, O. B. Paulson, T. L. Jernigan, and E. Rostrup. Diffusion tensor imaging during recovery from severe traumatic brain injury and relation to clinical outcome: a longitudinal study. *Brain*, 131:559–572, Feb 2008.

[179] A. Seewann, H. Vrenken, E. J. Kooi, P. van der Valk, D. L. Knol, C. H. Polman, P. J. Pouwels, F. Barkhof, and J. J. Geurts. Imaging the tip of the iceberg: visualization of cortical lesions in multiple sclerosis. *Mult. Scler.*, 17:1202–1210, Oct 2011.

[180] H. E. Hulst and J. J. Geurts. Gray matter imaging in Multiple Sclerosis: what have we learned? *BMC Neurol*, 11:153, Dec 2011.

[181] R. H. Lazeron, D. W. Langdon, M. Filippi, J. H. van Waesberghe, V. L. Stevenson, J. B. Boringa, D. Origgi, A. J. Thompson, M. Falautano, C. H. Polman, and F. Barkhof. Neuropsychological impairment in multiple sclerosis patients: the role of (juxta)cortical lesion on FLAIR. *Mult. Scler.*, 6:280–285, Aug 2000.

[182] C. Christodoulou, L. B. Krupp, Z. Liang, W. Huang, P. Melville, C. Roque, W. F. Scherl, T. Morgan, W. S. MacAllister, L. Li, L. A. Tudorica, X. Li, P. Roche, and R. Peyster. Cognitive performance and MR markers of cerebral injury in cognitively impaired MS patients. *Neurology*, 60:1793–1798, Jun 2003.

[183] M. Calabrese, M. A. Rocca, M. Atzori, I. Mattisi, A. Favaretto, P. Perini, P. Gallo, and M. Filippi. A 3-year magnetic resonance imaging study of cortical lesions in relapse-onset multiple sclerosis. *Ann. Neurol.*, 67:376–383, Mar 2010.

[184] M. Calabrese, M. Battaglini, A. Giorgio, M. Atzori, V. Bernardi, I. Mattisi, P. Gallo, and N. De Stefano. Imaging distribution and frequency of cortical lesions in patients with multiple sclerosis. *Neurology*, 75:1234–1240, Oct 2010.

[185] J. C. Haselgrove and J. R. Moore. Correction for distortion of echo-planar images used to calculate the apparent diffusion coefficient. *Magn Reson Med*, 36:960–964, Dec 1996.

[186] L. H. Lu, X. J. Zhou, S. K. Keedy, J. L. Reilly, and J. A. Sweeney. White matter microstructure in untreated first episode bipolar disorder with psychosis: comparison with schizophrenia. *Bipolar Disord*, 13:604–613, 2011.